

# DYNAMIC PROCESSES IN COMPLEX COMMUNITIES: INTERPLAY OF NOISE, NONLINEARITY, AND NETWORK STRUCTURE

*A Thesis Submitted*

*In Partial Fulfilment of the Requirements*

*for the Degree of*

## DOCTOR OF PHILOSOPHY

by

**Arzoo Narang**

**(2018MAZ0002)**

*Under the Supervision of*

**Dr. Partha S. Dutta**



DEPARTMENT OF MATHEMATICS

INDIAN INSTITUTE OF TECHNOLOGY ROPAR

December, 2023

Arzoo Narang: *Dynamic processes in complex communities: Interplay of noise, nonlinearity, and network structure*

Copyright ©2023, Indian Institute of Technology Ropar

All Rights Reserved



*To my parents  
For their love and support*

## Declaration of Originality

The author hereby declares that the work presented in the thesis entitled **Dynamic Processes in Complex Communities: Interplay of Noise, Nonlinearity, and Network Structure** submitted as partial fulfillment for the degree of Doctor of Philosophy to the Department of Mathematics, Indian Institute of Technology Ropar, has been carried out under the supervision of Dr. Partha S. Dutta, Associate Professor, IIT Ropar. To the best of my knowledge, it is an original work, both in terms of research content and narrative, and has not been submitted or accepted elsewhere, in part or in full, for the award of any degree, diploma, fellowship, associateship, or similar title of any university or institution. Further, due credit has been attributed to the relevant state-of-the-art and collaborations with appropriate citations and acknowledgements, in line with established ethical norms and practices. I also declare that any idea/data/fact/source stated in my thesis has not been fabricated/ falsified/ misrepresented. All the principles of academic honesty and integrity have been followed. I fully understand that if the thesis is found to be unoriginal, fabricated, or plagiarized, the Institute reserves the right to withdraw the thesis from its archive and revoke the associated Degree conferred. Additionally, the Institute also reserves the right to appraise all concerned sections of society of the matter for their information and necessary action (if any). If accepted, I hereby consent for my thesis to be available online in the Institute's Open Access repository, inter-library loan, and the title & abstract to be made available to outside organizations.



Signature

Name: Arzoo Narang

Entry Number: 2018MAZ0002

Program: PhD

Department: Mathematics

Indian Institute of Technology Ropar

Rupnagar, Punjab 140001

Date: 11-12-23

---

# Acknowledgements

First and foremost, I express my deep gratitude to God for bestowing upon me the blessings and strength to embark on this journey. I am thankful for His unconditional love and grace.

I extend my sincere gratitude to my supervisor Dr. Partha S. Dutta for not only providing me this opportunity but also for his invaluable guidance throughout the process. His knowledge, experience, patience, and motivation have allowed me to grow as a researcher. I am thankful to him for his insightful comments and encouragement, which have been substantial in this accomplishment.

I sincerely acknowledge the support of members of the doctoral committee at IIT Ropar: Dr. S. C. Martha, Dr. A. Sairam Kaliraj, Dr. Arun Kumar from the Department of Mathematics, and Dr. Lipika Kabiraj from the Department of Mechanical Engineering. I appreciate the cooperation provided by Neeraj Ji, the senior lab assistant, and the department staff over these years.

I want to take this moment to express my heartfelt gratitude to the friends I was fortunate to have during this journey. I am immensely thankful to Bipasha for standing by me at all times, and for being the one I can always count on. To Param, Monika, Shagun, and Manju, I extend my gratitude for being there when I needed someone to listen, for providing valuable advice, for the shared laughter, and for the support in times of sorrow, all of which have made this journey truly memorable. I thank the members of the Dutta group, Dr. Sukanta Sarkar and Ravi, for their valuable discussions and selfless help. A special mention goes to Dr. Subhendu for his indispensable support and guidance during the initial stages, and to Smita for always being there to help whenever I needed it. I must also mention Dr. Taranjot, who started as a senior and later became a cherished friend, sharing our passion, secrets, and delightful conversations. I also appreciate Aditi, Sonam, Vikash, Niharika, Jasbir, and Bharti for their support during the tough phase. I thank Amrendra Bhayia for being there and Krishnendu Bhayia for our invaluable discussions and for sharing with me the joy of hearty laughter. Special thanks to Karan, and Hafsoah for the sweet memories. A heartfelt thanks to Priti Di, who, despite the distance has always been there, patiently listening, supporting, and encouraging me.

I express my deep sense of gratitude towards my parents, for making my dreams their own. I owe them for believing in me, for being unconditionally supportive, and for the countless sacrifices they have made throughout the process. Their patience, love, and blessings have made me complete this journey.

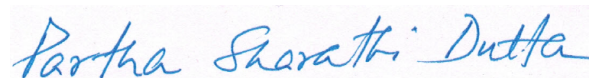
Finally, I thank IIT Ropar for providing me with the fellowship (through MHRD), giving me all the necessary resources for my research, as well as the financial support

I needed to present my work at various conferences during my doctoral study. Also, this work was partially supported by the FIST program of the Department of Science and Technology, Government of India, Reference No. SR/FST/MS-I/2018/22(C).

# Certificate

This is to certify that the thesis entitled **Dynamic Processes in Complex Communities: Interplay of Noise, Nonlinearity, and Network Structure**, submitted by **Arzoo Narang (2018MAZ0002)** for the award of the degree of **Doctor of Philosophy** of Indian Institute of Technology Ropar, is a record of bonafide research work carried out under my guidance and supervision. To the best of my knowledge and belief, the work presented in this thesis is original and has not been submitted, either in part or full, for the award of any other degree, diploma, fellowship, associateship or similar title of any university or institution.

In my opinion, the thesis has reached the standard fulfilling the requirements of the regulations relating to the Degree.



Signature of the Supervisor

Name: Dr. Partha S. Dutta

Department: Mathematics

Indian Institute of Technology Ropar

Rupnagar, Punjab 140001

Date: 11-12-23

# Abstract

Mathematical modeling of spatial ecological systems has significantly contributed to our understanding of population dynamics, species' distribution across space, collective behavior, and ecological stability. The theory of dynamical systems and diverse numerical methods are instrumental in studying spatial population models. In this thesis, we study various mathematical models of spatial ecological systems to understand the effect of demographic and environmental stochasticity, dispersal network topology, species movement patterns, and arrangement of landscape on ecosystem dynamics.

Noise-induced symmetry breaking has barely been unveiled on ecological grounds, though its occurrence may elucidate mechanisms responsible for maintaining biodiversity and ecosystem stability. We study an ecological network model and demonstrate that the interplay of network structure and noise intensity manifests a transition from homogeneous steady state to inhomogeneous steady states, resulting in noise-induced symmetry breaking. Further, we move beyond dyadic couplings and consider the higher-order species interactions in an ecological network. We study the synchrony patterns and observe that higher-order interactions bring about significant changes in collective behavior compared to the conventional pairwise interaction. We also find the region where the synchronous state is stable using the master stability function. The ability of species to move between fragmented landscapes is an essential factor in ascertaining the dynamics and spatial distribution of populations. Further, the effect of resource pulses on ecological processes due to environmental variation in the context of foraging strategies remains largely unexplored. Considering resource pulses, we analyze the unified impact of foraging behavior and species' life-history traits on the structure and dynamics of ecosystems. We find that a Lévy walk is consistently effective as a movement strategy. We also find that the optimal foraging behavior shifts from Brownian to ballistic as the mortality rate of grazers increases. In addition, our study comprehends how climate warming and spatial separation between habitat patches influence species' collective dynamics. We find that rising habitat temperature has the potential to destabilize ecological dynamics, and density-dependent species dispersal can mitigate these adverse effects. Moreover, long-range dispersal works out as the driving force for species persistence in extreme temperature conditions of habitat.

**Keywords:** ecological networks; habitat fragmentation; network topology; excitable system; noise-induced symmetry breaking; higher-order interaction; synchrony; chimera; resource pulse; foraging; Lévy walk; climate warming; long-range dispersal

# Contents

---

<b>Declaration</b>	<b>iv</b>
<b>Acknowledgement</b>	<b>v</b>
<b>Certificate</b>	<b>vii</b>
<b>Abstract</b>	<b>viii</b>
<b>List of Figures</b>	<b>xiii</b>
<b>List of Tables</b>	<b>xxiii</b>
<b>1 Introduction</b>	<b>1</b>
1.0.1 Network models . . . . .	2
1.0.2 Cellular automata . . . . .	2
1.0.3 Spatial ecology and conservation . . . . .	3
1.1 Stochasticity in nonlinear systems . . . . .	3
1.1.1 Noise in ecology . . . . .	4
1.2 Network topology and ecosystems dynamics . . . . .	5
1.2.1 An overview of the influence of the number of nodes and interaction strength . . . . .	6
1.2.2 Random pairwise interactions . . . . .	6
1.2.3 Higher-order interactions . . . . .	8
1.3 Landscape structure . . . . .	9
1.3.1 Foraging theory . . . . .	9
1.3.2 Random walk . . . . .	10
1.3.3 Resource pulse . . . . .	10
1.4 Role of species dispersal in population dynamics . . . . .	11
1.4.1 Temperature: an environmental stressor influencing species dispersal . . . . .	12
1.4.2 Density-dependent dispersal . . . . .	12
1.4.3 Dispersal distance . . . . .	13
1.5 Objectives and Scope . . . . .	13
1.6 Outline of the Thesis . . . . .	15
1.6.1 Noise-induced symmetry breaking in a network of excitable ecological systems . . . . .	15

1.6.2	Effect of higher-order interactions on the stability of ecological communities . . . . .	16
1.6.3	Resource pulses and foraging behavior shape spatial population dynamics . . . . .	17
1.6.4	Climate warming and dispersal strategies determine species persistence in a metacommunity . . . . .	17
1.6.5	Long-range dispersal promotes species persistence in climate extremes . . . . .	18
<b>2</b>	<b>Noise-induced symmetry breaking in a network of excitable ecological systems</b>	<b>19</b>
2.1	Introduction . . . . .	19
2.2	Model of an ecological network . . . . .	21
2.3	Results . . . . .	22
2.4	Conclusion . . . . .	27
2.5	Appendix 1: Stochastic consumer dynamics . . . . .	28
2.6	Appendix 2: Ecological network with stochastic birth and death rates	29
2.6.1	Effect of habitat connectance in a regular network ( $p = 0$ ) . . . . .	30
2.6.2	Effect of increasing habitat connectance in different network topologies (WS, BA, and ER) . . . . .	32
<b>3</b>	<b>Effect of higher-order interactions on the stability of ecological communities</b>	<b>35</b>
3.1	Introduction . . . . .	35
3.2	Model and Methods . . . . .	37
3.2.1	An ecological dispersal network with higher-order interactions	37
3.2.2	Linear stability analysis of synchronized solution with higher-order interactions . . . . .	39
3.3	Results . . . . .	43
3.3.1	Role of random network topology on synchronization in the presence of higher-order interaction . . . . .	43
3.3.2	Cluster analysis . . . . .	43
3.3.3	Effect of higher-order interaction strength on synchrony in a network with all-to-all coupling . . . . .	44
3.3.4	Using the master stability function approach to determine the coupling range of stable synchronous solution in a global network with higher-order interactions . . . . .	46
3.3.5	Synchronization error . . . . .	46



3.4	Conclusions . . . . .	47
<b>4</b>	<b>Resource pulses and foraging behavior shape spatial population dynamics</b>	<b>49</b>
4.1	Introduction . . . . .	49
4.2	A stochastic vegetation-grazer model in fragmented landscapes . . . .	52
4.3	Results . . . . .	52
4.3.1	Population dynamics with different movement strategies . . .	52
4.3.2	Vegetation's reproduction rate and foraging behavior . . . . .	56
4.4	Discussion . . . . .	58
4.5	Appendix . . . . .	59
4.5.1	Spatial configuration at $m = 0.2$ . . . . .	59
4.5.2	Stochastic lattice vegetation-grazer model . . . . .	59
4.5.3	Detailed model description . . . . .	61
<b>5</b>	<b>Climate warming and dispersal strategies determine species persistence in a metacommunity</b>	<b>63</b>
5.1	Introduction . . . . .	63
5.2	Models and Methods . . . . .	65
5.2.1	A two patch metacommunity model . . . . .	65
5.2.2	Metacommunity with a large number of patches . . . . .	68
5.3	Results . . . . .	69
5.3.1	Spatial synchrony . . . . .	70
5.3.2	Variance and mean of regional abundance . . . . .	72
5.3.3	Spatiotemporal dynamics for a metacommunity with many patches . . . . .	73
5.4	Discussion . . . . .	74
5.5	Appendix . . . . .	77
5.5.1	Variance and mean of regional abundance for $d_n > d_p$ . . . . .	77
5.5.2	Temperature sensitivity of the half-saturation constant ( $N_0$ ) and the carrying capacity ( $K$ ) . . . . .	80
5.5.3	Spatiotemporal dynamics for different choices of temperature .	81
<b>6</b>	<b>Long-range dispersal promotes species persistence in climate extremes</b>	<b>83</b>
6.1	Introduction . . . . .	83
6.2	Materials and Methods . . . . .	86
6.2.1	A metapopulation model . . . . .	86
6.2.2	Characteristic measures . . . . .	88
6.3	Results . . . . .	91

---

6.3.1	Time series analyses and predator amplitude . . . . .	91
6.3.2	Cluster analysis . . . . .	91
6.3.3	Interpatch synchrony . . . . .	92
6.3.4	Median predator amplitude and mean transient fraction . . . .	93
6.3.5	Cross wavelet analysis . . . . .	94
6.4	Discussion . . . . .	95
<b>7</b>	<b>Conclusions</b>	<b>99</b>
7.1	Key findings . . . . .	99
7.2	Future directions . . . . .	101
	<b>References</b>	<b>103</b>
	<b>List of Publications</b>	<b>128</b>

# List of Figures

---

- 1.1 Phase portrait and time series of the model (1.1a). (a) Phase portrait depicting a chaotic trajectory. (b)-(e) Time series exhibiting synchronous or asynchronous behavior of populations depending upon the network size ( $n$ ) and the interaction strength ( $\epsilon$ ): (b)  $n = 2$ ,  $\epsilon = 0$ : asynchrony, (c)  $n = 2$ ,  $\epsilon = 0.03$ : phase synchrony, (d)  $n = 2$ ,  $\epsilon = 0.075$ : phase and amplitude synchrony, and (e)  $n = 10$ ,  $\epsilon = 0.03$ : phase and amplitude synchrony. Other model parameters are  $a = 1, d = 1, c = 10, \beta_1 = 0.2, \beta_2 = 1, k_1 = 0.05$ , and  $z^* = 0.006$ . . . . . 7
- 1.2 A system with interacting units represented as (a) a network, where the interactions occur pairwise between nodes and depicted as edges, (b) hypergraph, which facilitates group interactions. In this context, shaded groups of nodes represent hyperedges, (c) simplicial complex, edges correspond to 1-simplices, and full triangles representing 2-simplices are shown in green. . . . . 8
- 2.1 Time series of the resource population ( $x$ ) for the model (1.1a) with,  $\sigma = 0$  and  $a = 9$  (the system is in the excitable region): (a) For zero noise intensity ( $D = 0$ ) the system settles into a steady state; inset: nullclines of the resource ( $x$ ) and the consumer ( $y$ ). (b) For a non-zero noise intensity ( $D = 0.00005$ ) there exist noise-induced oscillations; inset: stochastic cyclic attractor. Other model parameters are:  $r = 1$ ,  $b = 7$ ,  $m = 1$ ,  $\epsilon = 0.01$ , and  $N = 101$ . . . . . 20
- 2.2 (a)-(d) Space-time (left column) and corresponding time series plots (right column) of resource  $x_i$  for  $P = 8$ ,  $\sigma = 0.1$  with varying noise intensities: (a)  $D = 0$ ; steady state, (b)  $D = 0.00001$ ; symmetry breaking, (c)  $D = 0.000033$ ; stochastic switching between two resource densities, and (d)  $D = 0.005$ ; asynchronous oscillations. (e)-(h) Space-time (left column) and corresponding time series (right column) plots for  $D = 0.00001$ ,  $\sigma = 0.6$  with varying coupling range  $s$ : (e)  $s = 0.01$  (local coupling); asynchronous oscillations, (f)  $s = 0.04$ ; symmetry breaking, (g)  $s = 0.25$ ; symmetry breaking with most nodes settling at the lower branch, and (h)  $s = 0.5$  (global coupling); steady state. Other model parameters are  $r = 1$ ,  $a = 9$ ,  $b = 7$ ,  $m = 1$ ,  $\epsilon = 0.01$ , and  $N = 101$ . . . . . 21

- 2.3 Phase portraits exhibiting the long stay of attractor in the two domains around  $x_i = 0.1$  and  $x_i = 0.55$  for (a) one oscillator (15th node), and (b) all the oscillators, at noise intensity  $D = 0.005$ . (c) Center of mass ( $x_{c.m.}$ ), and (d) phase portrait at a particular time along with density distribution of  $y_i$  corresponding to NISB for non-local coupling ( $P = 8$ ) at noise intensity  $D = 0.00001$ . The histogram in the right panel of (d) represents the number of oscillators in either of the two states. Other model parameters are  $r = 1$ ,  $a = 9$ ,  $b = 7$ ,  $m = 1$ ,  $\epsilon = 0.01$ ,  $\sigma = 0.1$ , and  $N = 101$ . . . . . 24
- 2.4 Phase diagrams in the (a)  $(s, D)$  plane for  $\sigma = 0.1$ , and (b)  $(s, \sigma)$  plane for  $D = 0.00001$ , where NIO: noise-induced oscillations, SS: Stochastic switching, NISB: noise-induced symmetry breaking, and HSS: Homogeneous steady state. (c)-(e) Distribution of the eigenvalues for different values of  $s$  for  $\sigma = 0.6$  and  $D = 0$ . Other model parameters are the same as in Fig. 2.2. . . . . 25
- 2.5 Species dynamics of the uncoupled deterministic model: (a) One-parameter bifurcation diagram with variation in the parameter  $a$ . (b) Two-parameter bifurcation diagram in the  $(a, \epsilon)$ -plane. Shaded regions: [A] corresponds to the region where the system exhibits steady state dynamics. [B] is the region where species abundance depicts oscillatory behavior. (c-d) Time series of the resource ( $x$ ) for  $a = 8$ , and  $a = 9$ , respectively. Other parameter values are  $\epsilon = 0.01$ ,  $b = 7$ ,  $r = 1$ , and  $m = 1$ . . . . . 28
- 2.6 (a)-(d) Space-time (left column) and corresponding time series plots (right column) of consumer  $y_i$  for  $P = 8$ ,  $\sigma = 0.1$  with varying noise intensities: (a)  $D = 0$ ; steady state, (b)  $D = 0.00001$ ; symmetry breaking, (c)  $D = 0.000033$ ; stochastic switching between two consumer densities, and (d)  $D = 0.005$ ; frequent spiking. (e)-(h) Space-time (left column) and corresponding time series (right column) plots for  $D = 0.00001$ ,  $\sigma = 0.6$  with varying coupling range  $s$ : (e)  $s = 0.01$  (local coupling); asynchronous oscillations, (f)  $s = 0.04$ ; symmetry breaking, (g)  $s = 0.25$ ; most nodes settling at the lower branch, and (h)  $s = 0.5$  (global coupling); steady state. Other model parameters are  $r = 1$ ,  $a = 9$ ,  $b = 7$ ,  $m = 1$ ,  $\epsilon = 0.01$ , and  $N = 101$ . . . 29

- 2.7 Space-time plot (left column) and time series plot (right column) in a regular network ( $p = 0$ ) for  $D = 1$  and,  $\sigma = 1$  with varying average degree  $k$ : (a)  $k = 2$  (nearest neighbor connections); asynchronous oscillations, (b)  $k = 10$ ; stochastic switching, (c)  $k = 40$ ; symmetry breaking, and (d):  $k = 100$  (global connectivity); symmetry breaking. Other parameters are  $r = 1$ ,  $a = 9$ ,  $b = 7$ ,  $m = 1$ ,  $\epsilon = 0.01$ , and  $N = 101$ . . . . . 31
- 2.8 Center of mass  $x_{c.m.}(i)$  (left column) and phase portraits (right column) for  $p = 0$ ,  $D = 1$ , and  $\sigma = 1$  with varying average degree  $k$ : (a)  $k = 2$ , (b)  $k = 10$ , and (c)  $k = 100$ , respectively. Other parameters are the same as in Fig. 2.7. . . . . 32
- 2.9 Time series of resource  $x_i$  in WS ((a)-(c)) with  $p = 0.4$ , BA ((d)-(f)), and ER ((g)-(i)) networks with varying average degree  $k$ : [(a), (d), (g)]  $k = 4$ , [(b), (e), (h)]  $k = 10$ , [(c), (f), (i)]  $k = 40$ . Other parameters are  $r = 1$ ,  $a = 9$ ,  $b = 7$ ,  $m = 1$ ,  $\epsilon = 0.01$ ,  $N = 101$ ,  $\sigma = 1$ , and  $D = 1$ . . . . . 33
- 3.1 Networks representing pairwise and higher-order interactions between nodes. (a) A network with pairwise interactions between nodes connected by edges. (b) Higher-order interaction between nodes in a network is modeled using simplicial complexes, where edges correspond to 1-simplices, and full triangles represent 2-simplices (shown in green). . . . . 36
- 3.2 Phase portrait and time series of the food-chain model (3.1) in the absence of coupling (i.e., when  $\sigma_1 = \sigma_2 = 0$ ). (a) Phase portrait exhibiting a chaotic attractor. Time series representing the abundances of (b) the resource, (b) the consumer, and (c) the top predator. Model parameters are  $a_1 = 5$ ,  $a_2 = 0.1$ ,  $b_1 = 3$ ,  $b_2 = 2$ ,  $m_1 = 0.4$ , and  $m_2 = 0.01$ . . . . . 38
- 3.3 Space-time plots (left column) and corresponding time series plots (right column) of the top predator  $z$  in a network with average degree 8 for  $\sigma_1 = 0.004$ : (a) a regular network exhibiting complete synchrony for  $\sigma_2 = 0$ ; (b) a random network with asynchronous oscillations for  $\sigma_2 = 0$ ; and (c) a random network with suppressed asynchrony for  $\sigma_2 = 0.002$ . Other parameters are  $a_1 = 5$ ,  $a_2 = 0.1$ ,  $b_1 = 3$ ,  $b_2 = 2$ ,  $m_1 = 0.4$ ,  $m_2 = 0.01$ , and  $N = 21$ . . . . . 42

- 3.4 Frequency of cluster states for different network topologies when  $\sigma_1 = 0.004$ : (a) regular network exhibiting one cluster solution for  $\sigma_2 = 0$ ; (b) random network exhibiting a high number of clusters for  $\sigma_2 = 0$ ; and (c) random network exhibiting two to three clusters for  $\sigma_2 = 0.01$ . The frequency of each cluster is shown using  $10^2$  independent simulations. Other parameters are  $a_1 = 5, a_2 = 0.1, b_1 = 3, b_2 = 2, m_1 = 0.4, m_2 = 0.01$ , and  $N = 21$ . . . . . 44
- 3.5 Space-time plots (left column) and corresponding time series plots (right column) of the top predator  $z$  in a regular network with all-to-all coupling for  $\sigma_1 = 10^{-6}$  with varying higher-order coupling strength  $\sigma_2$ : (a)  $\sigma_2 = 10^{-6}$  results in strong asynchrony between the nodes; (b)  $\sigma_2 = 10^{-5}$  results in asynchrony with many cluster solutions; and (c)  $\sigma_2 = 10^{-4}$  results in complete synchrony. Other parameters are  $a_1 = 5, a_2 = 0.1, b_1 = 3, b_2 = 2, m_1 = 0.4, m_2 = 0.01$ , and  $N = 21$ . . . . . 45
- 3.6 Master stability function for the model (3.1) in the context of global coupling. The maximum Lyapunov exponent (MLE) is calculated to analyze the stability of synchronous solution: (a) MLE depicted in  $(\sigma_1, \sigma_2)$  parameter space. (b) The MLE ( $\Lambda$ ) plots exhibiting variation along  $\sigma_2$  for different values of  $\sigma_1$ . On increasing second-order interaction strength ( $\sigma_2$ ), a stable synchronous state is achieved even for the lower value of  $\sigma_1$ . . . . . 46
- 3.7 Synchronization error  $E$  in  $(\sigma_2, \sigma_1)$  plane for different network topologies: (a) random network, the value of  $E$  varies from 7 to 4 with increasing  $\sigma_2$ , and (b) after a region of asynchrony, the global network exhibits a completely synchronous solution ( $E = 0$ ). . . . . 47
- 4.1 A schematic representation of different stages of vegetation and grazers incorporated in the model. A resource pulse is incorporated periodically after every  $t_v$  time (upper panel) in which vegetation can either die naturally (pink circle) or reproduce in the nearest empty cell (yellow circle). The lower panel corresponds to the three stages of a grazer. A randomly selected grazer (blue square) disperses to a new site, as shown by an arrow. It attacks and consumes vegetation (red circle), making the cell vacant. It then reproduces at the site. . . 51

- 4.2 Evolution of the spatially averaged densities  $v(t)$  (vegetation) and  $g(t)$  (grazers) where the mortality rate of grazers are considered as  $m = 0.07$  (in (a)-(c)), and  $m = 0.2$  (in (d)-(f)). Time series and the corresponding power spectrum illustrate three different population scenarios: extinction of grazers, steady state coexistence, or oscillatory coexistence, depending upon the value of  $\beta$ , which determines the range of movement: (a), (d)  $\beta = 1.1$ ; (b), (e)  $\beta = 2.2$ ; and (c), (f)  $\beta = 3.5$ . Other parameters are  $p = 0.7$ ,  $\mu = 0.2$ , and  $L = 100$ . . . . . 53
- 4.3 Initial (left panel) and final (right panel) time configurations of grazers (in red) and vegetation (in green) at an intermediate rate of mortality ( $m = 0.07$ ). (a)  $\beta \sim 1$  (highly superdiffusive grazers): the left panel shows the initial time density configuration when grazers have outreached vegetation. This leads to the extinction of grazers on reaching the final time (right panel) and the rejuvenation of vegetation due to resource pulse, (b)  $\beta = 3.5$  (Brownian grazers): grazers and vegetation coexist in the final time (right panel). Other parameters are  $p = 0.7$ ,  $\mu = 0.2$ , and  $L = 100$ . . . . . 54
- 4.4 Cluster size distribution of vegetation (red) and grazers (green) for different values of  $m$  and  $\beta$ . Left ((a)-(c)) and right panels ((d)-(f)) show the trends corresponding to  $m = 0.07$ , and  $m = 0.2$ , respectively, where in (a), (d)  $\beta \sim 1$ ; (b), (e)  $\beta \sim 2.2$ ; and (c), (f)  $\beta > 3$ . Other parameters are  $\mu = 0.2$ ,  $p = 0.7$ , and  $L = 100$ . . . . . 55
- 4.5 Phase diagrams in the  $(\beta, p)$ -plane depicting various dynamical regimes corresponding to (a)  $m = 0.04$ , (b)  $m = 0.07$ , and (c)  $m = 0.2$ . Other parameters are  $\mu = 0.2$ , and  $L = 100$ . . . . . 56
- 4.6 Average grazer density as a function of  $p$  at (a)  $m = 0.07$ , and (b)  $m = 0.2$  for three different values of  $\beta$ . The shaded region corresponds to the oscillatory population dynamics and is represented by the 95% confidence interval. Other parameters are  $\mu = 0.2$ , and  $L = 100$ . . . . 57
- 4.7 Initial (left panel) and final (right panel) time configurations of grazers (in red) and vegetation (in green) at a high rate of mortality ( $m = 0.2$ ) for (a) highly superdiffusive grazers ( $\beta \sim 1$ ), (b) Brownian grazers ( $\beta = 3.5$ ). Other parameters are  $p = 0.7$ ,  $\mu = 0.2$ , and  $L = 100$ . 60
- 5.1 Temperature-dependent species biological traits: (a) Intrinsic growth of resource with varying temperature ( $T$ ). (b) Thermal response of consumer's attack rate. (c) Temperature-dependent mortality of consumers. . . . . 67

- 5.2 Schematic representation of different types of dispersal mechanisms, where  $N$  and  $P$  are the resource and consumer abundance, respectively. '+' sign describes the positive effect of resource abundance ( $N$ ) or consumer abundance ( $P$ ) on dispersal, and '-' sign symbolizes the negative effect of resource abundance ( $N$ ) on dispersal of consumer from the patch. . . . . 68
- 5.3 Species collective dynamics when  $d_n < d_p$ : Spatial synchrony with changing dispersal rates of resource ( $d_n$ ) and consumer ( $d_p = 100d_n$ ) at different temperatures ( $T$ ): For (a), (d), (g)  $T = 10^\circ C$ ; (b), (e), (h)  $T = 20^\circ C$ ; (c), (f), (i)  $T = 29^\circ C$ , in two distinct patches. (a)-(c) correspond to the dynamics for CD where  $x_{\alpha\beta} = 0$ . Intraspecific (dots) and interspecific (triangles) DD in resource and consumer follow the dynamics depicted in (d)-(f) and (g)-(i), respectively. . . . . 70
- 5.4 Species collective dynamics when  $d_n > d_p$ : Spatial synchrony of two patch metacommunity with changing dispersal rates of resource ( $d_n$ ) and consumer ( $d_p = 0.01d_n$ ) at different temperature ( $T$ ). For (a), (d), (g)  $T = 10^\circ C$ ; (b), (e), (h)  $T = 20^\circ C$ ; (c), (f), (i)  $T = 29^\circ C$ , in two distinct patches. (a)-(c) correspond to the dynamics for CD where  $x_{\alpha\beta} = 0$ . Intraspecific (dots) and interspecific (triangles) DD in resource and consumer follow the dynamics depicted in (d)-(f) and (g)-(i), respectively. . . . . 71
- 5.5 Mean and CV of resource abundance when  $d_n < d_p$ : Temporal mean (upper sub-graph) and coefficient of variation (lower sub-graph) of regional resource abundance as a function of maximal resource dispersal rates ( $d_n$ ) at different temperatures ( $T$ ). Consumer dispersal rates  $d_p = 100d_n$ . For (a), (d), (g)  $T = 10^\circ C$ ; (b), (e), (h)  $T = 20^\circ C$ ; (c), (f), (i)  $T = 29^\circ C$ , in two distinct patches. (a)-(c) correspond to the dynamics for CD where  $x_{\alpha\beta} = 0$ . Intraspecific (dots) and interspecific (triangles) DD in resource and consumer follow the dynamics depicted in (d)-(f) and (g)-(i), respectively. . . . . 73



- 5.6 Mean and CV of consumer abundance when  $d_n < d_p$ : Temporal mean (upper sub-graph) and coefficient of variation (lower sub-graph) of regional consumer abundance as a function of maximal resource dispersal rates ( $d_n$ ) at different temperatures ( $T$ ). Consumer dispersal rates  $d_p = 100d_n$ . For (a), (d), (g)  $T = 10^\circ C$ ; (b), (e), (h)  $T = 20^\circ C$ ; (c), (f), (i)  $T = 29^\circ C$ , in two distinct patches. (a)-(c) correspond to the dynamics for CD where  $x_{\alpha\beta} = 0$ . Intraspecific (dots) and interspecific (triangles) DD in resource and consumer follow the dynamics depicted in (d)-(f) and (g)-(i), respectively. . . . . 74
- 5.7 Interplay of coherence and incoherence in population abundance at an intermediate temperature: (a) Spatiotemporal plot of consumer  $P_i$ , (b) snapshot of  $P_i$  at  $t = 4200$  (red(dotted) lines are for visual guidance), and (c) mean phase velocity ( $w_i$ ), for  $n = 100$  patches. Coupling strength  $d_n = 10^{-6}$  and  $d_p = 10^{-4}$ ,  $T = 20^\circ C$ . . . . . 75
- 5.8 Mean and CV of resource abundance when  $d_n > d_p$ : Temporal mean (upper sub-graph) and coefficient of variation (lower sub-graph) of regional resource abundance as a function of maximal resource dispersal rates ( $d_n$ ) at different temperature ( $T$ ). Consumer dispersal rates  $d_p = 0.01d_n$ . For (a), (d), (g)  $T = 10^\circ C$ ; (b), (e), (h)  $T = 20^\circ C$ ; (c), (f), (i)  $T = 29^\circ C$ , in two distinct patches. (a)-(c) Correspond to the dynamics for CD where  $x_{\alpha\beta} = 0$ . Intraspecific (dots) and interspecific (triangles) DD in resource and consumer follow the dynamics depicted in (d)-(f) and (g)-(i), respectively. . . . . 78
- 5.9 Mean and CV of consumer abundance when  $d_n > d_p$ : Temporal mean (upper sub-graph) and coefficient of variation (lower sub-graph) of regional consumer abundance as a function of maximal resource dispersal rates ( $d_n$ ) at different temperature ( $T$ ). Consumer dispersal rates  $d_p = 0.01d_n$ . For (a), (d), (g)  $T = 10^\circ C$ ; (b), (e), (h)  $T = 20^\circ C$ ; (c), (f), (i)  $T = 29^\circ C$ , in two distinct patches. (a)-(c) correspond to the dynamics for CD where  $x_{\alpha\beta} = 0$ . Intraspecific (dots) and interspecific (triangles) DD in resource and consumer follow the dynamics depicted in (d)-(f) and (g)-(i), respectively. . . . . 79

- 5.10 Thermal sensitivity of species half-saturation constant ( $N_0$ ) and carrying capacity ( $K$ ): Two-parameter bifurcation diagram in the (a)  $T - N_0$  plane, and (b)  $T - K$  plane. Shaded regions: [A] corresponds to the region where species abundance shows oscillatory behavior. [B] determines the region where the system exhibits steady state dynamics, and [C] is the region where stability fails and consumers become extinct.  $HB$ , and  $TB$  represent the Hopf bifurcation and the transcritical bifurcation, respectively. . . . . 80
- 5.11 Interplay of coherence and incoherence in population abundance at  $T = 10^\circ C$ : (a) Spatiotemporal plot of consumer  $P_i$ , (b) snapshot of  $P_i$  at  $t = 9500$  (red (dotted) lines are for visual guidance), and (c) mean phase velocity ( $w_i$ ), for  $n = 100$  patches. Coupling strength  $d_n = 10^{-6}$  and  $d_p = 10^{-4}$ . . . . . 81
- 5.12 Interplay of coherence and incoherence in population abundance at  $T = 20^\circ C$ : (a) Spatiotemporal plot of consumer  $P_i$ , (b) snapshot of  $P_i$  at  $t = 9500$  (red(dotted) lines are for visual guidance), and (c) mean phase velocity ( $w_i$ ), for  $n = 100$  patches. Coupling strength  $d_n = 10^{-6}$  and  $d_p = 10^{-4}$ . . . . . 82
- 5.13 Global synchronized oscillations at  $T = 29^\circ C$ : (a) Spatiotemporal plot of consumer  $P_i$ , (b) snapshot of  $P_i$  at  $t = 9500$  (red(dotted) lines are for visual guidance), and (c) mean phase velocity ( $w_i$ ), for  $n = 100$  patches. Coupling strength  $d_n = 10^{-6}$  and  $d_p = 10^{-4}$ . . . . . 82
- 6.1 Thermal dependence of dispersal of spatially separated species. At extreme temperatures (either very low or high) species are less likely to disperse. . . . . 87
- 6.2 Time series of predator species, predator amplitude, and cumulative distributions of predator amplitude along the thermal gradient  $T$ : for (a), (f), (k)  $T = 0^\circ C$ ; (b), (g), (l)  $T = 5^\circ C$ ; (c), (h), (m)  $T = 10^\circ C$ ; (d), (i), (n)  $T = 15^\circ C$ ; and (e), (j), (o)  $T = 20^\circ C$ . Local dynamics are governed by  $\theta = 0.3$ ,  $\eta = 1$  and  $\phi = 3$ . Dispersal strengths are:  $\epsilon_h = 2^{-5}$  and  $\epsilon_p = 2^{-6}$ .  $k$  denotes clusters count at different values of  $T$ . . . . . 89

- 6.3 Frequency of cluster states for different values of  $T$ : (a)  $T = 0^\circ\text{C}$ , (b)  $T = 5^\circ\text{C}$ , (c)  $T = 10^\circ\text{C}$ , (d)  $T = 15^\circ\text{C}$ , and (e)  $T = 20^\circ\text{C}$ . The system converges to high or low number of clusters depending upon the temperature. The number of clusters decreases with the increasing temperature. Local dynamics are governed by  $\theta = 0.3$ ,  $\eta = 1$  and  $\phi = 3$ . Dispersal strengths are:  $\epsilon_h = 2^{-5}$  and  $\epsilon_p = 2^{-6}$ . Each panel is the result of 100 independent simulations. . . . . 92
- 6.4 Synchrony measure  $\sigma$  with changing  $T$ . The triangles represent the estimated value of  $\sigma$  at different values of  $T$ . The solid line is the best curve fit to the estimations. The other parameters are  $\epsilon_h = 2^{-10}$ ,  $\epsilon_p = 2^{-10}$ ,  $\phi = 2$ ,  $\eta = 1$ , and  $\theta = 0.3$ . . . . . 93
- 6.5 Median predator amplitude and transient duration. (a) Median predator amplitude for the transient (red) and asymptotic (blue) solution values of  $T$ . (b) The mean fraction of the total time duration the system remains in the transient solutions concerning temperature  $T$ . Parameter values are:  $\theta = 0.3$ ,  $\eta = 1$ ,  $\phi = 3$ ,  $\epsilon_h = 2^{-5}$ , and  $\epsilon_p = 2^{-6}$ . 94
- 6.6 Time series (left panels) and cross wavelet spectra (right panels) of the predator  $p_i$ . For two distinct temperatures: (a)-(c)  $T = 0^\circ\text{C}$  and (f)-(h)  $T = 20^\circ\text{C}$ , are the time series of predator density  $p_i$ , where  $i = 1, 3, 16$  is the patch index, in three distinct patches. (d), (i) Cross-wavelet spectra of the predator in two nearest patches  $p_1$  and  $p_3$ . (e), (j) Cross-wavelet spectra of the predator in two farthest patches  $p_1$  and  $p_{16}$ . At  $T = 0^\circ\text{C}$ , in case of nearest patches ((a), (b); (d)) the predator species oscillates in phase angle of  $\approx 30^\circ$ ; for the farthest patches ((b), (c); (e)) interactions lead to different phase angles ( $\approx 90^\circ$ ). At  $T = 20^\circ\text{C}$ , species, in the nearest patches oscillate in phase i.e  $0^\circ$  ((f), (g); (i)); in case of farthest patches ((g), (h); (j)) predator species show a phase drift of  $\approx 45^\circ$ . The black contour in cross-wavelet spectra encloses a significant region (95% confidence level) of consideration. The color code follows a pattern from blue to yellow; the blue color indicates the region with low power whereas the yellow region is with high power. Other parameter values are:  $n = 33$ ,  $\theta = 0.3$ ,  $\eta = 1$ ,  $\phi = 3$ ,  $\epsilon_h = 2^{-5}$ , and  $\epsilon_p = 2^{-6}$ . . . . . 95



# List of Tables

---

5.1	Species collective dynamics in two patch system for low to intermediate values of $d_n$ . For large $d_n$ values system dynamics synchronize completely ( $r_{ij} = 1$ ). . . . .	72
-----	---	----



# Chapter 1

## Introduction

---

Biological systems show complex patterns of species distribution in both space and time. Synthesizing the relationship between connectivity, diversity, and stability of communities is one of the goals of ecology. Over the years, several theoretical and empirical investigations have highlighted the potential role of space in exhibiting unexpected and intriguing dynamics ([Gause, 1935](#); [Huffaker, 1958](#)). [Hastings \(1992\)](#) considering a discrete time and space model showed that an equilibrium that would remain stable without diffusion could become unstable, forming stationary patterns, cyclic behaviors, or even chaotic dynamics. Yet another aspect that introduces new levels of uncertainty in spatial populations is the presence of multiple coexisting attractors ([Sole et al, 1992](#); [Hastings, 1993](#); [Guttal and Jayaprakash, 2009](#); [Pal et al, 2022](#)). A system with the same parameter values but different initial conditions evolves toward different dynamics, which can result in the coexistence of multiple attractors.

The influence of spatial structure on ecological processes can be understood in a metapopulation and landscape ecology ([Hanski and Gilpin, 1991](#); [Moilanen and Hanski, 2001](#)). Many species' populations are composed of spatially separated sub-populations rather than being continuously distributed. Dispersal plays the primary role in connecting multiple sub-populations, forming a metapopulation. The metapopulation approach has a long history ([Levins, 1969](#)) that focused on highly fragmented habitats known to affect the colonization and extinction of species, and understanding the influence of dispersal on population dynamics is a central concern in ecology. In this context, two well-established effects of dispersal are spatial synchrony, which involves positively correlated population dynamics across different spatial locations, and dispersal-induced stability, a phenomenon where populations exhibit less extinction-prone dynamics when they are connected by dispersal compared to when they are isolated ([Abbott, 2011](#)). The field of landscape ecology is motivated by a “need to understand the development and dynamics of pattern in ecological phenomena, the role of disturbance in ecosystems, and characteristic spatial and temporal scales of ecological events” ([Urban et al, 1987](#)). It emphasizes “broad spatial scales and the ecological effects of the spatial patterning of ecosystems” ([Turner, 1989](#)) and “deals with the effects of the spatial configuration of mosaics on a wide variety of ecological phenomena” ([Wiens et al, 1993](#)). Thus,

landscape ecology focuses on the ecological dynamics influenced by patch shape and quality of habitat matrix ([Hanski, 1998](#)).

At the heart of spatial ecology lies a central challenge: unraveling the impact of spatial factors on the dynamics of populations and the composition and structure of ecological communities. Mathematical modeling is an essential tool in this quest ([Goldwasser et al, 1994](#); [Molofsky, 1994](#); [Tilman et al, 1997](#)), as it plays a crucial role in studying population dynamics, conservation biology, and a wide range of spatial ecological phenomena. Mathematical models facilitate a deeper understanding of how spatial factors influence population growth, distribution, and persistence in heterogeneous landscapes.

We will now provide a brief overview of two modeling approaches employed in this thesis and underscore their significance in the context of conservation.

### 1.0.1 Network models

The theory of complex networks played a pivotal role in describing and understanding complexity sciences ([Amaral et al, 2000](#); [Albert and Barabási, 2002](#); [Montoya et al, 2006](#)). The study of complex networks aims to model and understand diverse real-world systems ranging from technological networks to ecological webs. Emerging research has focused on the suitability of network theory to the study of spatial ecology ([Fortuna et al, 2006](#); [Rayfield et al, 2011](#); [Jacoby and Freeman, 2016](#)). Majorly, spatial ecological networks are built by graph-theoretic approaches by considering habitat patches as the nodes and species movement as the links connecting the nodes. This approach's significance is evident in phenomena like chaos arising from non-linear interactions among species and environmental factors, symmetry-breaking characterized by the emergence of new patterns in populations transitioning from a symmetrical state, synchronization revealing coordinated ecological processes, chimera illustrating the coexistence of synchronized and unsynchronized dynamics within a community, or critical transitions denoting abrupt and irreversible shifts in the state of an ecosystem ([Arenas et al, 2008](#); [Dakos and Bascompte, 2014](#); [Kobayashi, 2011](#)).

### 1.0.2 Cellular automata

Cellular automata have been widely used to model spatial processes in ecology ([Pascual et al, 2002](#); [Langmead and Sheppard, 2004](#)). A key feature of cellular automata is that the patches are identical cells on a regular grid. The dispersal is distance-dependent, and the transitions between states are governed by rules that may be deterministic or stochastic. The application of cellular automaton



models in ecology has facilitated examining the role of landscape structure on species persistence.

### 1.0.3 Spatial ecology and conservation

Connectivity between habitat patches has been recognized as an influential factor in determining species distributions ([With et al, 1997](#); [Hanski, 1998](#); [Tischendorf and Fahrig, 2000](#)). Habitat connectivity is defined as the degree to which the landscape facilitates or inhibits the movement of species within it ([Taylor et al, 1993](#); [Tischendorf and Fahrig, 2000](#)). It is an essential factor in determining a broad spectrum of ecological phenomena, including seed dispersal, range expansion, invasion, and biodiversity maintenance ([Moilanen and Nieminen, 2002](#); [Kareiva and Wennergren, 1995](#); [Moilanen et al, 2005](#); [WF, 2006](#)). Habitat loss and fragmentation constitute a significant threat to Earth's biological diversity. Habitat loss can increase the distance between the patches by reducing connectivity ([Hanski, 1998](#)). Fragmentation results in loss of area and increasing spatial isolation, thus escalating the extinction risk of species ([Fahrig, 2003](#)). Hence, there is a substantial need for research to understand the factors determining the persistence of populations and communities. Achieving this necessitates an exploration of species interactions, dispersal patterns of a metapopulation, environmental factors, landscape characteristics, and the role of stochasticity, which may all have a considerable impact on species viability.

Deterministic and stochastic mathematical models used in the applied aspects of ecology are tailored to address specific questions related to conservation, assessment, and restoration. [Bascompte and Solé \(1996\)](#) used spatially explicit metapopulation models to demonstrate the existence of extinction thresholds that occur when a certain fraction of habitat is destroyed. As shown by [Ovaskainen et al \(2008\)](#), a model parameterized using data from a reference landscape effectively predicted the movements of clouded Apollo butterflies within a landscape that differed significantly in structure. As highlighted by [Kareiva and Odell \(1987\)](#) and [Moorcroft and Lewis \(2013\)](#), one of the advantages of using mechanistic models is their potential to allow for making predictions about responses to habitat alterations and inquiring how parameters might evolve in both current and altered landscapes.

## 1.1 Stochasticity in nonlinear systems

Stochasticity, or noise, is prevalent in the real world and affects a system's dynamics. Various factors like external noise, inherent variability, or uncertainty in initial conditions or parameters can lead to the emergence of stochasticity ([Melbourne](#)

and Hastings, 2008). This randomness can lead to a wide range of behaviors, including the emergence of chaotic dynamics (Billings and Schwartz, 2002), the presence of bistability (Biancalani et al, 2014), modulation of transients (Hastings et al, 2021) and the unpredictability of system trajectories. Understanding and modeling stochasticity is crucial in analyzing uncertainty and variability within real-world systems. Another interesting phenomenon observed in natural systems is the excitability. A common characteristic of all the excitable systems is the unperturbed system stays in the rest state, and small perturbations result in a small amplitude motion around a steady state. At the same time, strong perturbations can evoke large amplitude fluctuations before relaxing to a rest state. So excitability is a dynamic phenomenon far from equilibrium (Haken, 1975).

There is rich literature on excitability in deterministic nonlinear systems with applications in different areas (Murray, 1993). However, the dynamics of excitable systems are significantly influenced by the presence of noise. Stochastically perturbed excitable systems result in the occurrence of sustained oscillations or resonance purely under the effect of noise (Sigeti and Horsthemke, 1989; Sieber et al, 2007; Schwabedal and Pikovsky, 2010), thus exhibiting stochastic limit cycles. The resonance effect is often accompanied by stochastic resonance (Benzi et al, 1981; Gammaitoni et al, 1998) or coherence resonance (Gang et al, 1993; Pikovsky and Kurths, 1997). *Coherence resonance* corresponds to the noise-sustained oscillations in the excitable regime, which are most coherent or regular at an optimal noise intensity. A driving force in the presence of noise can result in *stochastic resonance*. Therefore, the system's behavior is enhanced to a signal by adding noise.

In addition to intriguing temporal dynamics, a large array of coupled excitable oscillators provides a glimpse into the affluence of spatiotemporal behavior. The role of noise in extended excitable systems is observed in the context of noise-enhanced propagation (Lindner et al, 1998), noise-induced spiral waves (Gu et al, 2013), spiral chaos (García-Ojalvo and Schimansky-Geier, 1999), the occurrence of chimera states (Semenova et al, 2016; Khatun et al, 2022), noise-induced synchronization (Neiman et al, 1999; Kurrer and Schulten, 1995) as well as spatiotemporal stochastic resonance (Jung and Mayer-Kress, 1995), and array enhanced coherence resonance (Hu and Zhou, 2000).

### 1.1.1 Noise in ecology

Fluctuations observed in species abundances are the result of intrinsic factor (demographic stochasticity) or extrinsic factor (environmental stochasticity) (Higgins et al, 1997; Lundberg et al, 2000). Stochasticity is often believed to obscure the deterministic patterns (Knape and de Valpine, 2012). However, extensive

research on stochastic ecological systems has revealed that noise can lead to many novel phenomena. The potential effect of noise in sustaining *hare-lynx* cycle was analyzed by Beninca et al (2011). The work by Stenseth et al (1996) showed that environmental stochasticity ensued oscillations. Stochasticity can even allow the coexistence of species in the scenario where one of them potentially becomes extinct in the deterministic framework (Chesson and Ellner, 1989).

Further, alternative stable states in ecological communities have been a dominant framework for decades (Lewontin, 1969). Ecologists envisage that strong fluctuations in population densities or changing the parameters determining the population's behavior could shift the communities from one state to another. Thus, stochastic switching between two regimes is a generic phenomenon due to stochasticity and alternative stable states interplay. The work by D'Odorico et al (2005) on the dryland plant model showed that noise could enhance stability by forming an intermediate statistically stable state between the two alternative stable states. Noise can even reduce the deterministic symmetry by inducing bistability in situations where only one stable branch is present without fluctuations, thus exhibiting noise-induced symmetry breaking (NISB) (Kobayashi, 2011). However, there is limited research on NISB, and so far, its ecological aspect still requires considerable attention.

## 1.2 Network topology and ecosystems dynamics

The dispersal network of a metapopulation governs the species' colonization routes between habitat patches. Therefore, the connectivity of a network is determined by the dispersal linking the patches. Over the years, considerable attention has been given to uncovering the effects of dispersal network structure on the ecological dynamics (Fahrig and Merriam, 1985; Holland and Hastings, 2008). The rationale behind the spatial structure being widely recognized in population biology is the belief that spatial ecological interactions influence populations as much as predation, competition, birth, and death rates. The network of interconnected communities, facilitated by the dispersal of species, is collectively termed a metacommunity. The maintenance of biodiversity and ecosystem functionality is possible by the ability of the species to move across habitat patches. Therefore, studying the degree distribution of patches (nodes of a network) that correspond to the dispersal route is crucial in determining species persistence. Below, we have outlined some fundamental network properties (Newman, 2018) that are essential for comprehending the results presented in this thesis:

**Degree of a node:** It is the number of links ( $k$ ) or neighbors connected to the

node.

**Degree distribution:** The degree distribution ( $p(k)$ ) is defined as the probability that any randomly chosen node has degree  $k$ .

**Clustering coefficient ( $C_i$ ):** It measures the connectivity between the neighborhood of node  $i$ .  $C_i = 0$  if there are no interconnections present, whereas,  $C_i = 1$  if all neighbors of the  $i$ -th node are connected.

### 1.2.1 An overview of the influence of the number of nodes and interaction strength

The complexity of a network largely influences the ecological processes. Below, we illustrate the role of node number and coupling strength on the collective dynamics of an ecological network composed with a tri-trophic foodweb model, namely, the Blasius-Huppert-Stone model (Blasius et al, 1999). The following equations govern the dynamics of the ecological network:

$$\frac{dx_i}{dt} = ax_i - \beta_1 \frac{x_i y_i}{1 + k_1 x_i}, \quad (1.1a)$$

$$\frac{dy_i}{dt} = \beta_1 \frac{x_i y_i}{1 + k_1 x_i} - \beta_2 y_i z_i - dy_i + \epsilon \sum_{j=1}^n (y_j - y_i), \quad (1.1b)$$

$$\frac{dz_i}{dt} = \beta_2 y_i z_i - c(z_i - z^*) + \epsilon \sum_{j=1}^n (z_j - z_i), \quad (1.1c)$$

where  $n$  is the number of interacting nodes and  $\epsilon$  is the interaction strength between the nodes.  $x_i$ ,  $y_i$ , and  $z_i$  represent vegetation, herbivore, and predator populations, respectively, in the  $i$ -th patch. We take fixed values for the parameters  $a, \beta_1, k_1, \beta_2, d, c$ , and  $z^*$ , which regulate the local dynamics. The system exhibits chaos for  $\epsilon = 0$  and a specific range of parameter values, and the corresponding attractor is depicted in Fig. 1.1(a). In the absence of dispersal ( $\epsilon = 0$ ) and for  $n = 2$ , the uncoupled populations remain unsynchronized both in phase and amplitude as is seen in the time series of predator populations (Fig. 1.1(b)). In contrast, for  $\epsilon = 0.03$ , the two patches show phase locking, i.e., the populations are synchronized in phase but not in amplitude (Fig. 1.1(c)), which with further increase in the coupling strength ( $\epsilon = 0.075$ ) exhibit complete synchrony (Fig. 1.1(d)). However, as observed from Fig. 1.1(e), increasing the network size to  $n = 10$  induces full synchronization even in a weak coupling limit ( $\epsilon = 0.03$ ).

### 1.2.2 Random pairwise interactions

Random connections allow long-distance interactions between patches (Watts and Strogatz, 1998). The work by Holland and Hastings (2008) shows that randomizing

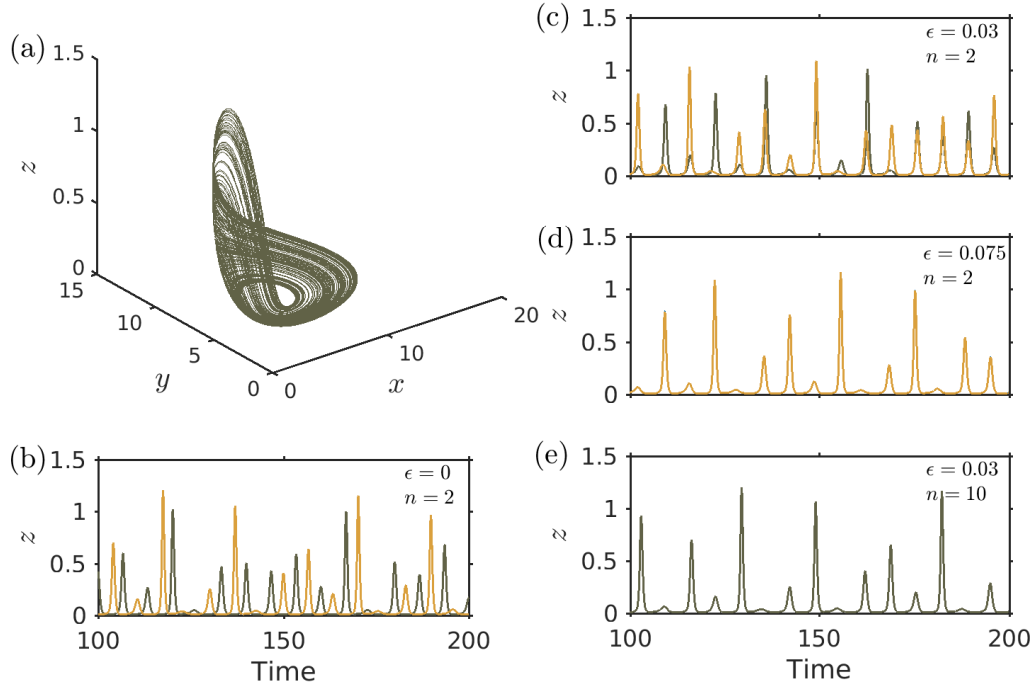


**Figure 1.1.** Phase portrait and time series of the model (1.1a). (a) Phase portrait depicting a chaotic trajectory. (b)-(e) Time series exhibiting synchronous or asynchronous behavior of populations depending upon the network size ( $n$ ) and the interaction strength ( $\epsilon$ ): (b)  $n = 2$ ,  $\epsilon = 0$ : asynchrony, (c)  $n = 2$ ,  $\epsilon = 0.03$ : phase synchrony, (d)  $n = 2$ ,  $\epsilon = 0.075$ : phase and amplitude synchrony, and (e)  $n = 10$ ,  $\epsilon = 0.03$ : phase and amplitude synchrony. Other model parameters are  $a = 1$ ,  $d = 1$ ,  $c = 10$ ,  $\beta_1 = 0.2$ ,  $\beta_2 = 1$ ,  $k_1 = 0.05$ , and  $z^* = 0.006$ .

the structure of dispersal networks tends to favour asynchrony. [Gilarranz and Bascompte \(2012\)](#) investigated the impact of network heterogeneity on regional abundance under the influence of demographic patterns. The study observed that uniform or random networks exhibit the lowest regional abundances, while scale-free networks demonstrate the highest abundance. The following random network topologies broadly capture real interaction patterns in higher dimensional systems: the Watts-Strogatz (WS) model, the Erdős-Rényi (ER) model, and the Barabási-Albert (BA) model ([Bhandary et al, 2022](#)). For the WS network, the interactions between the nodes with regular links are replaced by the random ones depending upon the rewiring probability  $p$ . For instance, when  $p = 0$ , the network is regular. Increasing the likelihood  $p$  from 0 to 1 transits a network from order to completely random, and the WS network is small-world when the value of  $p$  lies in between 0 and 1 ([Watts and Strogatz, 1998](#)). The BA model follows power-law distribution and generates scale-free networks, whereas the ER model develops random networks and follows the Poisson distribution. The response of ecological communities towards varying network structures can help determine population dynamics and needs more attention.

### 1.2.3 Higher-order interactions

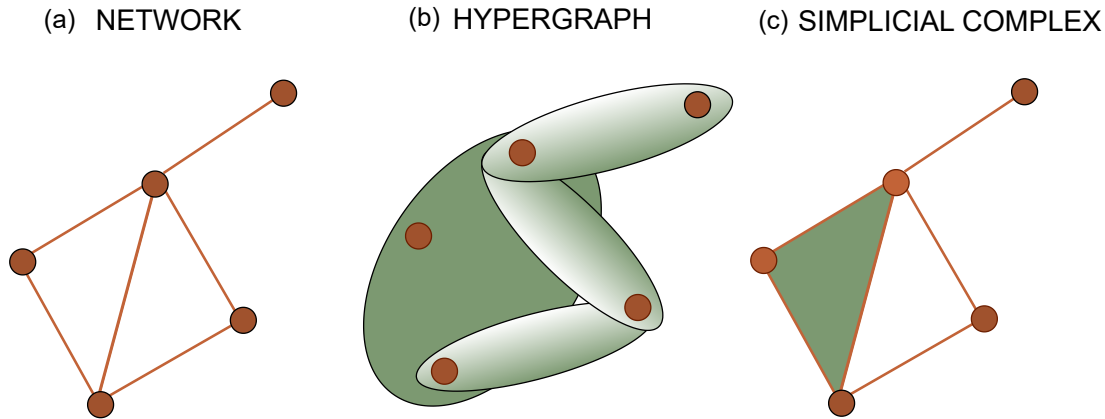


**Figure 1.2.** A system with interacting units represented as (a) a network, where the interactions occur pairwise between nodes and depicted as edges, (b) hypergraph, which facilitates group interactions. In this context, shaded groups of nodes represent hyperedges, (c) simplicial complex, edges correspond to 1-simplices, and full triangles representing 2-simplices are shown in green.

Over the decades, the architecture of complex systems has been modeled by networks where the nodes and the links encode pairwise interactions. This limitation of networks does not provide a significant description at the system level. Yet, interactions often occur in larger groups from human to ecological systems and cannot be described by dyadic couplings (Battiston et al, 2020). The work by Bairey et al (2016) shows that communities with greater diversity become more stable under higher-order interactions. Levine et al (2017) analyzed that incorporating higher-order interactions leads to species coexistence in competitive networks. Higher-order interactions play a stabilizing role in the dynamics of ecological communities, where the interactions between species are influenced by the presence of other species (Grilli et al, 2017). Other examples include neuronal (Schneidman et al, 2003), genetic systems (Ritz et al, 2014), and group interactions in social networks (Sekara et al, 2016). In complex systems, such interactions are often modeled using *hypergraphs* and *simplicial complexes* (Battiston et al, 2020). A simplicial complex is a particular type of hypergraph (Berge, 1973), where 1-simplex is a link, 2-simplex is a two-dimensional object made of three nodes, 3-simplex corresponds to four-node interaction and so on. A rich literature has shown the substantial impact of higher-order interactions on the dynamics of the networked systems, from synchronization (Millán et al, 2019) and diffusion (Carletti et al, 2020) to explosive transitions (Kuehn and Bick, 2021) and evolution (Alvarez-Rodriguez et al, 2021). Despite recognizing the fundamental importance of moving beyond dyadic couplings, there is still a substantial gap in our exploration of how many-body

interactions within ecological systems can reveal a new panorama of dynamical processes.

## 1.3 Landscape structure

Human activity often results in habitat fragmentation, which is one of the primary reasons for the changes in patterns of diversity and spatial distribution (Pereira et al, 2010; Rands et al, 2010). The number, size, shape, and position of patches within a landscape compose a landscape structure. Ecologists propose that these attributes of landscape structure are essential in determining the movement of animals between the habitats in a patchy landscape. Diffendorfer et al (1995) studied the effect of patch size on the movement of three mammal species. The authors predicted that animals would move farther in a more fragmented landscape to find resources. They found that two of the three species supported the hypothesis. Hanski et al (1994) found that the size and isolation of patches significantly affect the density of butterfly populations. Their analysis showed that the population size increased with the patch area. Therefore, the movement and the characteristics of populations are considerably affected by landscape structure.

### 1.3.1 Foraging theory

Mounting evidence suggests that the ability of organisms to move between spatially separated patches is a crucial factor in driving species dynamics in a fragmented landscape (Levins, 1969; Armsworth and Roughgarden, 2005; Niebuhr et al, 2015). Moreover, studies have shown that animals adjust their searching behavior following the availability of food resources (Benhamou and Bovet, 1989; Newlands et al, 2004; Nolet and Mooij, 2002; Bell, 2012). A general theory of foraging in ecology is that animals in areas of high resource abundance displace less, thereby increasing the usage of resources (Focardi et al, 1996; Turchin, 1991; Kareiva and Odell, 1987). Whereas, when the density of resources is less, the faster movements resulting in a large displacement increase the chance of food capture and thus are more efficient than the ones with high tortuosity (Turchin, 1991; Zollner and Lima, 1999; Bartumeus et al, 2005). Turchin (1998); Lima and Zollner (1996) consider that realistic animal movements comprise discrete series of displacement events separated by turning angles. Discretization of movement behavior determines the statistical distribution of displacement or step lengths and change of direction (i.e., turning angles). Such discretized movement paths can be examined through the techniques of random walk theory.



### 1.3.2 Random walk

The foraging path of an animal is effectively a random walk because the next move is based on the current location/state and the transition probability to the following location. A random walk is a stochastic process in which organisms move along random trajectories. Search strategies are one of the most prominent factors affecting the chances of an encounter. Lévy walk is a specific form of random walk composed of clusters of short steps with long travels between them (Viswanathan et al, 2011). It was Shlesinger and Klafter (1986) who first proposed that Lévy walks could be observed in animal search strategies. Further, various studies have reported Lévy walk searches in many animals for instance moths (*Agrotis segetum*) (Reynolds et al, 2007a), honeybees (*Apis mellifera*) (Reynolds et al, 2007b), and marine fish (Sims et al, 2008). Lévy walks are scale-free movements with uniform distribution for turning angles and power-law distribution  $P(l) \propto l^{-\beta}$  of step length ( $l$ ) with  $1 < \beta \leq 3$ . The parameter  $\beta$  describes the range of movement behaviors. For  $\beta \geq 3$ , the random walk is similar to Brownian motion. For  $1 < \beta < 3$ , the movement becomes super-diffusive (Lévy) and reaching to straight-line paths (ballistic motion) as  $\beta \rightarrow 1$ . Research suggests that Lévy walks optimize search strategies when resources are sparse and distributed in fragmented landscapes (Viswanathan et al, 2011; Bartumeus and Catalan, 2009). In a recent paper (Dannemann et al, 2018), the authors study the dynamics of population in the presence of foragers for different amounts of habitat availability. The work by Shlesinger and Klafter (1986); Dannemann et al (2018) employing analytical and simulated results shows that random walk significantly impacts the stability of metapopulations. The work suggests that Lévy walks optimize search in scarce environments, whereas Niebuhr et al (2015) observed straighter paths (Ballistic) as the optimal movement strategy in all situations.

### 1.3.3 Resource pulse

Another factor that profoundly affects population dynamics and communities is the temporal environmental variations (Mysterud et al, 2001; Schmidt and Ostfeld, 2003). Temporal variation in resource availability to a species can occur in the form of a resource pulse. Resource pulses are episodes of considerable magnitude, short-duration events of increased resource availability (Yang et al, 2008), that are prevalent in nature (Ostfeld and Keesing, 2000; Yang et al, 2008). Large fluctuations in resources can significantly vary the growth and reproduction of species (Ergon et al, 2001), which, in turn, also impacts the consumers of these species as they experience a pulse in the availability of resources. This correlation



between the resource pulse and consumer abundance can drastically alter the community dynamics (Yang et al, 2008). Witman et al (2003) studied the effect of massive sub-tidal prey recruitment on the community. The authors observed that this episodic increase in resources boosted consumer's abundance. However, at a later stage, this eliminated resources over large regions, which then triggered cannibalism in consumer species. Sommer et al (2002) reports the coexistence of competing phytoplankton through chemostat experiments. The episodic resource pulse was provided by diluting the medium at different intervals, facilitating the coexistence. Moreover, according to various studies, the interplay between resource pulse and dispersal can result in intriguing dynamics. The work by Keitt et al (2001) shows that the interplay of resource pulses and the Allee effect could expand species' distribution. In general, recurrent resource pulses can significantly and persistently impact communities.

Therefore, it is essential to examine how natural communities in fragmented landscapes, utilizing optimal foraging strategies, respond to these events. These responses have a direct impact on the diversity and stability of the ecosystem.

## 1.4 Role of species dispersal in population dynamics

Natural populations, functioning as complex nonlinear systems, often exhibit oscillatory dynamics. Amongst the emergent collective dynamics, synchronization is pervasive in a network of coupled oscillatory systems (Strogatz, 2004). Synchronization between populations with fluctuating abundances can be attributed to several factors, which include dispersal between populations, the Moran effect, and trophic interactions (Liebhold et al, 2004). Species dispersal can have conflicting consequences on population persistence. Asynchrony between the abundance of sub-populations leads toward regional stability (Briggs and Hoopes, 2004). Dispersal promotes stability by allowing recolonization, but it can sometimes elevate the chance of extinction by globally synchronizing populations. Dispersal, being sensitive to changing climatic conditions (Travis et al, 2013), patch size (Andreassen and Ims, 2001), food availability, population size (Matthysen, 2005), considerably varies within organisms. The partial synchronization patterns, such as the chimera state, are a fascinating effect gaining much attention. Chimera states correspond to a distinctive spatiotemporal pattern in which identical oscillators self-organize into coherent and incoherent co-existing domains. Several theoretical and experimental studies substantiate the existence of chimera in diverse fields of science and engineering (Hagerstrom et al, 2012; Zakharova et al, 2014). Therefore, various

processes in a metacommunity whereby dispersal can inhibit or promote synchrony should be examined.

### 1.4.1 Temperature: an environmental stressor influencing species dispersal

The rising temperature is known to lower species abundance, triggering extinction. For instance, current estimates of biodiversity loss predict that climate warming might lead to 3% to 78% of species extinction (Thomas et al, 2004; Thuiller et al, 2004). Temperature influences species abundance and complex interactions with other species in a community (Connell, 1961; Harrington et al, 1999; Walther, 2007). It is also evident from previous studies that species' response towards changing environmental conditions is carried out by changes in phenology and distribution (Sparks and Carey, 1995; Dunn and Winkler, 1999; Cayan et al, 2001). Dispersal is expressed through the interaction of an organism with its environment; therefore, it is influenced by environmental effects (Clobert et al, 2012). Walther et al (2005); Parmesan (2006) suggest species will disperse to a suitable climate niche responding to changing temperature. Moreover, Kuussaari et al (2016) found an increase in dispersal rates with increasing temperature and population abundance of the *Clouded Apollo* butterfly. In contrast, a study by Jourdan et al (2019) on the crane fly *Tipula maxima* reveals the negative effect of rising temperatures on their dispersal abilities.

### 1.4.2 Density-dependent dispersal

Emigration and immigration dispersal rates strongly influence the population dynamics in a patch, thus altering regional persistence. The dispersal rate is often considered constant, but it may be condition-dependent. Specifically, it may rely on species density in the local community. Hence, density-dependent dispersal builds a direct interaction between population dynamics and dispersal, thus impacting a community at a local and regional scale. Various studies have investigated the effect of density-dependent dispersal on population dynamics (Jánosi and Scheuring, 1997; Travis et al, 1999; Poethke and Hovestadt, 2002). Local populations might build even from low densities because of the density-dependent dispersal, which could minimize the emigration loss. Whereas high dispersal at more densities may restrain populations from outbreaks (Denno et al, 1994; Dixon, 1969). Ims and Andreassen (2005) and Li et al (2005) have shown that dispersal patterns depending upon local abundance result in diminishing synchrony compared to density-independent dispersal. Hauzy et al (2010) considering a mathematical

model studied the role of constant and density-dependent dispersal on the stability of a metacommunity. They find that density-dependent dispersal, particularly interspecific density-dependent dispersal, always results in asynchronous fluctuations in population abundance. Hence, in biodiversity maintenance, it is imperative to develop a mechanistic understanding of how dispersal, mediated by temperature and population abundance, can either stabilize or destabilize population dynamics.

### 1.4.3 Dispersal distance

The cost of dispersal is directly related to the distance between the habitat patches (Haddad, 1999). Studies suggest that predation risk might increase owing to large distance (Yoder et al, 2004). Another prominent factor that plays a crucial role in deciding how far a species can disperse is the environment. An experimental study by Baker and Rao (2004) demonstrated that increasing dispersal distance decreases the survival probability of desert isopods because of dehydration.

Dispersal kernel refers to a probability density function to describe the distribution of dispersal. It is based on the belief that distance is the underlying factor in determining the connection probability between two patches; the more distance, the lower the probability. Comprehensive literature suggests that research on dispersal has seen a paradigm shift from Gaussian and exponential to fat-tailed dispersal kernels (Kot et al, 1996; Clark et al, 1999). Specifically, an inverse power-law function, a fat-tailed distribution, is widely used as a dispersal kernel (Gupta et al, 2017). This particular type of dispersal kernel is motivated by the fact that long-range interaction plays a crucial role in many physical and biological systems. For example, in the one-dimensional Ising spin model (Kuo and Wu, 2015) and spin-glass model (Kotliar et al, 1983a), interaction among the spins is governed by long-range interaction that obeys a distance-dependent power law. In neuronal systems, long-range interaction with a specific scaling has been found that controls the connectivity among the neurons (Szaro et al, 1987). Dispersal, under the influence of climate change, has an impact on species range shifts (Brooker et al, 2007), either resulting in long-distance dispersal (LDD) or short-distance dispersal (SDD). However, a model incorporating temperature in spatial population movement to study dispersal-induced dynamics needs to be explored.

## 1.5 Objectives and Scope

This thesis aims to illustrate the impact of noise, changes in interaction topology, the effect of landscape structure, and abiotic conditions on the dynamics of coupled ecological systems. This thesis also studies many-body interactions between

ecological entities and elucidates different moving patterns adopted by foragers, which have important implications in determining ecological stability. The literature review has revealed several knowledge gaps, and these gaps give rise to the following questions that we aim to address in this thesis:

- Can noise break symmetry in an ecological network even when the deterministic processes are symmetric? How do random network topologies affect the dynamics in the presence of noise?
- How do higher-order interactions affect synchronization in different connectivity structures?
- How does a foraging strategy and resource pulse impact population viability in a patchy landscape?
- How does the interplay of dispersal strategies and temperature alter dynamical processes in a metacommunity?
- How does temperature-dependent dispersal influence synchrony, and thereby, species' persistence in an ecological network?

Stochasticity or noise is ubiquitous in ecosystems. The persuasive role of noise on the dynamics of excitable systems is observed in many disciplines, including noise-induced oscillations, the phenomenon of coherence resonance, the occurrence of chimera states, and noise-enhanced synchronization in coupled excitable systems (Neiman et al, 1999). The maintenance of biodiversity and ecosystem functionality is possible by the ability of the species to move across habitat patches, which is primarily hindered by habitat destruction and fragmentation. The prominence of spatial structure and habitat connectivity has widely been accepted to promote species persistence. In this thesis, we consider a network of excitable consumer-resource systems and study the interplay of network structure and noise intensity on the system's dynamics.

While most of the studies in networks consider only pairwise interactions, higher-order interactions are evident in many physical, social, and ecological systems. Research suggests that non-pairwise interactions lead to collective synchronization of the nodes (Gambuzza et al, 2021; Kovalenko et al, 2021). Moreover, considerable attention has been given to the interplay between the network topology and its synchronizability, particularly in weighted, multilayer, small-world networks. It is found that changing the connectivity by randomizing the dispersal network lowers synchrony (Holland and Hastings, 2008). To investigate this in the presence of higher-order interactions, we emphasize synchronization, which corresponds to the emergent collective behavior of networked coupled oscillators.

We consider different connectivity structures in simplicial complexes and analyze when the higher-order interactions lead to the synchronization of populations.

Movement strategies are crucial in maintaining connectivity and increasing survival in a fragmented landscape. Previous work (Dannemann et al, 2018) suggests that Lévy walks optimize search in scarce environments, whereas Niebuhr et al (2015) observed straighter paths (Ballistic) as the optimal movement strategy in all situations. However, research suggests that an environmental variation in the form of resource pulses can have profound consequences on the dynamics of populations and communities. Taking this into account and considering the phenomena of resource pulse in our stochastic framework, we analyze the unified effects the foraging behavior and life-history traits of species have on the structure and dynamics of natural communities.

Climate disruptions have already caused complex consequences to the distribution of species worldwide. Species dispersal also critically influences the balance between extinction and recolonization in a metacommunity. Hence, species may need effective dispersal strategies to cope with the changing environmental conditions to ensure metacommunity persistence. Motivated by this, we consider temperature-dependent functional traits of interacting species to elucidate dispersal effects in stabilizing population dynamics under climate warming.

Furthermore, the realization that the changing climate strongly impacts spatial populations, communities, and whole ecosystems triggered a lot of interest in investigating the effects of temperature-influenced dispersal on metapopulations (Bestion et al, 2015). Range interaction in species dispersal is an essential factor that drives interesting spatial dynamics (Banerjee et al, 2016). This motivates our investigation into species persistence within a spatial ecological model where dispersal is modeled as a temperature-dependent function.

## 1.6 Outline of the Thesis

After briefly introducing various factors, namely abiotic conditions, noise, species interactions, and their effects on the network of ecological communities, we move to the research questions we have addressed in this thesis.

### 1.6.1 Noise-induced symmetry breaking in a network of excitable ecological systems

In **Chapter 2**, we consider an ecological network of excitable resource-consumer systems. The consumers in each patch are connected with other patches via a diffusive coupling, where the connectivity pattern varies from local to global. There

is an additive Gaussian white noise that affects consumer abundance. We find that the network can be driven out of the resting state, leading to different collective dynamics, including regimes of heterogeneous steady states and asynchronous oscillatory states mediated by noise intensity and network topology. For non-local coupling and adequately tuning the noise intensity, we achieve an oscillatory regime due to the resonance effect or a region of inhomogeneous steady states termed NISB. Further, by keeping the noise intensity fixed while changing the coupling range from local to global, we identify a transition from an oscillatory domain to a region HSS through NISB. We also consider the effect of local heterogeneity (induced by considering stochastic components in species birth and death processes) and regional heterogeneity (in terms of varying node connectivity and network structure) on ecological dynamics. Here, noise is added as an intrinsic source to the system, arising from random fluctuations in the birth and death processes, and the connection between habitat patches follows the WS, BA, or ER model. We find that a noise-driven system with high habitat connectance potentially manifests symmetry breaking in all the network structures. Our findings are essential for understanding the mechanisms responsible for upholding biodiversity and ecosystem stability.

### 1.6.2 Effect of higher-order interactions on the stability of ecological communities

In **Chapter 3**, we consider an ecological network of spatially separated patches subjected not only to pairwise interactions but also to three-body higher-order coupling. Each node consists of a chaotic three-species food chain. A two-body interaction or a simplex of dimension 1 corresponds to a link, whereas a three-body interaction or a 2 simplex is a collection of 3 nodes, forming a triangle in a network. We carry forward our work up to 3 body interactions and study the collective behavior of the system. We focus on the role of network structure in influencing synchronous dynamics. We report that the inclusion of HOI in the dispersal network structure of an ecological community composed of chaotic three-species systems strongly affects the collective dynamics. We show that HOI in a random network can suppress asynchrony but does not result in complete synchronization. However, increasing the higher-order coupling strength in the network with all-to-all coupling (regular network) drives the system from asynchrony to complete synchrony, thus affecting species persistence. The observed synchronous state is stable over a range of coupling strengths, calculated using the master stability function. Overall, our study suggests that including HOI in species dispersal network structure can alter well-known results of ecological communities with pairwise interactions and demands more investigation.

### 1.6.3 Resource pulses and foraging behavior shape spatial population dynamics

In **Chapter 4**, we develop a stochastic vegetation-grazer model in a two-dimensional fragmented landscape. The two-dimensional plane is considered a periodic lattice divided into  $N$  square lattice sites. A fraction of the lattice sites are the initial vegetation habitat. The vegetation can then reach a steady state following the contact process model. A fraction of vegetation abundance at the steady state is introduced as the number of initial grazers into the system. At every discrete time step, a grazer dies with a specific rate or disperses to a new site following Lévy movement, where the dispersal length is drawn from the power-law distribution. The Lévy index  $\beta$  describes the range of movement behaviors. For  $\beta \geq 3$ , the random walk is similar to Brownian motion. For  $1 < \beta < 3$ , the movement becomes super-diffusive (Lévy) and reaching to straight-line paths (ballistic motion) as  $\beta \rightarrow 1$ . In our model, we consider the growth of vegetation to be seasonal. The rejuvenation of vegetation takes place at regular time intervals through resource pulses. Our analysis shows that the optimal foraging strategy highly depends upon the survival conditions and the amount of resources. We find that Lévy walk is always an effective movement strategy. However, the optimal foraging behavior changes from Brownian to ballistic with the increase in grazers' mortality rate. Our results demonstrate that grazer movement and resource pulses significantly enhance population viability and biodiversity in fragmented landscapes.

### 1.6.4 Climate warming and dispersal strategies determine species persistence in a metacommunity

In **Chapter 5**, we consider a theoretical metacommunity model that includes resource-consumer populations inhabited in patches. For simplicity, we start with a 2-patch metacommunity, where each patch behaves homogeneously in terms of resource-consumer interactions and phenotypes. The model assumes temperature-dependent life-history traits of species, which affect the metacommunity dynamics at the regional scale. The population in each patch is connected by dispersal, and the dispersal propensity is considered constant, or it depends upon the species abundance of the natal patch. We find that at low and intermediate temperatures, different dispersal strategies synchronize or desynchronize the population dynamics depending on dispersal rates. However, high temperatures synchronize the population trailing constant dispersal, weakening the stabilizing dynamics. Furthermore, density-dependent dispersal strongly affects the stability of the metacommunity at high temperatures by increasing or decreasing

spatial synchrony depending on dispersal rates. In metacommunities with many patches, conditional upon temperature, species abundance exhibits the coexistence of synchronous and asynchronous oscillations, namely the chimera state. Our results show that rising temperature may destabilize the dynamics by synchronizing populations; however, some dispersal mechanisms might impede the adverse outcomes.

### 1.6.5 Long-range dispersal promotes species persistence in climate extremes

Most of the results illustrating the effect of climate change on species dispersal are based on experimental studies. At the same time, only a few studies considering mathematical frameworks have elucidated the interplay between dispersal and temperature. In **Chapter 6**, we consider a regular network where all the patches are connected and hence accessible by the dispersing species from any patch, but the dispersal density may vary depending upon the distance between the patches as well as the temperature of the habitat. In the network, every patch is connected to all the other patches via the dispersal strength, modulated by the distance between patches and the temperature-dependent power law function. We consider the hypothesis that dispersal is strongest at the optimal temperature. We carry out different measures to learn the coherence/incoherence in species dynamics characterized by their amplitude of fluctuations, density correlations, and transient dynamics. Furthermore, we use cross-wavelet analyses to understand the long-term dynamics of the system through transients. We find that long-range dispersal at extreme temperatures turns out to be beneficial for the species' persistence. Finally, in **Chapter 7**, we summarize the key findings of our work. We also discuss future research directions.



# Chapter 2

## Noise-induced symmetry breaking in a network of excitable ecological systems

---

### 2.1 Introduction

A principle finding in theoretical ecology suggests that even a simple population model can manifest a range of dynamical scenarios, from stable equilibria to cyclic oscillations, through to chaos (May, 1974). Oscillatory dynamics has a long history, as summarized in diverse fields (Benincà et al, 2015; Elton, 1924; Rohani et al, 1999). Elucidating various mechanisms behind these oscillations is a major challenge and has been of persistent interest in ecology (Turchin and Ellner, 2000). As discussed in (Kingsland and Kingsland, 1995), endogenous causes are the plausible explanation for the generation of population cycles. Another well-studied nonlinear phenomenon observed in dynamical systems is *excitability* (Meron, 1992; Olla, 2013). Excitable dynamics are observed in a wide range of natural systems, which under strong perturbations can evoke large-amplitude fluctuations, before relaxing to a rest state (Izhikevich, 2007). These large amplitude transient fluctuations can sometimes turn into sustained oscillations due to stochastic perturbations, often called noise-induced oscillations (Nesse et al, 2008; Beninca et al, 2011). Here, by considering an ecological network of excitable systems, we address the following questions: Do noise-induced oscillations always directly transit from a steady state? Can other intermediate collective dynamics exist while the system shifts from a steady state to noise-induced oscillations?

Stochasticity or noise is ubiquitous in ecosystems. In recent years, extensive research on stochastic ecological systems has found that noise can lead to many novel phenomena, from population cycles to coexistence (Moran, 1953; Stenseth et al, 1996). The persuasive role of noise on the dynamics of excitable systems is observed in many disciplines, including noise-induced oscillations (Hillenbrand, 2002; Nesse et al, 2008), phenomenon of coherence resonance (Buldú et al, 2001; Ganopolski and Rahmstorf, 2002), occurrence of chimera states (Semenova et al,

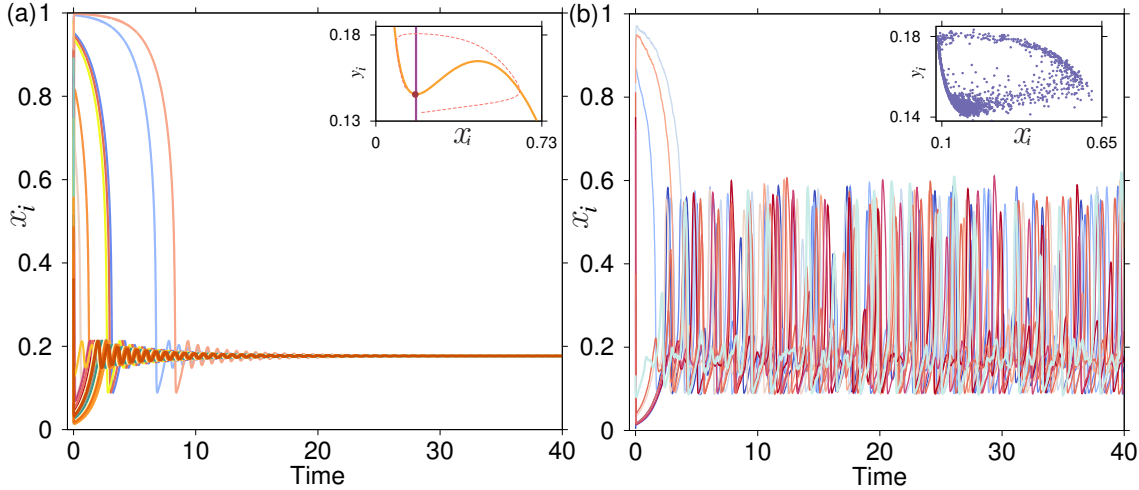


**Figure 2.1.** Time series of the resource population ( $x$ ) for the model (1.1a) with,  $\sigma = 0$  and  $a = 9$  (the system is in the excitable region): (a) For zero noise intensity ( $D = 0$ ) the system settles into a steady state; inset: nullclines of the resource ( $x$ ) and the consumer ( $y$ ). (b) For a non-zero noise intensity ( $D = 0.00005$ ) there exist noise-induced oscillations; inset: stochastic cyclic attractor. Other model parameters are:  $r = 1$ ,  $b = 7$ ,  $m = 1$ ,  $\epsilon = 0.01$ , and  $N = 101$ .

2016), and noise-enhanced synchronization in coupled excitable systems (Neiman et al, 1999; Boschi et al, 2001). An intriguing phenomenon that has received less attention is noise-induced symmetry breaking (NISB). NISB affirms reduced symmetric configuration (i.e. the perfect symmetry of the deterministic equilibrium state is disrupted) in the presence of noise, even though the underlying deterministic processes are symmetric, thus resulting in the occurrence of multiple stable states. There is limited research on NISB (Kobayashi, 2011; Jafarpour et al, 2017), and so far, its ecological facet remains to be studied.

Multiple stable solutions make it possible for populations in distinct patches/nodes to settle into different steady states. Therefore, minimizing the extinction risk and increasing the stability of spatial population through rescue effect (Amritkar and Rangarajan, 2006). The idea of spatial ecosystem functioning and species interactions go hand in hand. Spatially separated populations, which through dispersal may synchronize, are considered necessary to understand population cycles (Ranta et al, 1997). Researchers find that large systems of interacting oscillators have promising applications in various fluctuating systems (Izhikevich, 2007; Blasius et al, 1999). Further, species dispersal network structure is believed to influence the ecological dynamics strongly, as explored by recent studies (Holland and Hastings, 2008; Gupta et al, 2017). Following those lines of thought, here we report that an interplay of network structure and noise intensity results in a transition from homogeneous steady state to inhomogeneous steady states (multiple steady states) via NISB; before turning into noise-induced asynchronous oscillations. These results are explained numerically with the help of time series, spatiotemporal plots, and

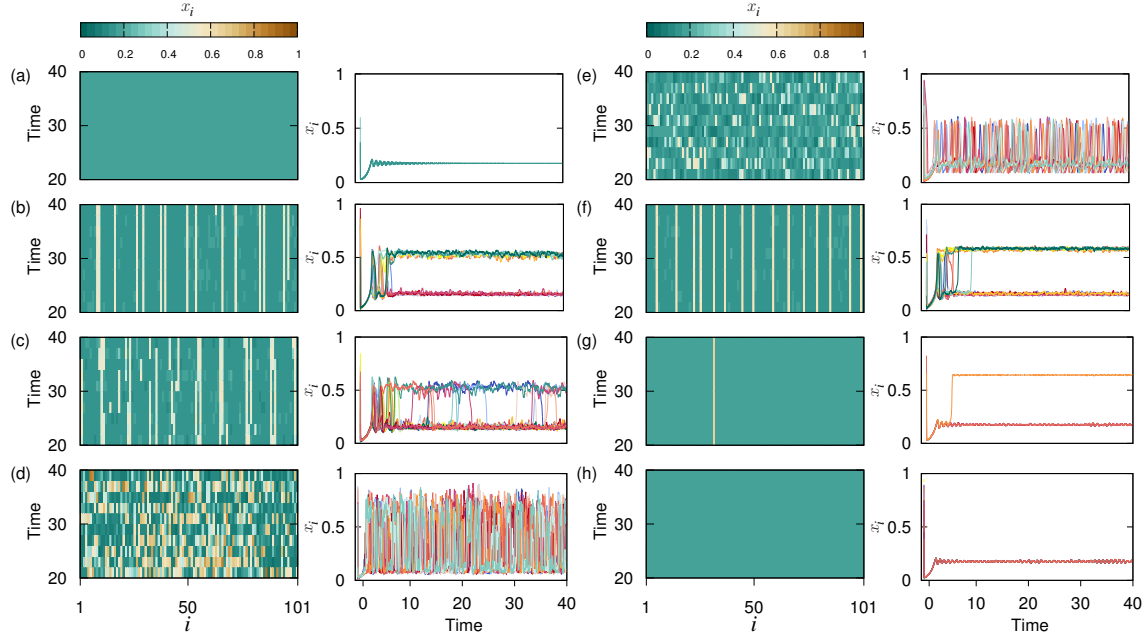


**Figure 2.2.** (a)-(d) Space-time (left column) and corresponding time series plots (right column) of resource  $x_i$  for  $P = 8$ ,  $\sigma = 0.1$  with varying noise intensities: (a)  $D = 0$ ; steady state, (b)  $D = 0.00001$ ; symmetry breaking, (c)  $D = 0.000033$ ; stochastic switching between two resource densities, and (d)  $D = 0.005$ ; asynchronous oscillations. (e)-(h) Space-time (left column) and corresponding time series (right column) plots for  $D = 0.00001$ ,  $\sigma = 0.6$  with varying coupling range  $s$ : (e)  $s = 0.01$  (local coupling); asynchronous oscillations, (f)  $s = 0.04$ ; symmetry breaking, (g)  $s = 0.25$ ; symmetry breaking with most nodes settling at the lower branch, and (h)  $s = 0.5$  (global coupling); steady state. Other model parameters are  $r = 1$ ,  $a = 9$ ,  $b = 7$ ,  $m = 1$ ,  $\epsilon = 0.01$ , and  $N = 101$ .

phase diagrams. Further, we show that the network model's linear stability analysis can help to explain the observed dynamics.

## 2.2 Model of an ecological network

We consider an ecological network with  $N$ -patches inhabiting resource-consumer (Truscott and Brindley, 1994) systems. The consumers in each patch are connected with other patches via a diffusive coupling, where the connectivity pattern varies from local to global. There is an additive Gaussian white noise  $\xi(t)$  that affects the consumer abundance. The network model, in the presence of stochastic perturbations, is given below:

$$\epsilon \frac{dx_i}{dt} = rx_i(1 - x_i) - \frac{a^2 x_i^2}{1 + b^2 x_i^2} y_i, \quad (2.1a)$$

$$\frac{dy_i}{dt} = \frac{a^2 x_i^2}{1 + b^2 x_i^2} y_i - m y_i + \frac{\sigma}{2P} \sum_{j=i-P}^{j=i+P} (y_j - y_i) + \sqrt{2D} \xi_i(t), \quad (2.1b)$$

where  $x_i$ , and  $y_i$ , respectively, determine resource and consumer abundance,  $i(= 1, 2, \dots, N)$  denotes the patch index (all indices are modulo  $N$ ). The parameter

$\epsilon > 0$  is responsible for a timescale separation between a fast resource population and a slow consumer population. The resource follows the logistic growth with an intrinsic growth rate  $r$ , and the interaction of resource and consumer is characterized by Holling's type-III grazing with parameters  $a$  and  $b$ .  $m$  is the natural mortality of the consumer. The parameter  $a$  describes the excitability threshold of the isolated system; in particular, it determines whether the system is in the excitable ( $a > 8.975$ ) or in the oscillatory ( $a \in [7.345, 8.975]$ ) regime. Excitability refers to a property of a system where a small perturbation can lead to a significant excursion in phase space before the system eventually returns to its equilibrium state. Here, we focus on the dynamics of the resource-consumer population in the excitable regime ( $a = 9$ ). The model assumes the movement of the consumer population between the patches, where the interaction is governed by the coupling strength  $\sigma$  and the parameter  $P$  controls the coupling range  $s = P/N$ , where  $1 \leq P \leq (N - 1)/2$  for an odd number of patches. Increasing the value of  $P$  from 1 to  $(N - 1)/2$  varies the network topology from local to global via non-local. Further,  $\xi_i(t) \in \mathbb{R}$  is the normalized Gaussian white noise that perturbs the consumer population in each  $i$ -th patch, i.e.,  $\langle \xi_i(t) \rangle = 0$  and  $\langle \xi_i(t) \xi_j(t') \rangle = \delta_{ij} \delta(t - t')$ ,  $\forall i, j$ , and  $D$  is the noise intensity. In the excitable region, the isolated system rests in a stable steady state in the absence of noise [see Fig. 2.1(a)]. Inducing stochastic perturbations beyond a threshold value of the noise amplitude drives the population to produce sustained oscillations, as seen in Fig. 2.1(b).

## 2.3 Results

The interplay of node dynamics, network topology, and noise introduced in the model (2.1a), gives rise to distinct dynamical regimes. We have numerically solved the stochastic model (2.1a) using the Euler-Maruyama method with integration step size  $10^{-3}$ , and initial conditions are randomly generated from the uniform distribution on the interval  $(0, 1)$ . Depending upon noise intensity  $D$ , we demonstrate four distinct space-time patterns for resource population in Fig. 2.2 (see Fig. 2.6 in the Appendix for the corresponding consumer dynamics). In the absence of noise ( $D = 0$ ) or for a low noise intensity, all the nodes rest in the steady state, thus giving a homogeneous steady state solution [Fig. 2.2(a)]. Now, in the presence of a weak noise strength, the system breaks into two sub-populations having two distinct noise-induced inhomogeneous steady states. The scenario is shown in Fig. 2.2(b) for  $D = 0.00001$ . The time series in the right panel of Fig. 2.2(b) shows two distinct branches of resource densities. Interestingly, the lower branch coincides with the deterministic steady state. However, the presence of noise gives birth to

an additional steady state, i.e., the upper branch. The spatiotemporal plot in the left panel of Fig. 2.2(b) depicts that the upper branch randomly appears in the background of the steady state of the lower branch. The presence of two steady states breaks the spatial symmetry of the system, and we get a new stationary state governed by noise-induced symmetry breaking. We find that the network exhibits stochastic switching between the two branches for an intermediate noise intensity. Fig. 2.2(c) demonstrates this scenario for  $D = 0.000033$ . For a large noise intensity ( $D = 0.005$ ), inhomogeneous steady states no longer exist; rather, stochastically spiking incoherent oscillations take place [see Fig. 2.2(d)].

Moreover, to provide an insight into the effects of network topology on the dynamics of the system, we fix the noise intensity  $D = 0.00001$ , coupling strength  $\sigma = 0.6$  and vary the connectivity from local ( $s = 0.01$ ) to global ( $s = 0.5$ ) via non-local ( $s = 0.03, s = 0.25$ ) coupling [see Figs. 2.2(e)-2.2(h)]. We find notable differences between dynamics with the changing network topology. Increasing the coupling range of the network not only reduces the number of solutions but also changes the dynamics from oscillatory to steady state. As observed from Fig. 2.2(e), local coupling favors oscillating populations with spatial incoherence, whereas increasing the coupling range shows a transition from oscillating populations [Fig. 2.2(e)] to inhomogeneous steady states [Figs. 2.2(f)-2.2(g)], through to homogeneous solutions [Fig. 2.2(h)]. Interestingly, in the presence of non-local coupling, as depicted in the space-time plot in Fig. 2.2(f), oscillators randomly rest at the lower or the upper branch; however, with the increasing network connectivity to global coupling, all the oscillators settle at the lower branch [Fig. 2.2(h)], which also incites towards homogeneous population densities. Thus, for a fixed noise intensity  $D$  and coupling strength  $\sigma$ , the network model (2.1a) experiences NISB while moving from global to local coupling.

The observed transition from oscillatory dynamics to inhomogeneous states impels us to investigate our system's qualitative behavior in these respective regimes. We analyze the features of the oscillatory region through phase portrait in Figs. 2.3(a)-2.3(b) for noise intensity  $D = 0.005$ . We observe that the density of phase points of stochastic limit cycle attractor for one oscillator [see Fig. 2.3(a)] and correspondingly for all the oscillators [see Fig. 2.3(b)] is larger around two population densities, i.e.,  $x_i = 0.1$  and  $x_i = 0.55$ . To further elaborate on the phenomenon of symmetry breaking observed in Fig. 2.2, we calculate the center of mass defined as (Zakharova et al, 2014):

$$x_{c.m.} = \frac{1}{T} \int_0^T x_i(t) dt, \quad (2.2)$$

where  $x_i$  is the resource density in each  $i$ -th patch, and  $T$  is taken sufficiently large. Resource population settles exactly into two branches as is characterized

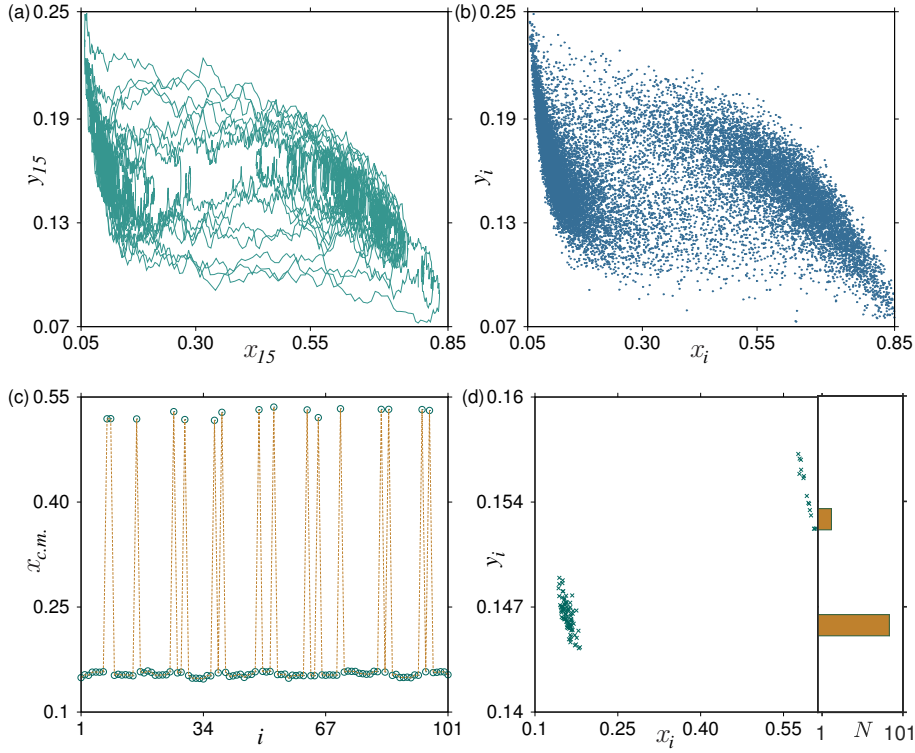


**Figure 2.3.** Phase portraits exhibiting the long stay of attractor in the two domains around  $x_i = 0.1$  and  $x_i = 0.55$  for (a) one oscillator (15th node), and (b) all the oscillators, at noise intensity  $D = 0.005$ . (c) Center of mass ( $x_{c.m.}$ ), and (d) phase portrait at a particular time along with density distribution of  $y_i$  corresponding to NISB for non-local coupling ( $P = 8$ ) at noise intensity  $D = 0.00001$ . The histogram in the right panel of (d) represents the number of oscillators in either of the two states. Other model parameters are  $r = 1$ ,  $a = 9$ ,  $b = 7$ ,  $m = 1$ ,  $\epsilon = 0.01$ ,  $\sigma = 0.1$ , and  $N = 101$ .

by two distinct values of center of mass [Fig. 2.3(c)], where for one part of the population  $x_{c.m.} \approx 0.15$  and for the other sub-population  $x_{c.m.}$  takes the value around 0.5, therefore exhibiting two nonuniform states. A relevant observation illustrated in the phase space [Fig. 2.3(d)] suggests an underlying mechanism for symmetry breaking, specifically NISB, clearly indicating the coexistence of two steady states in the network. We observe that wide distributions show up for two density values ( $\approx 0.15$  and  $\approx 0.5$ ), thus settling the system solely around these two states.

To gain a comprehensive view of the spatiotemporal dynamics in the network, we compute phase diagrams in the  $(s, D)$  and  $(s, \sigma)$  parameter planes [see Figs. 2.4(a) and 2.4(b), respectively]. Keeping the value of coupling strength  $\sigma$  fixed to 0.1, we vary  $s$  and  $D$  in Fig. 2.4(a). For stronger noise intensity  $D$ , in the entire range of  $s$ , the system resides in the asynchronous oscillatory regime. For weaker values of  $D$ , we observe either asynchronous oscillations or NISB, along with a region of stochastic switching, depending upon the coupling range  $s$ . NISB occurs for a certain threshold value of  $s > 0.07$ , i.e., when the coupling is non-local with around 8 nodes connected and persists up to  $s = 0.5$  (globally coupled). However, local coupling ( $s = 0.01$ ) and less connected nodes (up to 6) maintain the oscillatory

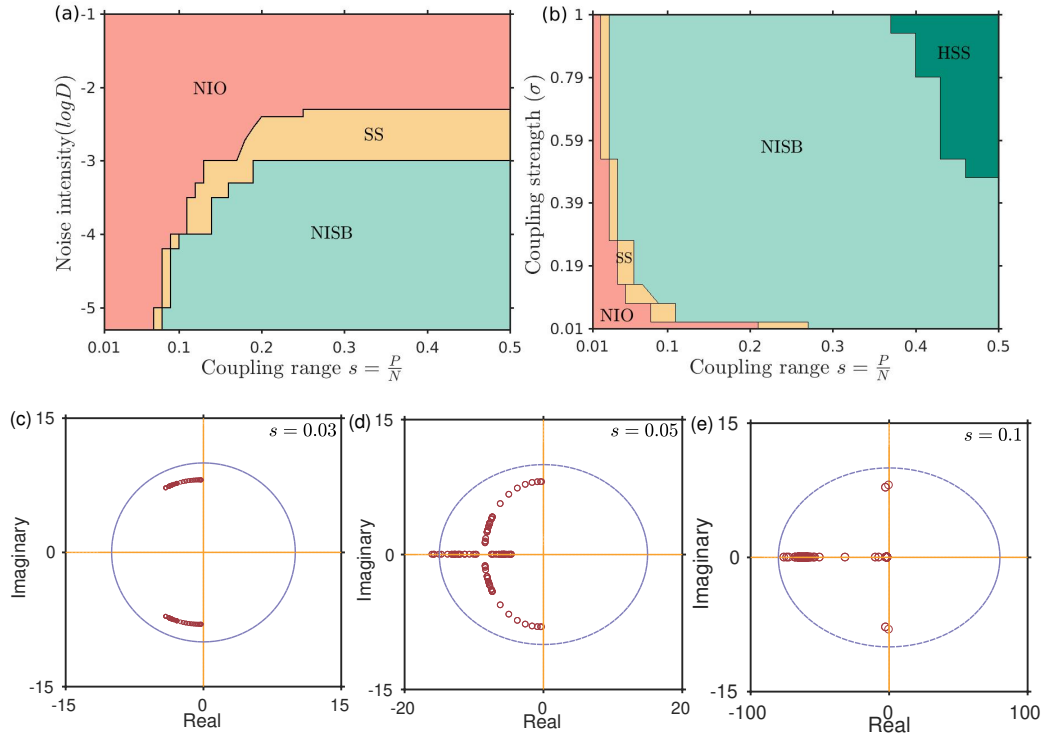


**Figure 2.4.** Phase diagrams in the (a)  $(s, D)$  plane for  $\sigma = 0.1$ , and (b)  $(s, \sigma)$  plane for  $D = 0.00001$ , where NIO: noise-induced oscillations, SS: Stochastic switching, NISB: noise-induced symmetry breaking, and HSS: Homogeneous steady state. (c)-(e) Distribution of the eigenvalues for different values of  $s$  for  $\sigma = 0.6$  and  $D = 0$ . Other model parameters are the same as in Fig. 2.2.

behavior. Moreover, a narrow zone of stochastic switching is observed between these two regimes. Oscillations in stochastic excitable systems are known to occur due to noisy perturbations (Hillenbrand, 2002). Noise-driven excitable systems possess noise-induced eigenfrequency and thus can exhibit stochastic oscillations. The work by Hidalgo et al (2012) describes the phenomenon of “stochastic amplification of fluctuations”. The mechanism is associated with the resonance amplification of some frequencies when the corresponding steady state equilibrium of the deterministic system has complex eigenvalues. Therefore, we infer that the transition from a steady state ( $D = 0$ ) to an oscillatory state or a region of SS ( $D \neq 0$ ) in our work is due to stochastic amplification of fluctuations. In Fig. 2.4(b), we explore the interplay of  $s$  and  $\sigma$ , with value of  $D$  being fixed to 0.00001. The oscillatory region observed for a large number of connected nodes  $s = 0.21$ , narrows down to  $s = 0.02$  with increasing coupling value  $\sigma$ , clearly determining the persisting oscillatory pattern for local coupling in the whole range of  $\sigma$ . Moreover, for a large value of  $\sigma$  ( $\approx 0.53$ ), a transition from oscillations to NISB via stochastic switching takes place for a lower coupling range. In contrast, with decreasing coupling strength, more connected nodes are required for the transition. In the direction of global coupling, beyond a threshold value of  $\sigma$ , the system traverses a synchronous steady state (HSS).



Our results can have significant implications for understanding the positive effects of noise on species diversity. Metapopulation is essential as it supports the persistence of many species under the events of local extinctions and re-colonization. Understanding the ecological effects of population cycles on ecosystem processes is also challenging. Studies ([Armstrong and McGehee, 1980](#); [Dutta et al, 2014, 2017](#)) suggest that cycles promote the coexistence of several consumers competing for shared resources. The work by [Eveleigh et al \(2007\)](#) shows that cyclic species can enhance biodiversity through the “bird-feeder effect”. Therefore, oscillatory dynamics may significantly contribute towards biodiversity maintenance ([Chesson, 2000](#)). Further, ecologists predict that large population fluctuations could shift communities from one state to another. The presence of alternative stable equilibria allows populations in different patches to settle in any stable states depending upon the initial conditions. Thus there is no spatial synchronization, which impedes extinction ([Amritkar and Rangarajan, 2006](#)) (local synchrony between a small number of patches may be possible, resulting in the formation of multi-cluster solutions).

The noise intensity  $D$  considered for our analysis is in the order of  $10^{-5}$  [see Fig. 2.2]. Thus, a careful investigation of the model (2.1a) in the deterministic limit can give an insight to explain the observed dynamics. Therefore, considering the deterministic framework, i.e.,  $D = 0$  in (2.1a), we carry the linear stability analysis. We calculate eigenvalues of the linearized system using the equilibrium points based upon the changing network topology ([Logofet, 2018](#)). Let  $(x^*, y^*) = (x_1^*, y_1^*, x_2^*, y_2^*, \dots, x_N^*, y_N^*)$  be a non-trivial equilibrium point of the system (2.1a) when  $D = 0$ . Linearization of the deterministic system in the neighborhood of the equilibrium point  $(x^*, y^*)$  yields the following block-structured matrix:

$$J = \begin{bmatrix} J_1(x_1^*, y_1^*) - \text{diag}\{0, 2P\} & \vdots & \text{diag}\{0, m_j\} & \vdots & \dots & \vdots & \text{diag}\{0, m_j\} \\ \text{diag}\{0, m_j\} & \vdots & J_2(x_2^*, y_2^*) - \text{diag}\{0, 2P\} & \vdots & \text{diag}\{0, m_j\} & \vdots & \dots \\ \vdots & \vdots & \vdots & \vdots & \vdots & \vdots & \vdots \\ \text{diag}\{0, m_j\} & \vdots & \text{diag}\{0, m_j\} & \vdots & \dots & \vdots & J_N(x_N^*, y_N^*) - \text{diag}\{0, 2P\} \end{bmatrix},$$

where  $J_i$  is the Jacobian of the isolated  $i$ -th patch at an equilibrium point  $(x_i^*, y_i^*)$  ( $i = 1, 2, \dots, N$ ) given as:

$$J_i = \begin{bmatrix} j_{11}^i & j_{12}^i \\ j_{21}^i & j_{22}^i \end{bmatrix},$$

with  $j_{11}^i = \frac{1}{\epsilon} - \frac{2x_i^*}{\epsilon} - \frac{1}{\epsilon} \frac{2a^2 x_i^* y_i^*}{1+b^2 x_i^{*2}}$ ,  $j_{12}^i = -\frac{1}{\epsilon} \frac{a^2 x_i^{*2}}{1+b^2 x_i^{*2}}$ ,  $j_{21}^i = \frac{2a^2 x_i^{*2} y_i^*}{(1+b^2 x_i^{*2})^2}$ , and  $j_{22}^i = \frac{a^2 x_i^{*2}}{1+b^2 x_i^{*2}} - 1$ . Further,  $m_j = 1$  if  $i$ -th and  $j$ -th nodes are connected, and  $m_j = 0$  otherwise.



The coupling strength  $\sigma = 0.6$  and noise intensity  $D = 0.00001$  manifest four distinct regimes based upon the value of  $s$ , as can be seen in Fig. 2.4(b). The transition from oscillatory dynamics to NISB via SS occurs for  $s = 0.05$ , further traversing HSS around  $s = 0.41$ . Here we intend to investigate whether the node dynamics and network structure determine the dominant pattern of NISB in the limiting value of  $D$  tending to 0. Figs. 2.4(c)- 2.4(e) show the distribution of eigenvalues with varying coupling range  $s$ . We observe complex conjugate eigenvalues ( $\lambda_i$ ) for  $s$  ranging from 0.01 to 0.04 as shown for  $s = 0.03$  in Fig. 2.4(c). It is ascertained from Fig. 2.4(c) that the fixed point obtained at  $D = 0$  for  $s = 0.03$  is a stable spiral since  $\text{Real}(\lambda_i) < 0 \forall i$ . However, as analyzed from Fig. 2.4(b) for the same coupling range ( $s = 0.03$ ), the presence of noise in the system results in the occurrence of oscillations or SS. A recent study (Hutt et al, 2016) demonstrated the impact of additive noise on networks, tuning their spectral properties. The work showed that increasing noise intensity could coerce the eigenvalues to cross the imaginary axis. The impact of noise on the eigenvalue spectrum that resulted in destabilizing the equilibrium point by crossing the imaginary axis, and hence the occurrence of Hopf bifurcation. Moving further to  $s = 0.05$ , we observe the emergence of a few real eigenvalues [see Fig. 2.4(d)], which also eventually tend towards 0 with increasing coupling range ( $s = 0.1$ ), as observed from Fig. 2.4(e). We also notice that the number of real eigenvalues increases in the passage of global coupling. Thus, we infer that the presence of noise in the network (2.1a) can lead the real eigenvalues to cross the origin, henceforth inducing NISB via a pitchfork bifurcation.

## 2.4 Conclusion

In conclusion, we have shown that an ecological network of identical excitable systems can be driven out of the resting state leading to different collective dynamics, including regimes of heterogeneous steady states and asynchronous oscillatory states, mediated by noise intensity and network topology. For non-local coupling and adequately tuning the noise intensity, we achieve an oscillatory regime due to the resonance effect (Beninca et al, 2011) or a region of inhomogeneous steady states (NISB). Further, by keeping the noise intensity fixed while changing the coupling range from local to global, we identify a transition from an oscillatory domain to a region HSS through NISB. While oscillatory and inhomogeneous steady states support the survival of species, the emergence of HSS during the transition to global coupling hinders biodiversity (Gupta et al, 2017). Our results are robust across a large region in the parameter space, as demonstrated via phase diagrams. Therefore, our findings could be important for understanding the mechanisms responsible for

upholding biodiversity and ecosystem stability. Finally, deriving the Fokker-Planck equation of stochastic ecological networks for the analytical tractability of the observed collective dynamics is an important future direction.

## 2.5 Appendix 1: Stochastic consumer dynamics

In each node of the network, we consider an ecological consumer-resource system whose dynamics are governed as:

$$\epsilon \frac{dx}{dt} = rx(1-x) - \frac{a^2 x^2}{1+b^2 x^2} y, \quad (2.3a)$$

$$\frac{dy}{dt} = \frac{a^2 x^2}{1+b^2 x^2} y - my, \quad (2.3b)$$

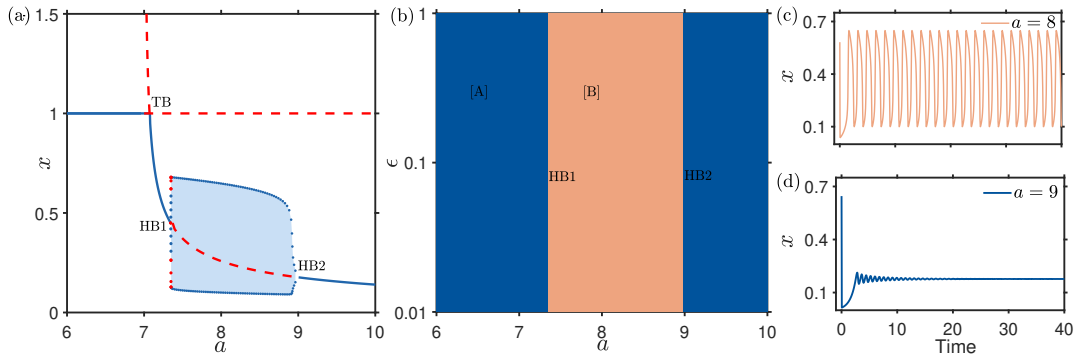


**Figure 2.5.** Species dynamics of the uncoupled deterministic model: (a) One-parameter bifurcation diagram with variation in the parameter  $a$ . (b) Two-parameter bifurcation diagram in the  $(a, \epsilon)$ -plane. Shaded regions: [A] corresponds to the region where the system exhibits steady state dynamics. [B] is the region where species abundance depicts oscillatory behavior. (c-d) Time series of the resource ( $x$ ) for  $a = 8$ , and  $a = 9$ , respectively. Other parameter values are  $\epsilon = 0.01$ ,  $b = 7$ ,  $r = 1$ , and  $m = 1$ .

Depending upon the value of the parameter  $a$ , the model shows the transition between cyclic and equilibrium dynamics. The underlying dynamics are depicted in Fig. 2.5, where the one parameter bifurcation diagram (see Fig. 2.5(a)) and the two-parameter bifurcation diagram (see Fig. 2.5(b)) show that the system remains in the steady state dynamics for  $a < 7.345$  and  $a > 8.975$ , however,  $a \in [7.345, 8.975]$  determines the oscillatory region (the fixed point becomes unstable) for the isolated system. Two representative time series are presented in Figs. 2.5(c)-2.5(d). As the time-scale separation parameter ( $\epsilon$ ) is known to significantly impact population dynamics, to analyze its sensitivity we plot the two-parameter bifurcation diagram in the  $(a, \epsilon)$ -plane.

In Fig. 2.6, we demonstrate the effect of noise intensity and network topology on consumer ( $y$ ) dynamics (corresponding to Fig. 2.2). For a fixed coupling range  $P = 8$  and in the absence of noise ( $D = 0$ ) we observe that all the nodes rest in the steady state [Fig. 2.6(a)]. Adding noise into the system ( $D > 0$ ), although with weak

intensity, results in two inhomogeneous steady solutions, as shown in Fig. 2.6(b) for  $D = 0.00001$ . However, due to the low population density maintained by consumers, the upper and the lower steady state branches do not have a large difference, as was in the case of resource ( $x$ ) densities [see Fig. 2.2(b)]. Further, increasing noise intensity results in the switching between the two branches of consumer densities [Fig. 2.6(c)]. For a large noise intensity ( $D = 0.005$ ), frequent spiking is noticed [see Fig. 2.6(d)]. Moving ahead, for a fixed noise intensity  $D = 0.00001$  and local

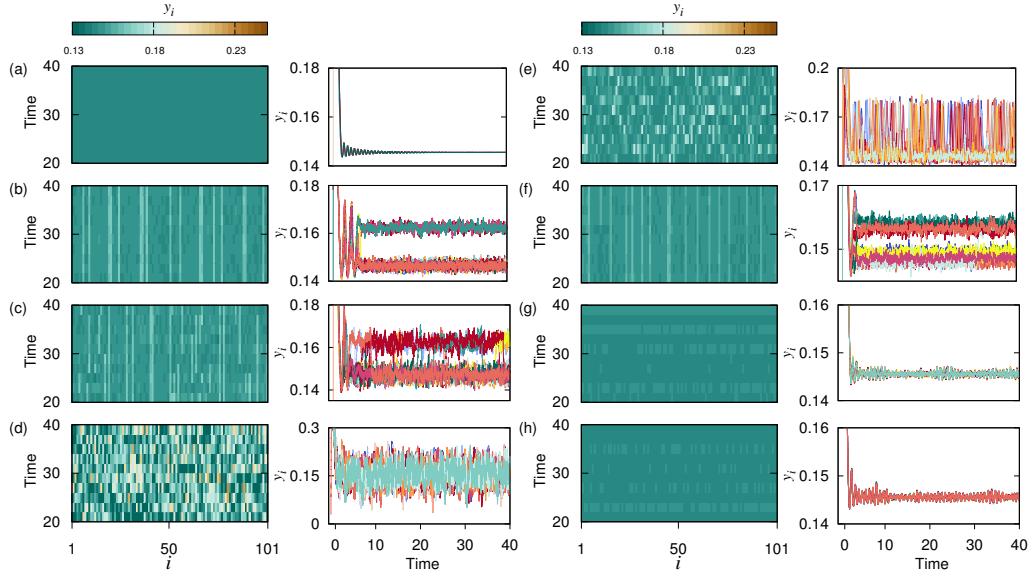


**Figure 2.6.** (a)-(d) Space-time (left column) and corresponding time series plots (right column) of consumer  $y_i$  for  $P = 8$ ,  $\sigma = 0.1$  with varying noise intensities: (a)  $D = 0$ ; steady state, (b)  $D = 0.00001$ ; symmetry breaking, (c)  $D = 0.000033$ ; stochastic switching between two consumer densities, and (d)  $D = 0.005$ ; frequent spiking. (e)-(h) Space-time (left column) and corresponding time series (right column) plots for  $D = 0.00001$ ,  $\sigma = 0.6$  with varying coupling range  $s$ : (e)  $s = 0.01$  (local coupling); asynchronous oscillations, (f)  $s = 0.04$ ; symmetry breaking, (g)  $s = 0.25$ ; most nodes settling at the lower branch, and (h)  $s = 0.5$  (global coupling); steady state. Other model parameters are  $r = 1$ ,  $a = 9$ ,  $b = 7$ ,  $m = 1$ ,  $\epsilon = 0.01$ , and  $N = 101$ .

coupling ( $s = 0.01$ ), we observe oscillating dynamics of the consumer population from Fig. 2.6(e). Increasing the coupling range results in symmetry breaking as is exhibited by the consumer population settling in the two branches [see Fig. 2.6(f)], where the densities of the upper and the lower branches are not very significantly apart. Therefore, any further increase in connectivity leads to the collision of the two states, thus resulting in a single steady-state solution [Figs. 2.6(g)-2.6(h)].

## 2.6 Appendix 2: Ecological network with stochastic birth and death rates

The noise in (2.1a) is incorporated extrinsically (additive), we now investigate how an ecological network of stochastic excitable systems responds toward heterogeneity

in network structure (due to varying degree distribution) and habitat patches (due to stochasticity in the birth and death rates). Noise is added as an intrinsic source to the system, arising from random fluctuations in the birth and death processes. The dynamics of species in the  $i$ -th patch can be read as:

$$\epsilon \frac{dx_i}{dt} = r(1 + D\zeta_i(t))x_i(1 - x_i) - \frac{a^2 x_i^2}{1 + b^2 x_i^2} y_i, \quad (2.4a)$$

$$\frac{dy_i}{dt} = \frac{a^2 x_i^2}{1 + b^2 x_i^2} y_i - m(1 + D\zeta_i(t))y_i + \sigma \sum_{j=1}^{j=N} A_{ij}(y_j - y_i). \quad (2.4b)$$

The species interaction across patches in a network occurs through the consumer movement, where  $\sigma$  determines the coupling strength and  $A_{ij}$  is the entry of adjacency matrix  $A$  (representative of the network structure). Here, we consider three different network topologies: the Watts-Strogatz (WS) (Watts and Strogatz, 1998) model, the Barabási-Albert (BA) (Barabási and Albert, 1999) model, and the Erdős-Rényi (ER) model (Erdős and Rényi, 1959). For the WS network, the interactions between the nodes with regular links are replaced by the random ones depending upon the rewiring probability  $p$ . Increasing the probability  $p$  from 0 to 1 transits a network from order to completely random, and the WS network is small-world when the value of  $p$  lies in between 0 and 1. The BA model follows power-law distribution and generates scale-free networks, whereas, the ER model generates random networks and follows the Poisson distribution.

### 2.6.1 Effect of habitat connectance in a regular network

( $p = 0$ )

The effect of changing the average degree  $k$  (patch connectance) on population dynamics (2.4a) is depicted in Fig. 2.7. We fix the noise intensity  $D = 1$  and coupling strength  $\sigma = 1$  and increase the average degree. As observed from Fig. 2.7(a), the system with a low average degree or less habitat connectance ( $k = 2$ ) exhibits asynchronous oscillatory solutions. On increasing the spatial connectivity (Figs. 2.7(b)-2.7(c)), we observe that the underlying symmetry of the deterministic skeleton breaks with the occurrence of alternative steady states. It is noticed that for  $k = 10$  (see Fig. 2.7(b)), the population keeps shifting between the two states giving rise to stochastic switching (SS), whereas, the average degree  $k = 40$  (see Fig. 2.7(c)) completely settles the resource densities in the respective two branches, thus resulting in noise-induced symmetry breaking (NISB). Further, as noticed from Fig. 2.7(d), the global connectivity ( $k = 100$ ) between the habitat patches also results in symmetry breaking.

To further comprehend the observed scenarios, namely oscillatory, SS, and NISB

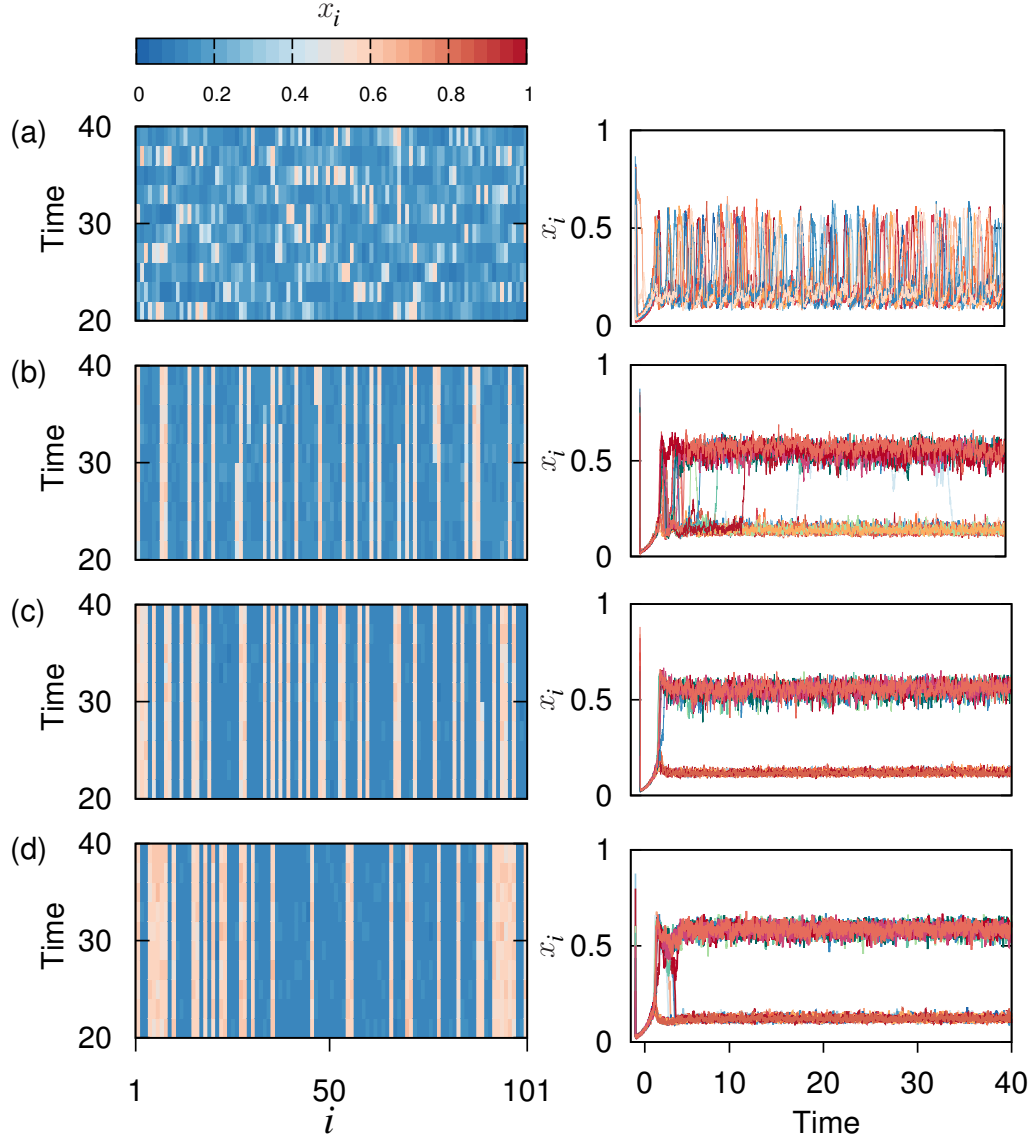


**Figure 2.7.** Space-time plot (left column) and time series plot (right column) in a regular network ( $p = 0$ ) for  $D = 1$  and,  $\sigma = 1$  with varying average degree  $k$ : (a)  $k = 2$  (nearest neighbor connections); asynchronous oscillations, (b)  $k = 10$ ; stochastic switching, (c)  $k = 40$ ; symmetry breaking, and (d):  $k = 100$  (global connectivity); symmetry breaking. Other parameters are  $r = 1$ ,  $a = 9$ ,  $b = 7$ ,  $m = 1$ ,  $\epsilon = 0.01$ , and  $N = 101$ .

by the changing average degree we calculate the center of mass (2.2). The low average degree resulting in incoherent oscillating dynamics is depicted from the rapid fluctuations between the values of the center of mass and the corresponding stochastic limit cycle as observed in Fig. 2.8(a). Resource densities occasionally fluctuate between the two branches for  $k = 20$  as can be seen from Fig. 2.8(b), whereas, the population completely resides in the respective states for global connectivity, suggesting NISB (see Fig. 2.8(c)). The value of  $x_{c.m.}(i) \approx 0.55$  for one resource sub-population and the other sub-population settles at  $x_{c.m.} \approx 0.12$ , which is also clearly exhibited in the phase space that shows the wide distribution of resource population wholly around two densities  $x_i \approx 0.12$  and  $\approx 0.55$ .

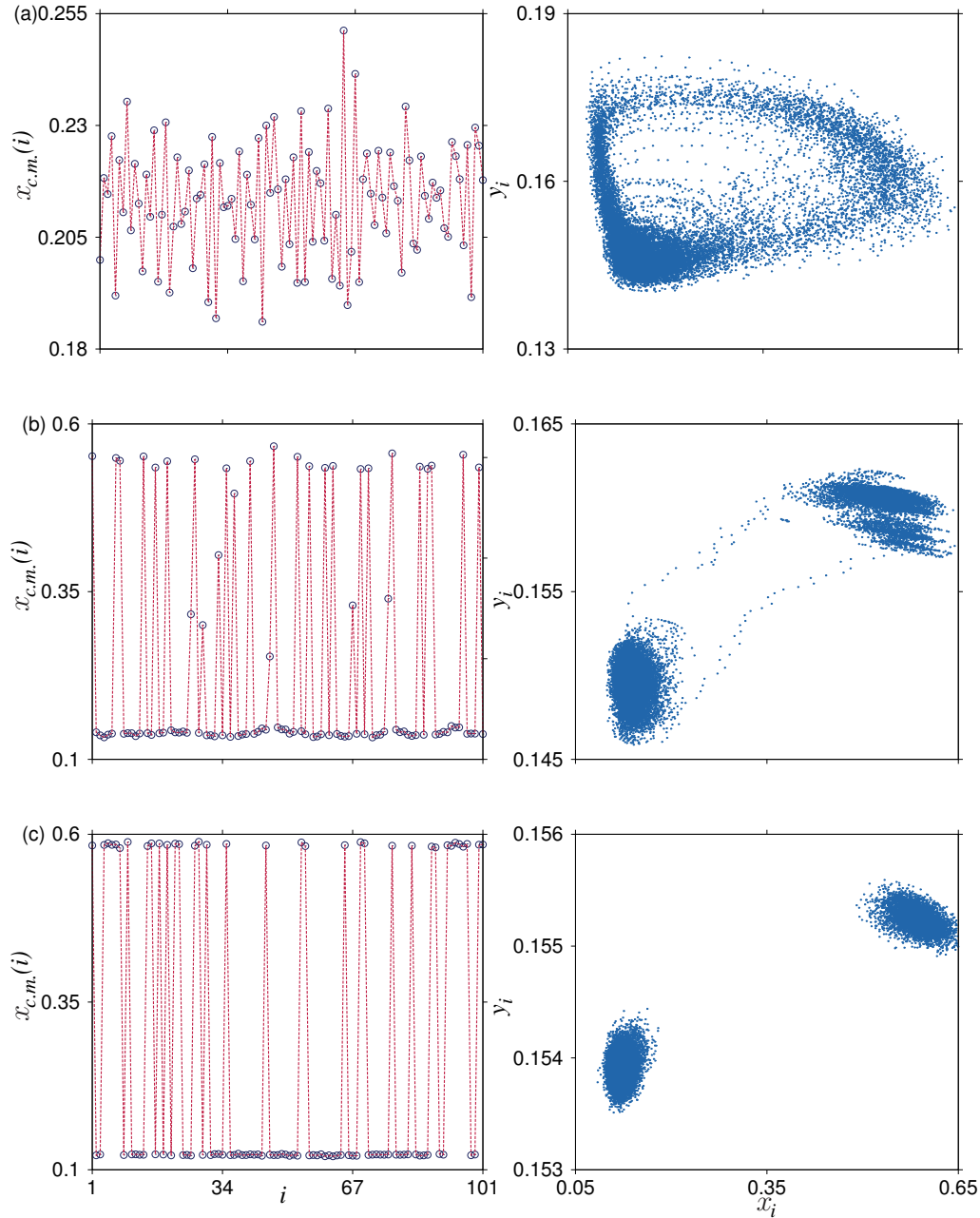


**Figure 2.8.** Center of mass  $x_{c.m.}(i)$  (left column) and phase portraits (right column) for  $p = 0$ ,  $D = 1$ , and  $\sigma = 1$  with varying average degree  $k$ : (a)  $k = 2$ , (b)  $k = 10$ , and (c)  $k = 100$ , respectively. Other parameters are the same as in Fig. 2.7.

### 2.6.2 Effect of increasing habitat connectance in different network topologies (WS, BA, and ER)

Next, we explore the effect of increasing patch connectivity ( $k$ ) in changing network topologies. As observed in Fig. 2.9(a) and Fig. 2.9(d), WS and BA networks result in noise-induced oscillating solutions, whereas ER model exhibits switching between the alternate stable states (see Fig. 2.9(g)), when the connections between habitat patches are less ( $k = 4$ ). Increasing the average degree to  $k = 10$  transits

WS, and BA models from oscillatory dynamics to a regime of stochastic switching (see Fig. 2.9(b) and Fig. 2.9(e)), and in ER network, the system gives rise to inhomogeneous steady-state solutions, as seen in Fig. 2.9(h). Moving towards more habitat connections ( $k = 40$ ), under all three network topologies (WS, BA, and ER), the system breaks into sub-populations resulting in symmetry breaking (see Fig. 2.9(c), Fig. 2.9(f), and Fig. 2.9(i)). Therefore, remarkably, the occurrence of NISB can easily be achieved for a higher average degree irrespective of the properties of a random network.

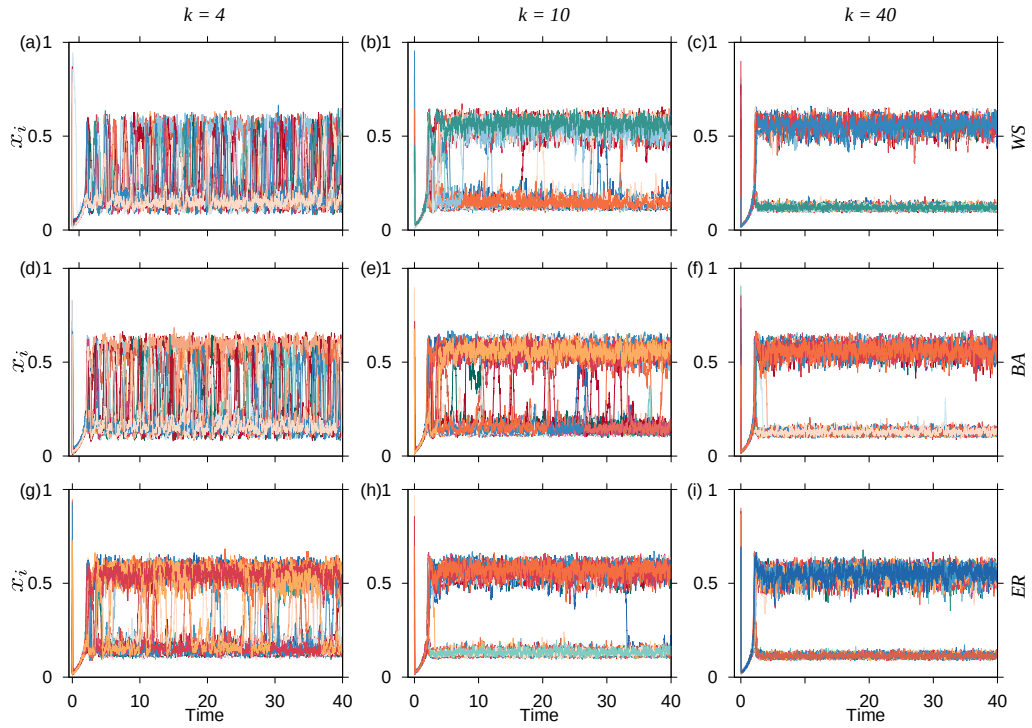


**Figure 2.9.** Time series of resource  $x_i$  in WS ((a)-(c)) with  $p = 0.4$ , BA ((d)-(f)), and ER ((g)-(i)) networks with varying average degree  $k$ : [(a), (d), (g)]  $k = 4$ , [(b), (e), (h)]  $k = 10$ , [(c), (f), (i)]  $k = 40$ . Other parameters are  $r = 1$ ,  $a = 9$ ,  $b = 7$ ,  $m = 1$ ,  $\epsilon = 0.01$ ,  $N = 101$ ,  $\sigma = 1$ , and  $D = 1$ .





# Chapter 3

## Effect of higher-order interactions on the stability of ecological communities

---

### 3.1 Introduction

In the study of complex networks, recent years have been of scientific growth, successfully providing new insights into the organization and functioning of nonlinear systems of interacting entities. An underlying assumption in representing networks is that they capture only pairwise interactions ([Boccaletti et al, 2006](#)). However, in complex systems comprising many units, any pairwise interaction is likely to be influenced by the presence of other nodes. Growing evidence suggests that in human dynamics ([Cencetti et al, 2021](#)), ecological systems ([Grilli et al, 2017](#)), brain networks ([Petri et al, 2014](#)), and many physical and social systems, the interactions cannot be decomposed into pairwise couplings ([Battiston et al, 2020](#)), hence, the higher-order interactions are considered for the proper characterization of the system.

Higher-order interactions are known to impact the collective dynamics of the networked systems substantially, from synchronization ([Millán et al, 2019](#)), diffusion ([Carletti et al, 2020](#)), explosive transitions ([Kuehn and Bick, 2021](#)) and evolution ([Alvarez-Rodriguez et al, 2021](#)). In complex systems, such interactions are often modeled using the simplicial complexes ([Salnikov et al, 2018](#)), which describe different kinds of mathematical structures present in the network, including not only nodes and links but also triangles, tetrahedron, etc. (see Fig. 3.1). The consideration of three-way interactions in the context of species migration between patches introduces a nuanced perspective that extends beyond the standard pairwise connections. The movement of species depends on the collective conditions of multiple neighboring patches concurrently. Some species exhibit spatial memory that involve considering multiple patches in their decision-making process, for instance, the availability of resources or suitable habitats in distant patches might influence the migration choices of a species. Despite the recognition of the

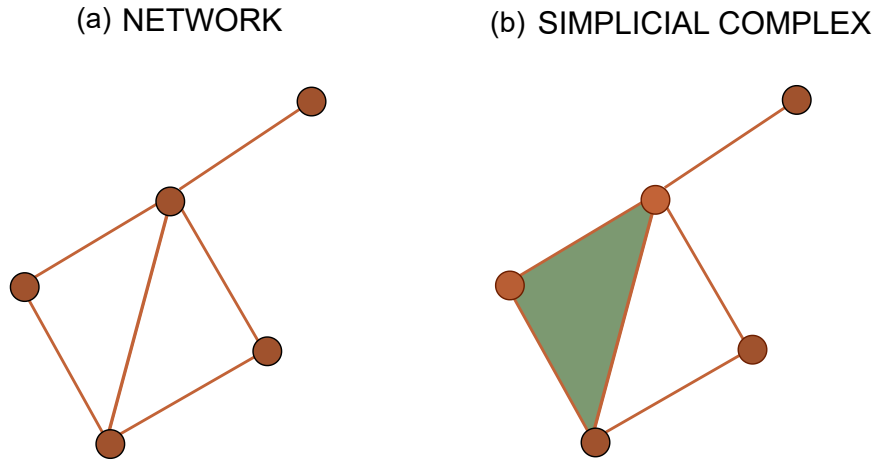


**Figure 3.1.** Networks representing pairwise and higher-order interactions between nodes. (a) A network with pairwise interactions between nodes connected by edges. (b) Higher-order interaction between nodes in a network is modeled using simplicial complexes, where edges correspond to 1-simplices, and full triangles represent 2-simplices (shown in green).

fundamental importance of moving beyond the dyadic couplings (Salnikov et al, 2018; Gong and Pikovsky, 2019; Arnaudon et al, 2022), a study of how the many-body interactions in spatial ecological communities can lead to new dynamical processes still needs to be explored. To investigate this, we focus on synchronization, a nonlinear collective phenomenon observed in coupled oscillators (Shahal et al, 2020; Boccaletti et al, 2018). Considerable attention has been given to studying the interplay between the network topology and its synchronizability, particularly in weighted (Chavez et al, 2005), multilayer (Del Genio et al, 2016), small-world networks (Barahona and Pecora, 2002). The work by Holland and Hastings (2008) revealed that changing the connectivity by randomizing the dispersal network in a spatial predator-prey model reduces synchrony. Moreover, recently, a stream of research has shown that the inclusion of HOI can lead to collective synchronization of the nodes (Gambuzza et al, 2021; Kovalenko et al, 2021; Parastesh et al, 2022). Therefore, a careful investigation of synchronization for different structures of connectivity with higher-order interactions is of great interest in ecology. This is because complete synchronization in population abundance between spatially separated patches can trigger global extinction and, hence, reduce ecosystem stability.

In this chapter, we study the collective behavior of an ecological network within simplicial complexes and analyze when the higher-order interactions can promote synchronization. In particular, we observe that moving from a regular to an irregular network topology (formed by randomizing the connectivity) results in asynchronous solutions as reported in Holland and Hastings (2008). However, incorporating higher-order interactions into the system favors synchrony, but

complete synchronization does not exist when the considered network is random. We then use the concept of clustering frequency to analyze the coherence or incoherence in species dynamics. Further, we find that for all-to-all coupling, the network with HOI exhibits global synchrony in a bounded region, which we have calculated using the master stability function (MSF). Finally, we corroborate our results by measuring the synchronization error which depending upon the interaction strengths decreases to zero in the case of all-to-all coupling but remains high with a random network topology.

## 3.2 Model and Methods

### 3.2.1 An ecological dispersal network with higher-order interactions

Here, we consider an ecological network of  $N$  spatially separated patches subjected not only to pairwise interactions but also to three-body higher-order interactions. Each node in the network inhabits a food chain with a basal resource ( $x$ ), an intermediate consumer ( $y$ ), and a top predator ( $z$ ) (Hastings and Powell, 1991). The dynamics of the food chain in each patch are described by the logistic growth and Holling's type-II functional response. We make the assumption that when three patches, denoted as  $i, j$ , and  $k$  are interconnected in a manner where both  $j$  and  $k$  are neighbors of  $i$ , and they are also neighbors of each other. Then in addition to considering standard pairwise dispersal among the patches, there is also the presence of a linear (or nonlinear) diffusion process connecting these patches (HOI). The considered ecological network, with HOI between the nodes, is given by the following model:

$$\frac{dx_i}{dt} = x_i(1 - x_i) - \frac{a_1 x_i y_i}{1 + b_1 x_i}, \quad (3.1a)$$

$$\begin{aligned} \frac{dy_i}{dt} = & \frac{a_1 x_i y_i}{1 + b_1 x_i} - \frac{a_2 y_i z_i}{1 + b_2 y_i} - m_1 y_i + \sigma_1 \sum_{j=1}^N a_{ij}^{(1)} (y_j - y_i) \\ & + \sigma_2 \sum_{j=1}^N \sum_{k=1}^N a_{ijk}^{(2)} (y_j + y_k - 2y_i), \end{aligned} \quad (3.1b)$$

$$\begin{aligned} \frac{dz_i}{dt} = & \frac{a_2 y_i z_i}{1 + b_2 y_i} - m_2 z_i + \sigma_1 \sum_{j=1}^N a_{ij}^{(1)} (z_j - z_i) \\ & + \sigma_2 \sum_{j=1}^N \sum_{k=1}^N a_{ijk}^{(2)} (z_j + z_k - 2z_i), \end{aligned} \quad (3.1c)$$

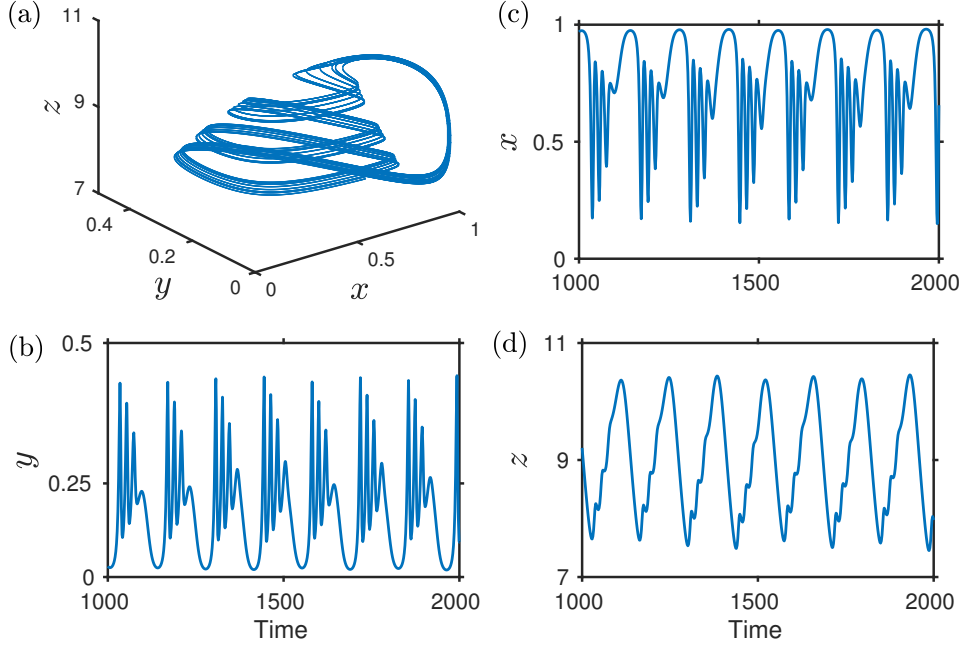


**Figure 3.2.** Phase portrait and time series of the food-chain model (3.1) in the absence of coupling (i.e., when  $\sigma_1 = \sigma_2 = 0$ ). (a) Phase portrait exhibiting a chaotic attractor. Time series representing the abundances of (b) the resource, (b) the consumer, and (c) the top predator. Model parameters are  $a_1 = 5, a_2 = 0.1, b_1 = 3, b_2 = 2, m_1 = 0.4$ , and  $m_2 = 0.01$ .

where  $i(= 1, 2, \dots, N)$  denotes the node index. The mortality of consumers and top predators is determined by the rates  $m_1$  and  $m_2$ , respectively.  $\sigma_1$  and  $\sigma_2$  are the coupling strengths corresponding to two-body and three-body interactions. A two-body interaction or a simplex of dimension-1 corresponds to a link. Whereas a three-body interaction or a 2 simplex is a collection of 3 nodes, forming a triangle in a network and representing HOI in a network.  $a_{ij}^{(1)}$  are entries of a  $N \times N$  adjacency matrix  $A^{(1)}$ , which takes the value 1 if  $i$ -th and  $j$ -th nodes are connected, and which is 0 otherwise. For a two-dimensional object we define a  $N \times N \times N$  adjacency tensor  $A^{(2)}$  whose entry  $a_{ijk}^{(2)} = 1$  if the nodes  $i, j, k$  form a triangle, otherwise  $a_{ijk}^{(2)} = 0$ .

The Laplacian matrix  $L = l_{ij}$  for a graph is defined as  $L = D - A$ , where  $D$  is the diagonal matrix with degree of each node as its diagonal entries and  $A$  is the adjacency matrix. Therefore, for simplicial complexes, the first-order Laplacian matrix  $L^{(1)}$  is the standard Laplacian matrix with:

$$d_i^{(1)} = \sum_{j=1}^N a_{ij}^{(1)}, \quad (3.2)$$

denoting the degree of node  $i$ .  $d_i^{(2)}$  counts the number of triangles in which  $i$  belongs,

given as:

$$d_i^{(2)} = \frac{1}{2} \sum_{j=1}^N \sum_{k=1}^N a_{ijk}^{(2)}, \quad (3.3)$$

and  $d_{ij}^{(2)}$  characterizes the degree of the link  $(i, j)$ , i.e, the number of 2-simplices to which  $(i, j)$  participates:

$$d_{ij}^{(2)} = \sum_{k=1}^N a_{ijk}^{(2)}. \quad (3.4)$$

The second-order Laplacian matrix  $L^{(2)}$  is thus defined as:

$$L_{ij}^{(2)} = \begin{cases} 0 & \text{for } i \neq j \text{ and } a_{ij}^{(1)} = 0, \\ -d_{ij}^{(2)} & \text{for } i \neq j \text{ and } a_{ij}^{(1)} \neq 0, \\ 2d_i^{(2)} & \text{for } i = j. \end{cases} \quad (3.5)$$

Here, we focus on the role of network structure in influencing synchronous dynamics of model (3.1). We begin the modeling of a dispersal network by considering a regular network of degree eight (each patch or node is connected to its four neighbors on either side of a ring). We then randomize the structure by rewiring the edges, i.e., we replace the existing connection between two patches with a new random connection and analyze the effect the heterogeneity in the dispersal network has on the system's behavior. We further investigate the influence of HOI on synchronization in the random network. To investigate the effect of connections between the nodes, we also analyze how HOI shapes the population dynamics when the network is globally coupled (i.e., the degree of each node is considered  $(N - 1)$  - all to all coupling).

### 3.2.2 Linear stability analysis of synchronized solution with higher-order interactions

Apart from the nodal dynamics and network topology, the interaction strength between spatially separated nodes of the coupled oscillators plays a crucial role in governing the collective dynamics of a network. We now investigate the synchronization in global network for two-body and three-body interaction strengths using the master stability function (MSF) approach (Pecora and Carroll, 1998). Considering simplicial complexes up to order two, a network of identical oscillators with HOI can be written in general form as:

$$\begin{aligned} \dot{X}_i = & F(X_i) + \sigma_1 \sum_{j=1}^N a_{ij}^{(1)} H^{(1)}(X_i, X_j) \\ & + \sigma_2 \sum_{j=1}^N \sum_{k=1}^N a_{ijk}^{(2)} H^{(2)}(X_i, X_j, X_k), \quad i = 1, 2, \dots, N \end{aligned} \quad (3.6)$$

where  $X_i$  is the  $m$ -dimensional state vector and  $F : \mathbb{R}^m \rightarrow \mathbb{R}^m$  describes the dynamics of the  $i$ -th node.  $H^{(1)}$  and  $H^{(2)}$  are the coupling functions defining the interactions between different nodes in 1 and 2 simplex structures, respectively. The existence of the synchronous solution  $X_1 = X_2 = \dots = X_N = X_s$  is guaranteed because the considered coupling functions are non-invasive (i.e.  $H^d(x, x, \dots, x) \equiv 0 \forall d$ ), where  $X_s$  is the synchronization manifold (Gambuzza et al, 2021). To investigate the stability of the synchronous solution, a tiny perturbation  $\delta X_i$  is added to the synchronous manifold  $X_s$  as  $\delta X_i = X_i - X_s$ . Thus, the perturbation equation corresponding to Eqn. (3.6) is as follows:

$$\begin{aligned} \delta \dot{X}_i &= DF(X_s) \delta X_i \\ &+ \sigma_1 \sum_{j=1}^N a_{ij}^{(1)} [DH^{(1)}(X_s, X_s) \delta X_i + DH^{(1)}(X_s, X_s) \delta X_j] \\ &+ \sigma_2 \sum_{j=1}^N \sum_{k=1}^N a_{ijk}^{(2)} [DH^{(2)}(X_s, X_s, X_s) \delta X_i \\ &+ DH^{(2)}(X_s, X_s, X_s) \delta X_j + DH^{(2)}(X_s, X_s, X_s) \delta X_k], \end{aligned} \quad (3.7)$$

where  $DF(X_s)$  is the  $m \times m$  Jacobian matrix of  $F$ , evaluated at the synchronous manifold  $X_s$ . Therefore, we have

$$\delta \dot{X}_i = \begin{cases} \delta \dot{x}_i = Df(X_s) \delta X_i, \\ \delta \dot{y}_i = Dg(X_s) \delta X_i + \sigma_1 \sum_{j=1}^N a_{ij}^{(1)} [\delta y_j - \delta y_i] \\ \quad + \sigma_2 \sum_{j=1}^N \sum_{k=1}^N a_{ijk}^{(2)} [\delta y_j + \delta y_k - 2\delta y_i], \\ \delta \dot{z}_i = Dh(X_s) \delta X_i + \sigma_1 \sum_{j=1}^N a_{ij}^{(1)} [\delta z_j - \delta z_i] \\ \quad + \sigma_2 \sum_{j=1}^N \sum_{k=1}^N a_{ijk}^{(2)} [\delta z_j + \delta z_k - 2\delta z_i]. \end{cases} \quad (3.8)$$

The Laplacian  $L^{(d)}$  of an adjacency matrix  $A^{(d)}$  is defined as  $L^{(d)} = D^{(d)} - A^{(d)}$ . Furthermore from Eqn. (3.2) and Eqn. (3.3) one has  $d_i^{(1)} = \sum_{j=1}^N a_{ij}^{(1)}$  and  $d_i^{(2)} = \frac{1}{2} \sum_{j=1}^N \sum_{k=1}^N a_{ijk}^{(2)}$ , respectively. Since in model (3.1) we have considered dispersal in

the intermediate consumer and the top predator, we here formulate  $\delta \dot{y}_i$  as:

$$\begin{aligned}
\delta \dot{y}_i &= Dg(X_s)\delta X_i + \sigma_1 \left[ \sum_{j=1}^N D_{ij}^{(1)} \delta y_j - \sum_{j=1}^N L_{ij}^{(1)} \delta y_j - \delta y_i \sum_{j=1}^N a_{ij}^{(1)} \right] \\
&\quad + \sigma_2 \left[ \sum_{j=1}^N \sum_{k=1}^N D_{ijk}^{(2)} [\delta y_j + \delta y_k] - \sum_{j=1}^N \sum_{k=1}^N L_{ijk}^{(2)} [\delta y_j + \delta y_k] - 2\delta y_i \sum_{j=1}^N \sum_{k=1}^N a_{ijk}^{(2)} \right] \\
&= Dg(X_s)\delta X_i - \sigma_1 \sum_{j=1}^N L_{ij}^{(1)} \delta y_j - \sigma_2 \left[ \sum_{j=1}^N \delta y_j \sum_{k=1}^N L_{ijk}^{(2)} + \sum_{k=1}^N \delta y_k \sum_{j=1}^N L_{ijk}^{(2)} \right] \\
&= Dg(X_s)\delta X_i - \sigma_1 \sum_{j=1}^N L_{ij}^{(1)} \delta y_j - \sigma_2 \left[ \sum_{j=1}^N L_{ij}^{(2)} \delta y_j + \sum_{k=1}^N L_{ik}^{(2)} \delta y_k \right] \\
&= Dg(X_s)\delta X_i - \sigma_1 \sum_{j=1}^N L_{ij}^{(1)} \delta y_j - 2\sigma_2 \sum_{j=1}^N L_{ij}^{(2)} \delta y_j,
\end{aligned} \tag{3.9}$$

$\delta \dot{z}_i$  can be extended on the same lines. Henceforth, Eqn. (3.8) can be considered as:

$$\delta \dot{X}_i = \begin{cases} \delta \dot{x}_i = Df(X_s)\delta X_i, \\ \delta \dot{y}_i = Dg(X_s)\delta X_i - \sigma_1 \sum_{j=1}^N L_{ij}^{(1)} \delta y_j - 2\sigma_2 \sum_{j=1}^N L_{ij}^{(2)} \delta y_j, \\ \delta \dot{z}_i = Dh(X_s)\delta X_i - \sigma_1 \sum_{j=1}^N L_{ij}^{(1)} \delta z_j - 2\sigma_2 \sum_{j=1}^N L_{ij}^{(2)} \delta z_j, \end{cases} \tag{3.10}$$

Eqn. (3.7) can thus be written as:

$$\begin{aligned}
\delta \dot{X}_i &= DF(X_s)\delta X_i - \sigma_1 \sum_{j=1}^N L_{ij}^{(1)} DH^{(1)}(X_s, X_s)\delta X_j \\
&\quad - \sigma_2 \sum_{j=1}^N L_{ij}^{(2)} DH^{(2)}(X_s, X_s, X_s)\delta X_j,
\end{aligned} \tag{3.11}$$

Now writing Eqn. (3.11) in block form we get the variational equation of the system (Eqn. (3.6)) as:

$$\delta \dot{X} = \left[ I_N \otimes DF - \sigma_1 L^{(1)} \otimes DH^{(1)} - \sigma_2 L^{(2)} \otimes DH^{(2)} \right] \delta X, \tag{3.12}$$

where  $I_N$  is the  $N \times N$  identity matrix,  $\otimes$  symbolises the Kronecker product. For the all to all network configuration, we have  $L^{(2)} = (N-2)L^{(1)}$ . Therefore, Eqn. (3.12) reduces to

$$\delta \dot{X} = \left[ I_N \otimes DF - \sigma_1 L^{(1)} \otimes DH^{(1)} - \sigma_2 (N-2)L^{(1)} \otimes DH^{(2)} \right] \delta X. \tag{3.13}$$

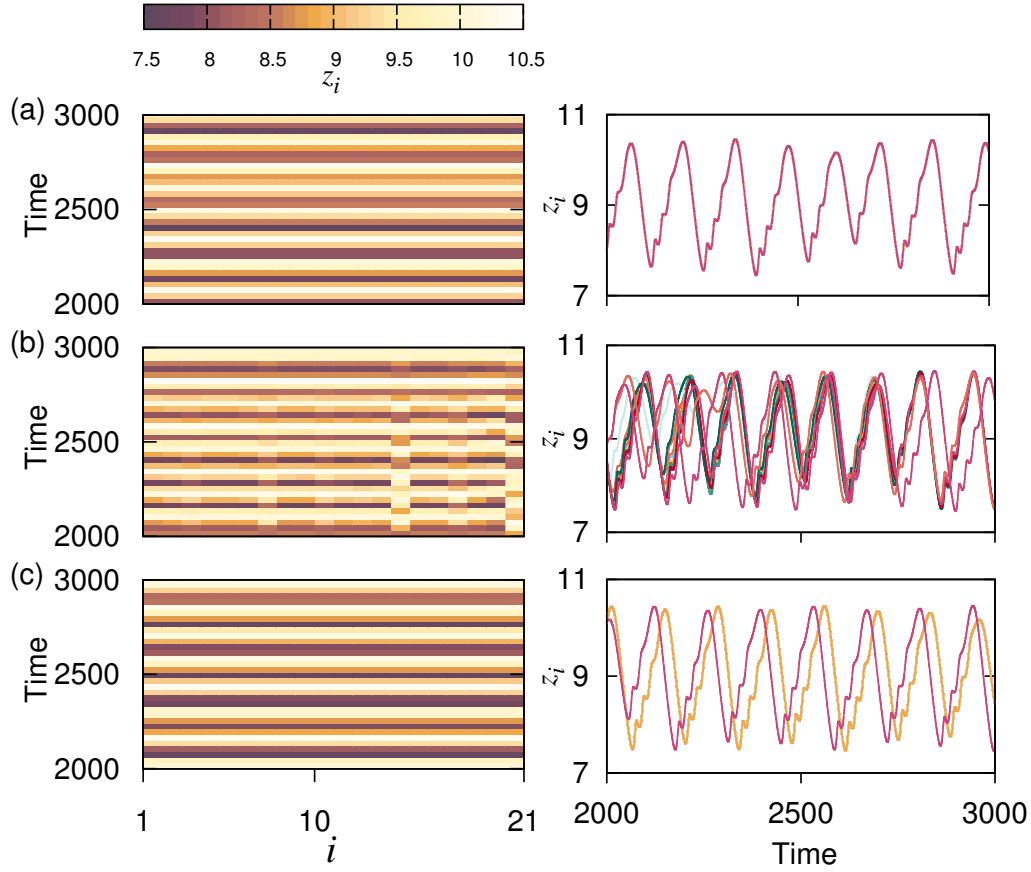


**Figure 3.3.** Space-time plots (left column) and corresponding time series plots (right column) of the top predator  $z$  in a network with average degree 8 for  $\sigma_1 = 0.004$ : (a) a regular network exhibiting complete synchrony for  $\sigma_2 = 0$ ; (b) a random network with asynchronous oscillations for  $\sigma_2 = 0$ ; and (c) a random network with suppressed asynchrony for  $\sigma_2 = 0.002$ . Other parameters are  $a_1 = 5, a_2 = 0.1, b_1 = 3, b_2 = 2, m_1 = 0.4, m_2 = 0.01$ , and  $N = 21$ .

Hence,

$$\delta \dot{X}_i = DF(X_s) \delta X_i - (\sigma_1 + 2\sigma_2(N-2)) \sum_{j=1}^N L_{ij}^{(1)} \delta X_j. \quad (3.14)$$

Considering new variables  $\xi = (Q^{-1} \otimes I_m) \delta X$  and taking into account the eigenvalue of  $L^{(1)}$ , i.e.,  $\lambda_1 = 0$  and  $\lambda_2 = \dots = \lambda_N = N$ . Hence, for  $i \in \{2, 3, \dots, N\}$  we get

$$\dot{\xi}_i = [DF - \sigma_1 NDH^{(1)} - \sigma_2 N(N-2)DH^{(2)}] \xi_i. \quad (3.15)$$

The first eigenvalue, denoted as  $\lambda_1 = 0$ , signifies that the system evolves along the synchronization manifold. In contrast, for the remaining eigenvalues  $\lambda_2, \dots, \lambda_N$ , the system's evolution is transverse to the synchronization manifold. The stability of the synchronous state is examined by computing the maximum Lyapunov exponent ( $\Lambda$ ), which in this case is a function of  $\sigma_1$ ,  $\sigma_2$  and  $N$ . Negative values of  $\Lambda$ , i.e.,  $\Lambda < 0$  for  $\lambda = N$ , indicate the stability of the synchronization manifold.



### 3.3 Results

#### 3.3.1 Role of random network topology on synchronization in the presence of higher-order interaction

We find notable differences between the collective dynamics depending upon the type of interactions among the nodes. For different network topologies, we demonstrate different space-time patterns for the population of top-predators in Fig. 3.3. In the absence of higher-order interactions ( $\sigma_2 = 0$ ) and for a regular network with a nodal degree 8, we observe complete synchrony even for a weak two-body interaction strength  $\sigma_1 = 0.004$  (see Fig. 3.3(a)). On randomizing the network (with the average degree 8), asynchronous oscillations are observed, as shown in Fig. 3.3(b). However, considering three-body interactions in the random network in the presence of weak coupling strength ( $\sigma_2 = 0.002$ ), the system settles into two cluster solutions (all the oscillators settle into two branches) (see Fig. 3.3(c)). Hence, for a random network, the inclusion of HOI is capable of reducing the degree of asynchrony through multi-cluster solutions.

#### 3.3.2 Cluster analysis

The above-mentioned results show a transition from complete synchrony to the asynchronous solution through to the system exhibiting two oscillatory solutions with the changing network topology and interaction type. Therefore, to gain information on the system's collective dynamics, we analyze the distribution of clusters (see Fig. 3.4). We calculate the correlation coefficient ( $\rho_{ij}$ ) to study the coherence between predator species ( $z$ ) abundances of  $i$ -th and  $j$ -th patches, which is given as:

$$\rho_{ij} = \frac{\langle z_i z_j \rangle - \langle z_i \rangle \langle z_j \rangle}{\sqrt{\langle z_i^2 \rangle - \langle z_i \rangle^2} \sqrt{\langle z_j^2 \rangle - \langle z_j \rangle^2}}, \quad (3.16)$$

where  $z_i$  is the predator density in the  $i$ -th patch and  $\langle \dots \rangle$  is the average over the time interval  $[t, t + \bar{t}]$ , and  $\bar{t}$  is a large time-period. The set of patches is considered to form a 1-cluster when  $\rho_{ij} \approx 1$ . Out of the  $N$  patches, the network can exhibit  $1 \leq k \leq N$  cluster solutions where 1-cluster represents complete synchrony, and  $N$ -clusters correspond to complete asynchrony. The frequency of  $k$  clusters is determined as:

$$\text{Frequency} = \frac{\text{No. of } \leq k\text{-clusters}}{\text{No. of simulations}}. \quad (3.17)$$

The 1-cluster solution shown in Fig. 3.4(a) for a regular network and  $\sigma_2 = 0$  corresponds to complete synchrony. Randomization of the network increases

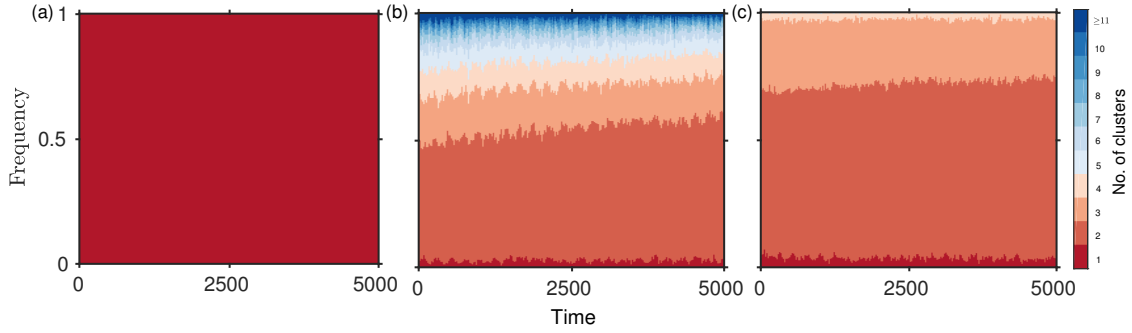


**Figure 3.4.** Frequency of cluster states for different network topologies when  $\sigma_1 = 0.004$ : (a) regular network exhibiting one cluster solution for  $\sigma_2 = 0$ ; (b) random network exhibiting a high number of clusters for  $\sigma_2 = 0$ ; and (c) random network exhibiting two to three clusters for  $\sigma_2 = 0.01$ . The frequency of each cluster is shown using  $10^2$  independent simulations. Other parameters are  $a_1 = 5, a_2 = 0.1, b_1 = 3, b_2 = 2, m_1 = 0.4, m_2 = 0.01$ , and  $N = 21$ .

the proportion of solutions from a moderate to a high number of clusters (see Fig. 3.4(b)). However, by introducing higher-order interaction into the network, the frequency of getting 2-cluster solution increases (see Fig. 3.4(c)).

### 3.3.3 Effect of higher-order interaction strength on synchrony in a network with all-to-all coupling

Our analysis from Fig. 3.3 and Fig. 3.4 shows that once a network with degree eight results in asynchronous solutions from complete synchrony (due to rewiring edges), introducing many-body interactions with any range of coupling strength (even  $\sigma_2 = 0.01$ ) does not ensure complete synchrony. This compels us to investigate the collective dynamics of a network with a higher degree of connectivity under many-body interactions. Therefore, by increasing the degree of each node to  $N - 1$  leading to all-to-all or global coupling, we study the effect of HOI strength ( $\sigma_2$ ) on the collective dynamics. For coupling values of  $\sigma_1 = 10^{-6}$  and  $\sigma_2 = 10^{-6}$ , we observe many cluster solutions, representing strong asynchrony (see Fig. 3.5(a)). However, with increasing the value of  $\sigma_2$  ( $\sigma_1$  is kept fixed) even to a very weak coupling limit we perceive from Fig. 3.5(b) the suppression of asynchrony which on further increase in  $\sigma_2$  ( $=10^{-4}$ ) leads to one cluster solution (see Fig. 3.5(c)).

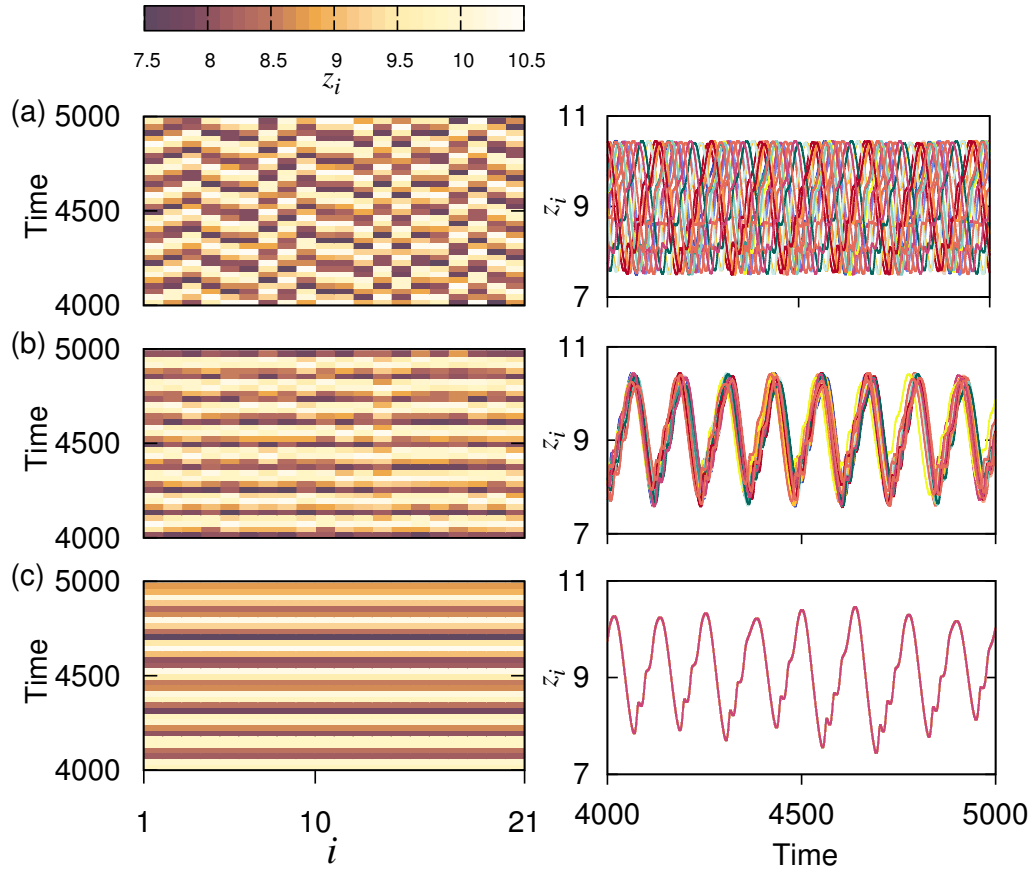


**Figure 3.5.** Space-time plots (left column) and corresponding time series plots (right column) of the top predator  $z$  in a regular network with all-to-all coupling for  $\sigma_1 = 10^{-6}$  with varying higher-order coupling strength  $\sigma_2$ : (a)  $\sigma_2 = 10^{-6}$  results in strong asynchrony between the nodes; (b)  $\sigma_2 = 10^{-5}$  results in asynchrony with many cluster solutions; and (c)  $\sigma_2 = 10^{-4}$  results in complete synchrony. Other parameters are  $a_1 = 5$ ,  $a_2 = 0.1$ ,  $b_1 = 3$ ,  $b_2 = 2$ ,  $m_1 = 0.4$ ,  $m_2 = 0.01$ , and  $N = 21$ .

### 3.3.4 Using the master stability function approach to determine the coupling range of stable synchronous solution in a global network with higher-order interactions

We now use the MSF approach to calculate the coupling range for pairwise interaction and HOI, aiming to analyze the stability of the synchronous solution. Fig. 3.6(a) illustrates the maximal Lyapunov exponent (MLE) for combinations of  $\sigma_1$  and  $\sigma_2$  in the case of global coupling. It shows that in the presence of second-order interactions, synchronization can be achieved even with a weak coupling value of  $\sigma_1$  (characterized by a negative MLE). The curves of  $\Lambda$  plotted in Fig. 3.6(b) exhibit the effect of second-order interaction strength ( $\sigma_2$ ) on synchronization for different values of  $\sigma_1$ . We observe that even for a very low value of  $\sigma_1$  ( $=10^{-6}$ ), a critical value of HOI strength  $\sigma_2$  can stabilize the synchronous solution, evident by the MLE crossing the zero line. However, the threshold value for achieving stability decreases with an increase in the value of  $\sigma_1$ .

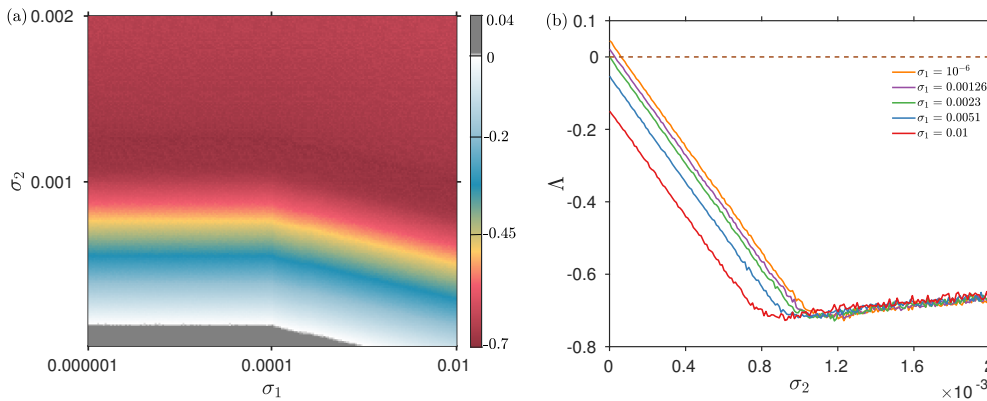


**Figure 3.6.** Master stability function for the model (3.1) in the context of global coupling. The maximum Lyapunov exponent (MLE) is calculated to analyze the stability of synchronous solution: (a) MLE depicted in  $(\sigma_1, \sigma_2)$  parameter space. (b) The MLE ( $\Lambda$ ) plots exhibiting variation along  $\sigma_2$  for different values of  $\sigma_1$ . On increasing second-order interaction strength ( $\sigma_2$ ), a stable synchronous state is achieved even for the lower value of  $\sigma_1$ .

### 3.3.5 Synchronization error

We investigate the synchronization of a random and global network with  $N$  patches for different pairwise and non-pairwise interaction strengths. We calculate the averaged synchronization error to evaluate the degree of synchrony, which is given as (Gambuzza et al, 2021):

$$E = \left\langle \left( \frac{1}{N(N-1)} \sum_{i,j=1}^N \|x_j(t) - x_i(t)\|^2 \right)^{\frac{1}{2}} \right\rangle_T. \quad (3.18)$$

We find that for a random network, low values of  $\sigma_1$  and  $\sigma_2$  result in a wide region exhibiting high synchronous error ( $E \approx 7$ ), as can be seen in Fig. 3.7(a). As perceived, the value of  $E$  keeps on decreasing with an increase in  $\sigma_2$ . However, even a large value of  $\sigma_2$  does not lead toward complete synchrony, and the system exhibits an asynchronous solution, with a minimum value of  $E$  reaching 4. On the contrary, for a network with global coupling (see Fig. 3.7(b)), we notice a transition from a narrow region with high synchrony error to a broad region with complete synchrony ( $E = 0$ ). The observed outcome is completely in line with the results of linear stability analysis (Fig. 3.6).

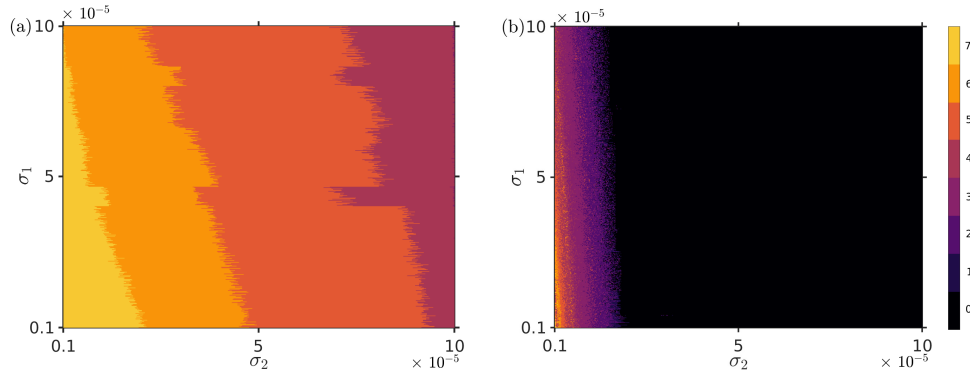


**Figure 3.7.** Synchronization error  $E$  in  $(\sigma_2, \sigma_1)$  plane for different network topologies: (a) random network, the value of  $E$  varies from 7 to 4 with increasing  $\sigma_2$ , and (b) after a region of asynchrony, the global network exhibits a completely synchronous solution ( $E = 0$ ).

### 3.4 Conclusions

The study of collective behavior in networks of coupled oscillators has always been a central issue in nonlinear dynamics. Synchronization is a prevalent phenomenon in natural systems that can be understood by analyzing the interactions in spatially extended systems. Here, considering an ecological network composed of tri-trophic food chains, we elucidate the effect of network structure and HOI on collective ecological dynamics. Our results illustrate that the interacting units in a network, along with non-pairwise coupling, influence population dynamics and can thus impact the stability of a community.

Synchrony has fundamental but conflicting implications for the persistence and stability of metapopulations at local and regional scales. Synchrony amplifies the risk of global extinction and consequently diminishes species persistence. Synchronization dynamics on complex networks has been widely studied in the literature, and it is known to be very significantly affected by the spectral properties of a dispersal network (Holland and Hastings, 2008; Gupta et al, 2017). In the presence of HOI, a regular network with a low average degree exhibits synchronous

behavior even in a weak coupling limit. Randomizing the network structure by rewiring the links induces asynchrony. However, incorporating three-body interactions in the system suppresses asynchrony and results in the system exhibiting two clusters. On the contrary, in global coupling (high node degree), the system with increasing higher-order coupling strength shows a transition from a region of asynchronous oscillations to a synchronous regime (one cluster solution).

In this chapter, we explore the stability of collective population dynamics within simplicial structures using the master stability function approach to analyze global synchrony scenarios. Our investigation shows that the synchronous manifold exhibits stability within a defined bounded region. We find that higher-order interaction suppresses asynchrony and leads to synchronous solutions. However, considering random network topology prevents complete synchrony, thus impeding global extinction risk. Overall, our results illustrate that the interacting units in a network and non-pairwise coupling influence population dynamics and can thus impact the stability of a community.

# Chapter 4

## Resource pulses and foraging behavior shape spatial population dynamics

---

### 4.1 Introduction

The recognition of the biodiversity effects on ecosystem stability has a long history in ecology ([Tilman, 1996](#); [Naeem et al, 1994](#)). However, anthropogenic stressors, abiotic conditions, and trophic structure have led to significant changes in the composition of ecological communities. Mounting evidence ([Chapin Iii et al, 2000](#); [Hooper et al, 2005](#); [Balvanera et al, 2006](#); [Cardinale et al, 2006](#)) report that the loss of species resulting in declining biodiversity has raised concern about its consequences on the functioning and services of ecosystems. Human domination over Earth's system has essentially altered biotic structure ([Vitousek et al, 1997](#)) concerning the number of coexisting species (species richness) and their relative abundance. Degradation and conversion of natural ecosystems are imperiling the species at an accelerating rate ([Steffen et al, 2007](#); [Vitousek et al, 1997](#)). Habitat loss and fragmentation are the underlying reasons for the changes in the population and distribution of organisms ([Pereira et al, 2010](#); [Rands et al, 2010](#)). Fragmentation results in loss of area and increasing spatial isolation, thus increasing the extinction risk of species due to demographic stochasticity ([Fahrig, 2003](#); [Lindenmayer and Fischer, 2013](#)). Therefore, understanding how species interactions and spatial change influence population dynamics is a longstanding issue in spatial ecology.

Ecologists find that the ability of organisms to move between spatially separated patches is a crucial factor in driving species dynamics in a fragmented landscape ([Levins, 1969](#); [Armsworth and Roughgarden, 2005](#); [Niebuhr et al, 2015](#)). However, increased fragmentation strongly impacts animal movements, leading to more considerable distances between the habitat patches, thus lowering the connectivity and the recolonization rates ([Brown and Kodric-Brown, 1977](#); [Hanski et al, 2004](#)). Hence, the movement pattern that animals adapt during foraging is essential in determining their survivability ([Viswanathan et al, 1999](#); [Zollner and Lima, 1999](#)).

Considerable attention has been paid to quantifying the movement strategies of foragers (Viswanathan et al, 1999; Turchin, 1998; Kareiva and Shigesada, 1983; Crist et al, 1992; Bartumeus et al, 2003; Austin et al, 2004). However, investigating the impact of demographic rates and movement behavior concerning the resource abundance to maintain ecological stability still needs to be explored.

Studies have shown that animals adjust their searching behavior following the availability of food resources (Benhamou and Bovet, 1989; Newlands et al, 2004; Nolet and Mooij, 2002; Bell, 2012). A general theory of foraging in ecology is that animals in areas of high resource abundance displace less, thereby increasing the usage of resources (Focardi et al, 1996; Turchin, 1991; Kareiva and Odell, 1987). Whereas, when the density of resources is less, the faster movements resulting in a large displacement increase the chance of food capture and thus are more efficient than the ones with high tortuosity (Turchin, 1991; Zollner and Lima, 1999; Bartumeus et al, 2005). Turchin (1998); Lima and Zollner (1996) consider that realistic animal movements comprise discrete series of displacement events separated by turning angles. Discretization of movement behavior determines the statistical distribution of displacement or step lengths and change of direction (i.e., turning angles). Such discretized movement paths can be examined through the techniques of random walk theory.

Lévy walk is a particular form of random walk composed of clusters of short steps with long travels between them (Viswanathan et al, 2011). It was Shlesinger and Klafter (1986) who first proposed that Lévy walks could be observed in animal search strategies. Further, various studies have reported Lévy walk searches in many animals, for instance moths (*Agrotis segetum*) (Reynolds et al, 2007a), honeybees (*Apis mellifera*) (Reynolds et al, 2007b), and marine fish (Sims et al, 2008). Lévy walks are scale-free movements with uniform distribution for turning angles and power-law distribution  $P(l) \propto l^{-\beta}$  of step length ( $l$ ) with  $1 < \beta \leq 3$ . Research suggests that Lévy walks optimize search strategies when resources are sparse and distributed in fragmented landscapes (Viswanathan et al, 2011; Bartumeus and Catalan, 2009). In a recent paper (Dannemann et al, 2018), the authors report the population dynamics in the presence of foragers for different amounts of habitat availability. Further, Nauta et al (2022) analyzes the effect of varying habitat fragmentation on the system's dynamics in fragmented landscapes. However, the resource pulse is an essential environmental factor that has not yet been studied much in landscape ecology theory in the context of foraging strategies. Resource pulses are episodes of considerable magnitude, short-duration events of increased resource availability (Yang et al, 2008), that are prevalent (Ostfeld and Keesing, 2000; Yang et al, 2008). Resource pulses are characterised by sudden and temporary increase in the availability of a resource. This increase is often short-lived with



a rapid but temporary change in the environment. An event of resource pulse substantially increases the proportion of resource availability in the system, and studies (Ostfeld and Keesing, 2000) report that rare events can have significant and persistent impacts on communities. Hence, how the natural communities in the fragmented landscapes with optimal foraging strategies respond to these events will directly influence the diversity and stability of the system and needs to be examined.

To study the interplay between foraging behavior, resource pulse, and the survival rates of species, we consider a spatially explicit stochastic vegetation-grazer model in a fragmented landscape. Resources are restricted to occupied sites, and grazers can disperse according to a power law kernel (Lévy random walk). By considering different demographic rates and movement strategies, we examine their effect on the persistence of populations. Our findings indicate that adopting an optimal foraging strategy, depending upon the demographic rates of species and the availability of resources has the potential to mitigate the effects of unfavorable conditions and promote species coexistence.

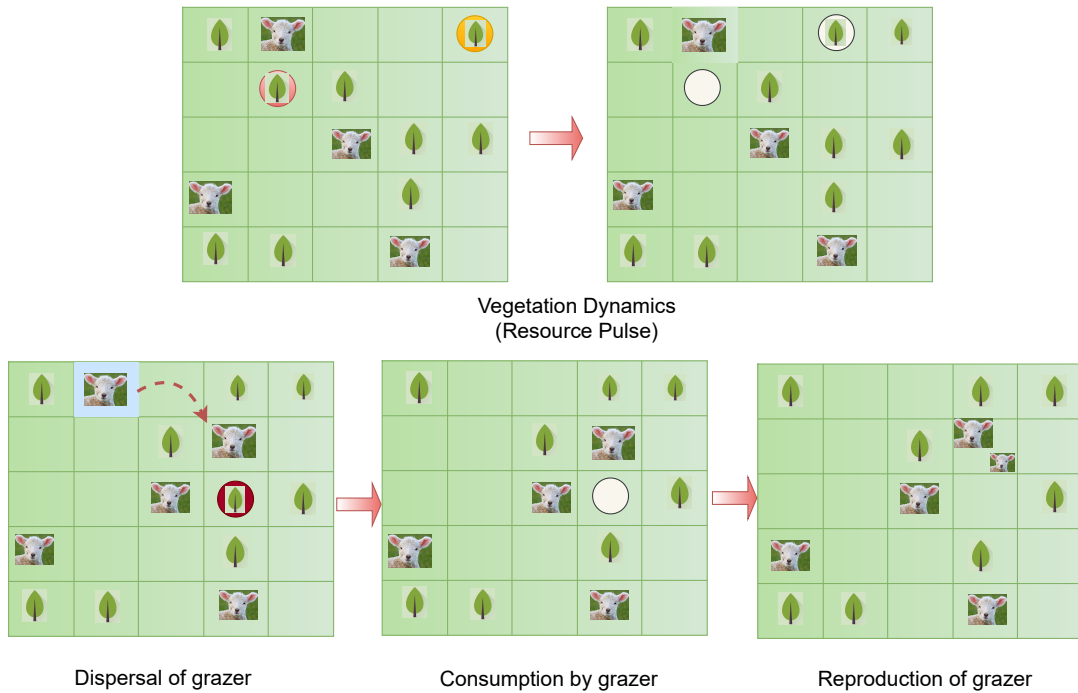


**Figure 4.1.** A schematic representation of different stages of vegetation and grazers incorporated in the model. A resource pulse is incorporated periodically after every  $t_v$  time (upper panel) in which vegetation can either die naturally (pink circle) or reproduce in the nearest empty cell (yellow circle). The lower panel corresponds to the three stages of a grazer. A randomly selected grazer (blue square) disperses to a new site, as shown by an arrow. It attacks and consumes vegetation (red circle), making the cell vacant. It then reproduces at the site.

## 4.2 A stochastic vegetation-grazer model in fragmented landscapes

Here, we develop a stochastic vegetation-grazer model in a two-dimensional fragmented landscape. The two-dimensional space is a periodic lattice divided into  $N$  square lattice sites. The initial vegetation habitat is a fraction  $\phi \in [0, 1]$  of the lattice sites. The vegetation is then allowed to reach a steady state following the contact process model, which has widely been used in epidemiology (Harris, 1974; Levin and Durrett, 1996), and also applied in ecology for modeling spatial dynamics of plant species (Barkham and Hance, 1982; Majumder et al, 2021). At each time step, vegetation reproduces with a probability  $p$  or may naturally die with a probability  $1 - p$ , and the following model governs the dynamics:

$$\frac{dv}{dt} = pv(1 - v) - v(1 - p). \quad (4.1)$$

Further, a fraction  $\rho \in [0, 1]$  of vegetation abundance at the steady state is introduced as the number of initial grazers into the system. At every discrete time step, a grazer dies with a rate  $m$  or disperses to a new site following Lévy movement, where the dispersal length  $l > 1$  is drawn from the power-law distribution  $P(l) = cl^{-\beta}$ , where  $\beta$  is the power-law exponent and  $c$  the normalization constant. The parameter  $\beta$  describes the range of movement behaviors. For  $\beta \geq 3$ , the random walk is similar to Brownian motion. For  $1 < \beta < 3$ , the movement becomes superdiffusive (Lévy) and reaching to straight-line paths (ballistic motion) as  $\beta \rightarrow 1$ . In our model, we consider that the encounter of grazer-vegetation results in the decay of vegetation with a probability  $\mu$ , and vegetation growth is seasonal. The rejuvenation of vegetation takes place at regular time intervals through resource pulses. We simulate the grazer-vegetation model on a 2D regular lattice of length  $L = 100$ , with the power-law exponent  $1 < \beta \leq 3.5$ . The spatially averaged grazer and vegetation densities are denoted by  $g$  and  $v$ , respectively. We initialize the simulations with  $g_0 = \rho \times v_s$  number of grazers randomly distributed into the matrix after the vegetation has reached a steady state abundance  $v_s$ .

## 4.3 Results

### 4.3.1 Population dynamics with different movement strategies

We analyze the population dynamics for different adapted movement strategies by the grazers. Allowing the vegetation to reach its equilibrium density for a fixed

reproduction rate ( $p$ ), grazers-vegetation dynamics is determined for a range of movement varying from ballistic ( $\beta \sim 1$ ) to Brownian ( $\beta \geq 3$ ) motion. We observe different vegetation and grazer interaction scenarios for a fixed rate of grazers' mortality ( $m$ ), we observe different vegetation and grazer interaction scenarios.

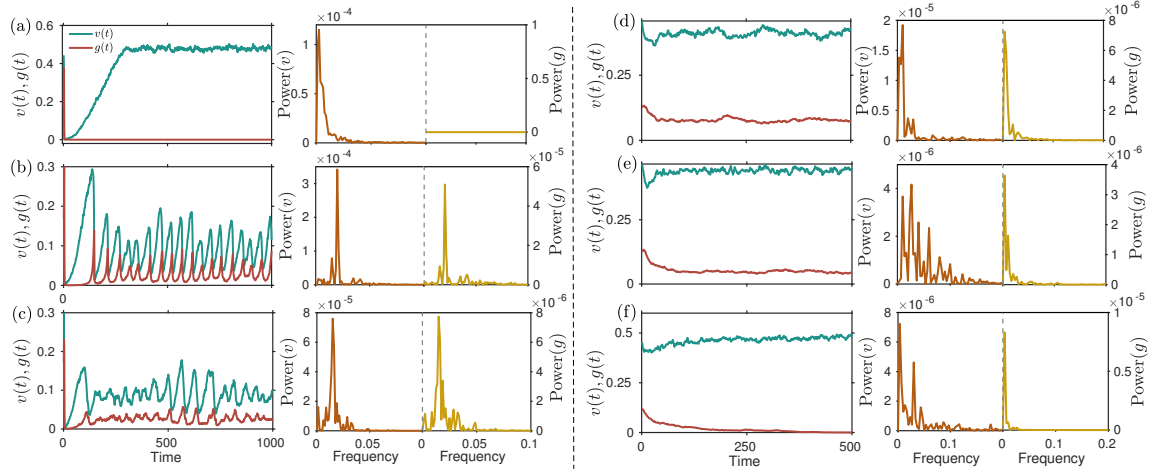


**Figure 4.2.** Evolution of the spatially averaged densities  $v(t)$  (vegetation) and  $g(t)$  (grazers) where the mortality rate of grazers are considered as  $m = 0.07$  (in (a)-(c)), and  $m = 0.2$  (in (d)-(f)). Time series and the corresponding power spectrum illustrate three different population scenarios: extinction of grazers, steady state coexistence, or oscillatory coexistence, depending upon the value of  $\beta$ , which determines the range of movement: (a), (d)  $\beta = 1.1$ ; (b), (e)  $\beta = 2.2$ ; and (c), (f)  $\beta = 3.5$ . Other parameters are  $p = 0.7$ ,  $\mu = 0.2$ , and  $L = 100$ .

As observed from Fig. 4.2(a), for an intermediate mortality rate ( $m = 0.07$ ), the highly superdiffusive grazers ( $\beta \sim 1$ ) in the initial time surpass the vegetation, which leads to the decay of vegetation (see Fig. 4.3(a) left). The random diffusion of grazers in space leads to the exploitation of vegetation to the extent that decreases grazers' density, which in the long term goes to zero. On the extinction of grazers, vegetation proliferates as a result of resource pulse and thus reaches its maximum abundance obtained from the contact process (see Fig. 4.3(a) right). In contrast, with the same parameter values, for the Brownian motion ( $\beta > 3$ ), our model predicts oscillatory species coexistence, clearly illustrated by the time-series and the corresponding spectral analysis in Fig. 4.2(c) and its configuration is depicted in Fig. 4.3(b).

Grazer-vegetation encounter shows drastically different dynamics in environments not favorable for grazers. The preceding results signify that the Brownian motion stabilizes coexistence compared to ballistic motion. However, in adverse conditions, when the mortality of grazers is high ( $m = 0.2$ ), we perceive the extinction of grazers for  $\beta > 3$  (see Fig. 4.2(f)). Due to its slow diffusion, a Brownian grazer has a high probability of staying in the vicinity of a focal cell, leading to poor utilization of the vegetation and, hence, the collapse of grazers. On the contrary, ballistic movements induce steady-state coexistence as observed from Fig. 4.2(d). Random motion of

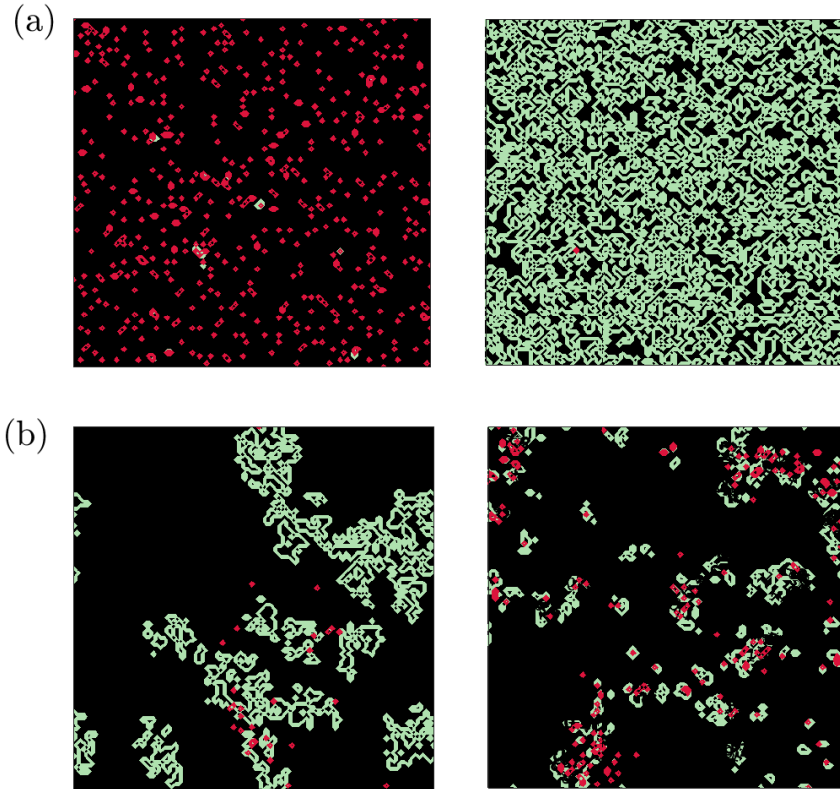


**Figure 4.3.** Initial (left panel) and final (right panel) time configurations of grazers (in red) and vegetation (in green) at an intermediate rate of mortality ( $m = 0.07$ ). (a)  $\beta \sim 1$  (highly superdiffusive grazers): the left panel shows the initial time density configuration when grazers have outreached vegetation. This leads to the extinction of grazers on reaching the final time (right panel) and the rejuvenation of vegetation due to resource pulse, (b)  $\beta = 3.5$  (Brownian grazers): grazers and vegetation coexist in the final time (right panel). Other parameters are  $p = 0.7$ ,  $\mu = 0.2$ , and  $L = 100$ .

the grazers increases its encountering probability with the vegetation. However, due to high mortality, grazers' abundance cannot exceed that of the vegetation, leaving time for vegetation to rejuvenate. Thus, resulting in species' coexistence (steady-state) of species, the spatial configuration is illustrated in Fig. 4.7. For the intermediate range of Lévy exponent ( $\beta \sim 2$ ), our model shows the coexistence of species determined by grazers adopting Lévy walk and the rate of mortality. We observe the oscillatory coexistence of vegetation and grazers for an intermediate rate of mortality (see Fig. 4.2(b)), whereas, at high mortality, population densities settle down to steady-states (coexisting) as shown in Fig. 4.2(e). Therefore, as analyzed from the dynamics, our model suggests that at the intermediate  $\beta$  value, mortality does not adversely affect the population abundance.

As observed, ballistic movements ( $\beta \sim 1$ ) can prevent extinction at high rates of grazers' mortality, which is not the case when  $m = 0.07$ , where the Brownian foragers

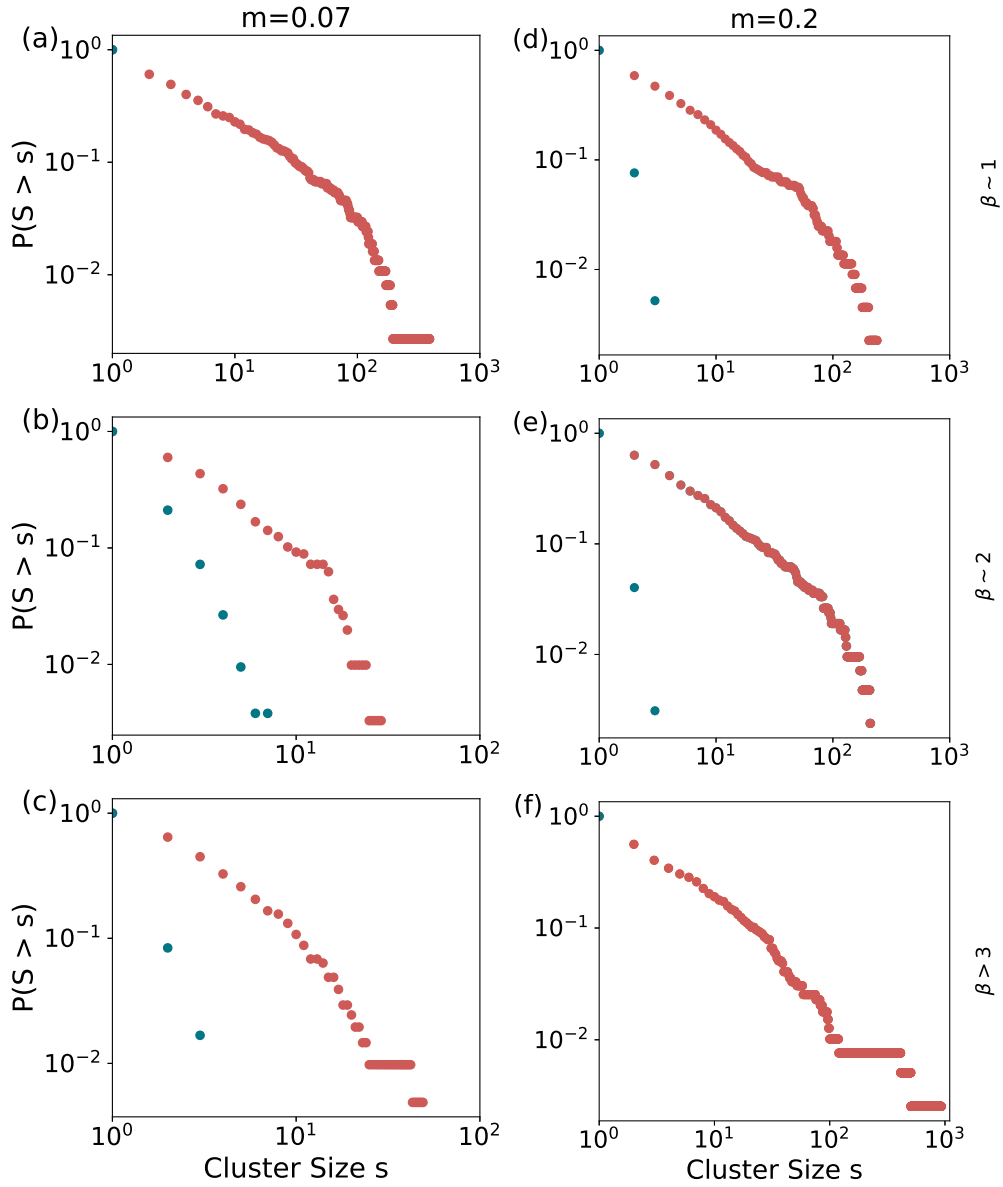


**Figure 4.4.** Cluster size distribution of vegetation (red) and grazers (green) for different values of  $m$  and  $\beta$ . Left ((a)-(c)) and right panels ((d)-(f)) show the trends corresponding to  $m = 0.07$ , and  $m = 0.2$ , respectively, where in (a), (d)  $\beta \sim 1$ ; (b), (e)  $\beta \sim 2.2$ ; and (c), (f)  $\beta > 3$ . Other parameters are  $\mu = 0.2$ ,  $p = 0.7$ , and  $L = 100$ .

are more likely to promote coexistence (see Fig. 4.2). Therefore, to investigate this, we analyze the population distribution in the landscape for different foraging strategies  $\beta$  and mortality rates ( $m$ ) through the cluster size distribution (CSD).

We calculate inverse cumulative distribution function (CDF) for  $m = 0.07$ , and  $m = 0.2$  at different values of  $\beta$  ranging from straight line paths ( $\beta \sim 1$ ) to Brownian movements ( $\beta > 3$ ) in Fig. 4.4. The CDF shows a declining trend, indicating the relatively small probability of the species being distributed in large clusters. However, the probability of the formation of large clusters increases as the value of  $\beta$  rises from 1.1 (see Fig. 4.4(a) and Fig. 4.4(d)) to  $\beta = 3.5$  as shown in Fig. 4.4(c)

and Fig. 4.4(f), which reflects the fact that the large  $\beta$  values makes the foragers sessile, restricting their movements to the nearby sites, hence, resulting in more particles in a cluster. Moreover, the effect of  $m$  on the distribution of grazers in the landscape is also well depicted in Fig. 4.4(a) and Fig. 4.4(f). As noticed, when  $m = 0.07$ , ballistic motion results in the complete elimination of grazers from the landscape (see Fig. 4.4(a)), and interestingly, this goes for the Brownian foragers when the mortality rate is increased to  $m = 0.2$  (see Fig. 4.4(f)).

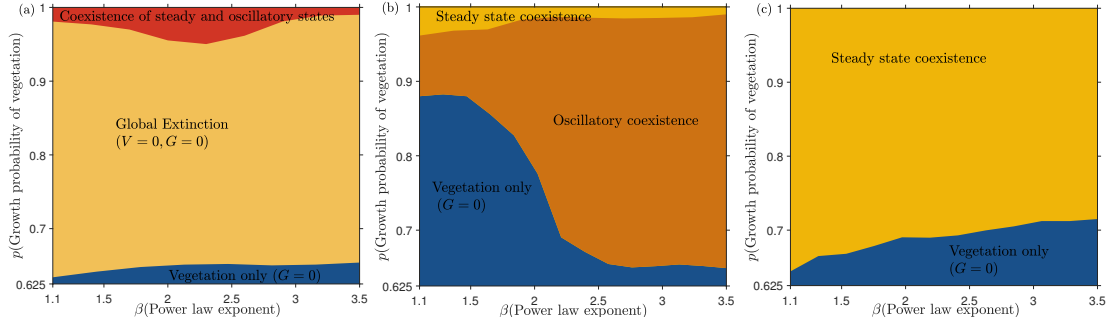


**Figure 4.5.** Phase diagrams in the  $(\beta, p)$ -plane depicting various dynamical regimes corresponding to (a)  $m = 0.04$ , (b)  $m = 0.07$ , and (c)  $m = 0.2$ . Other parameters are  $\mu = 0.2$ , and  $L = 100$ .

### 4.3.2 Vegetation's reproduction rate and foraging behavior

We here analyze the simultaneous effect of vegetation growth and Lévy exponent on spatiotemporal dynamics for which we compute the phase diagrams in  $(p, \beta)$  parameter planes. Keeping the mortality  $m$  fixed to 0.04, 0.07 and 0.2, we vary  $p$  and  $\beta$  correspondingly in Fig. 4.5(a), Fig. 4.5(b), and Fig. 4.5(c). We observe that the movement strategy ( $\beta$ ) does not affect the system's behavior for a low  $p$  value (meager resources), resulting in grazer extinction at all the considered mortality rates. However, increasing the value of  $p$  gives rise to different dynamical regimes depending upon the mortality rate  $m$  and the Lévy exponent ( $\beta$ ). As shown in the phase diagrams (see Fig. 4.5), the ballistic movements ( $\beta \sim 1$ ) and the Brownian grazers ( $\beta > 3$ ) show diverse outcomes in line with mortality  $m$ . According to Fig. 4.5(a), increasing vegetation growth enhances the chance of encountering grazers with vegetation. However, a very low mortality rate of grazers ( $m = 0.04$ ) leads to over-exploitation of vegetation, thus eventually resulting in global extinction. Further, higher  $p$  values increase the chance of vegetation survival, and hence, vegetation-grazer coexistence is observed. Further, Fig. 4.5(b) illustrates that for an intermediate rate of mortality ( $m = 0.07$ ) and the value of  $\beta > 3$ , the system transitions from a region of grazer extinction to the oscillatory regime for a much lower value of  $p$  ( $\sim 0.65$ ), which however increases to  $\sim 0.88$  as the foraging strategy changes from the Brownian to Ballistic movement. Further, increasing the value of

$p$  results in the transition from oscillatory coexistence to a region of steady-state coexistence. On the contrary, as analyzed, at a high rate of mortality ( $m = 0.2$ ), gazers with ballistic movements show a transition from extinction to a steady-state coexistence at a lower  $p$  value ( $\sim 0.65$ ), whereas, for the Brownian grazers, higher resource abundance ( $p \sim 0.72$ ) is required to promote the survivability.

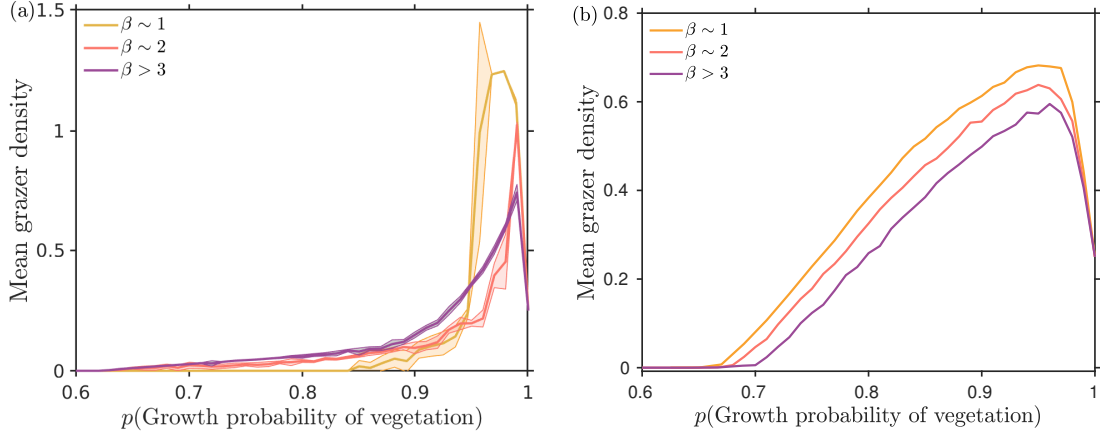


**Figure 4.6.** Average grazer density as a function of  $p$  at (a)  $m = 0.07$ , and (b)  $m = 0.2$  for three different values of  $\beta$ . The shaded region corresponds to the oscillatory population dynamics and is represented by the 95% confidence interval. Other parameters are  $\mu = 0.2$ , and  $L = 100$ .

To gain a comprehensive understanding, we calculate the average grazer abundance as a function of  $p$  for different values of  $\beta$  and  $m$  (see Fig. 4.6). We observe that beyond a threshold value of  $p$ , all the movement strategies effectively maintain the grazer's abundance; however, the effect of the Lévy exponent on the systems' dynamics largely depends upon the value of  $m$ . As shown in Fig. 4.6(a), for  $m = 0.07$ , the threshold value of  $p$  required for the transition to oscillatory state and the maintenance of abundance is high for the Ballistic grazers (also see Fig. 4.5(a)). We here observe that up to  $p \sim 0.92$ , the Brownian strategy leads to a relatively higher average abundance of grazers than Lévy and the ballistic movements. However, ballistic foragers result in high average density (irrespective of  $p$ ), in contrast to Lévy and Brownian movement for  $m = 0.2$ , as illustrated in Fig. 4.6(b). High mortality does not allow grazers to surpass vegetation, while ballistic motion increases the chances of an encounter, thus maintaining species richness. Another exciting result observed through this analysis is that after a certain threshold of  $p \sim 0.96$ , the grazer's abundance in the coexisting domain (steady state) drops somewhat, irrespective of the foraging strategy. Moreover, at a low growth rate ( $p \sim 7$ ), when resource density is less, Fig. 4.6(b) suggests that, at a high rate of mortality ( $m = 0.2$ ), ballistic movements ( $\beta \sim 1$ ), characterized by random large displacements can increase the probability of food capture and hence are more efficient than the Brownian foraging ( $\beta > 3$ ). However, the opposite results are observed in the case of a low rate of mortality ( $m = 0.07$ ) (see Fig. 4.6(a)).



## 4.4 Discussion

Although resource pulse promotes species coexistence (Chesson and Warner, 1981; Warner and Chesson, 1985), it does not avert the significant impacts the other mechanisms might have on ecosystems. Here, considering resource pulse in our stochastic vegetation-grazer model, we analyze the unified effects of foraging behavior and life-history traits on the dynamics of spatial ecosystems. When the vegetation has attained a state of equilibrium density, the adaptability of grazers to the landscape and the evolution of vegetation and grazers is determined primarily by the foraging strategy ( $\beta$ ) and the mortality rate of grazers ( $m$ ).

Movement strategies are vital in maintaining connectivity and increasing species survival in a fragmented landscape. The work by Shlesinger and Klafter (1986); Dannemann et al (2018) suggests that Lévy walks optimize search in scarce environments, whereas Niebuhr et al (2015) observed straighter paths (Ballistic) as the optimal movement strategy in all situations. Our study finds that the efficient search strategy changes depending on the species' mortality rate. As analyzed from Fig. 4.2(a-c), the overexploitation of vegetation at the initial time due to the lower mortality rate (higher grazing risk) leads to a significant drop in resource abundance (also see Fig. 4.3(a) (left panel)). The grazers of pulsed vegetation show an adaptive response through movement strategies, which affects their evolution. Lévy walk and Brownian foraging result in oscillatory species coexistence. However, straight search paths due to the high probability of missing an encounter with the vegetation, especially when the resources are scarce, result in the extinction of grazers (see Fig. 4.2(a)).

Results regarding the optimal search behavior are likely to reflect what happens when the mortality risk of grazers is increased. In contrast to low mortality, a high mortality rate decreases the grazing risk, due to which grazer's density does not exceed the vegetation abundance. Therefore, contrary to our previous findings where Lévy and Brownian searches happened to be effective search strategies by promoting species coexistence, here we observe that the optimal movement behavior changes from the Brownian to ballistic walk (see Fig. 4.2(d-f)). This reflects that under the risk of high mortality, the only way would be to increase the rate of finding a resource, which is only possible because of a straight-line search (Zollner and Lima, 1999). The long displacement in superdiffusive walk ( $\beta \sim 1$ ) counterbalances the effect of high mortality, which is not possible in the case of Brownian foragers.

Our analysis of an effective movement strategy at different mortality rates across a range of vegetation growth  $p$  aligns with Fig. 4.2. The results show that the Lévy walk can be an optimal foraging strategy in the discussed scenarios of  $m = 0.07$  and  $m = 0.2$ . However, as observed in Fig. 4.6, the Brownian movement at  $m = 0.07$



and the ballistic strategy at  $m = 0.2$  are relatively more effective in maintaining the population size with the amount of vegetation availability. Increasing the value of  $p$  to the maximum probability accelerates vegetation growth in the landscape. Because of the limited space, the abundance of vegetation cannot increase further in the absolute sense. However, it can increase if the abundance of the other species (grazers) relatively decreases (Chesson and Warner, 1981). Thus, due to the prominent effect of growth rate  $p$  on the vegetation abundance, we observed a sufficient decrease in the grazer abundance.

In summary, this chapter unveils the interdependence of movement behavior and species' survival rate. It reports the significant aspect of resource pulse on the persistence and stability of populations in the fragmented landscape. Our analysis shows that the optimal foraging strategy highly depends upon the survival conditions and the amount of resources. We observe that Lévy walk is always an effective movement strategy; however, the optimal foraging behavior changes from the Brownian to ballistic with the increase in the rate of mortality of grazers. However, considering the higher trophic interactions in a heterogeneous landscape, which incorporates the dispersal costs, is an important future direction to investigate the effect of movement on landscape connectivity and ecological stability.

## 4.5 Appendix

### 4.5.1 Spatial configuration at $m = 0.2$

The spatial distribution of the species clearly illustrates the evolution of vegetation and grazers subject to the movement behavior (see Fig. 4.7). The figure shows the configuration at initial and large time corresponding to Ballistic (Fig. 4.7(a)) and the Brownian grazers (Fig. 4.7(b)). As observed for  $\beta \sim 1$  in Fig. 4.7(a), our model predicts vegetation-grazer coexistence (also see Fig. 4.2(d)), whereas we perceive the extinction of grazers at large time for  $\beta > 3$  (see Fig. 4.7(b) and Fig. 4.2(f)).

### 4.5.2 Stochastic lattice vegetation-grazer model

**Stochastic rules** We consider the space to be a 2D lattice of  $N = L \times L$  square sites with periodic boundary conditions where the position of each site is labeled by a vector  $n \in \mathbb{Z}^2$ .  $L^2/4$  initial vegetation is randomly distributed in the landscape, where each site is then empty ( $\phi$ ), or vegetation occupied ( $V$ ). The state transitions for the vegetation corresponding to (4.1) are given as:

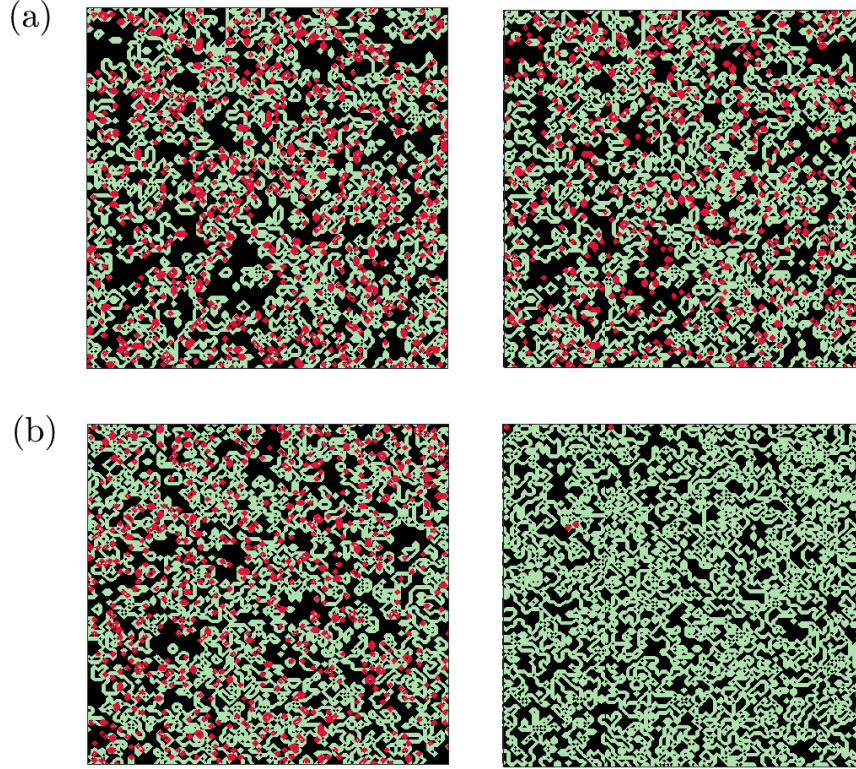


**Figure 4.7.** Initial (left panel) and final (right panel) time configurations of grazers (in red) and vegetation (in green) at a high rate of mortality ( $m = 0.2$ ) for (a) highly superdiffusive grazers ( $\beta \sim 1$ ), (b) Brownian grazers ( $\beta = 3.5$ ). Other parameters are  $p = 0.7$ ,  $\mu = 0.2$ , and  $L = 100$ .

$$\begin{aligned} V\phi &\xrightarrow{p} VV, \\ V\phi &\xrightarrow{1-p} \phi\phi, \\ VV &\xrightarrow{1-p} \phi V, \end{aligned}$$

where  $p$  is the reproduction rate of vegetation. The system is allowed to reach an equilibrium density where  $V_0$  is the total number of vegetation in the landscape of size  $N$ . Later,  $V_0/4$  initial grazers are randomly introduced in the lattice. Now, each site can be either empty ( $\phi$ ), vegetation occupied ( $V$ ), with vegetation and grazer ( $VG$ ), or with grazer reproduction ( $GG$ ). The stochastic state transitions governing the dynamics are then modeled as follows:

$$\begin{aligned} G &\xrightarrow{m} \phi, \\ G\phi &\xrightarrow{\lambda_0} \phi G, \\ GV &\xrightarrow{\mu} G\phi, \\ GV &\xrightarrow{\tilde{\mu}} GG, \\ V\phi &\xrightarrow{p} VV, \\ V\phi &\xrightarrow{1-p} \phi\phi, \\ VV &\xrightarrow{1-p} \phi V, \end{aligned}$$

where  $m, \lambda_0, \mu, \tilde{\mu}(= e\mu)$  are the grazer mortality rate, grazer dispersal rate, grazer attack rate, and grazer reproduction rate, respectively.

The average abundance of grazer ( $g$ ) and vegetation ( $v$ ) is defined as  $v = V/L^2$  and  $g = G/L^2$ , where  $V$  and  $G$  is the total number of vegetation and grazer in the  $L^2$  sites, respectively.

### 4.5.3 Detailed model description

**Monte Carlo simulation of the stochastic model:** We simulate the stochastic dynamics using the Monte Carlo method. A Monte Carlo time step corresponds to selecting all individuals on the lattice once on average.

An occupied site is chosen randomly at each elementary step and updated as follows:

#### Vegetation dynamics in the absence of grazers

We update the site using the contact process (Sankaran et al, 2019) by the rules:

- One of the four nearest neighbors of the chosen site (focal cell) is selected randomly. If that site is empty, vegetation reproduces there with the probability  $p$ ; else, the vegetation in the focal cell dies (the probability for which is  $(1 - p)$ ).
- If the randomly selected cell of the four nearest neighbors of the chosen site is occupied, the vegetation in the focal cell dies with probability  $(1 - p)$ .

The above rules are iterated  $L^2$  times in every discrete time step until the system reaches steady vegetation density.

#### Vegetation-grazer dynamics

Once the vegetation reaches an equilibrium density, its fraction  $\rho$  is introduced as the initial grazer density. Each grazer is assigned some random energy  $E_g$  in the range  $[1, E_t]$ , where  $E_t$  is the threshold energy, then the dynamics are given as follows:

- **Grazer death:** If the chosen site has a grazer, it dies with probability  $m$ .
- \* *If a grazer survives at the selected site,*
- **Grazer movement:** The selected grazer moves to a new site at a distance  $l > 1$ , where  $l$  is drawn from a power law distribution  $P(l) = cl^{-\beta}$ , with  $\beta$  as an exponent and  $c$  the normalization constant.

- **Grazer energy and resource consumption:** The total number of vegetation ( $V_c$ ) from the new site and the four nearest neighbors of the new site results in the energy gain of grazer, thus the energy of grazer is increased by  $N_c$ , i.e.,  $E_g = E_g + V_c$ . One site is chosen randomly from the  $V_c$  vegetation inhabited sites. The grazer consumes the vegetation in that site with the probability  $\mu$ .
- **Grazer reproduction:** The selected grazer reproduces with the probability  $\tilde{\mu} = \frac{E_i^2}{E_i^2 + E_g^2}$  in the new site. The energy of the reproduced grazer and the newborn grazer is updated to  $\frac{E_g}{2}$ .

The update rules are iterated for total time  $T$ , in which after every  $t_v = 50$  discrete time steps, vegetation rejuvenates (resource pulse) as per the rules of the contact process.

# Chapter 5

## Climate warming and dispersal strategies determine species persistence in a metacommunity

---

### 5.1 Introduction

Biological diversity is fundamental for the functioning of life on Earth, and rapid anthropogenic climate warming is likely to exacerbate the loss of global biodiversity. Extensive evidence suggests that climate disruptions have already caused complex consequences to the distribution of species all over the world ([Pimm, 2009](#); [Thomas et al, 2004](#); [Walther et al, 2002](#)). Changing climate outside the extent of species adaptability results in the collapse of ecosystem-level diversity. The rising temperature is known to lower species abundance which in turn triggers extinction. For instance, current estimates of biodiversity loss predict that climate warming might lead to 3% to 78% of species extinction ([Thomas et al, 2004](#); [Thuiller et al, 2004](#)). Biodiversity supports the functioning of ecosystems needed for human subsistence, which is now being affected by the rising temperature. Thus, anticipating species' response to climate warming to mitigate future extinction risks is important ([Dillon et al, 2010](#); [McMahon et al, 2011](#)). However, the resistance and resilience of biological communities to rising temperature and their possible implications on ecosystems remain uncertain.

Ecologists are trying to anticipate and assimilate what effect the rising temperature can have on species. This is a challenging question because increasing temperature does not only influence species abundance but also the complex interactions with other species in a community ([Connell, 1961](#); [Harrington et al, 1999](#); [Walther, 2007](#)). It is also evident from previous studies that the response of species towards changing environmental conditions is carried out by changes in phenology and distribution ([Sparks and Carey, 1995](#); [Dunn and Winkler, 1999](#); [Cayan et al, 2001](#)). Further evidence ([Walther et al, 2005](#); [Parmesan, 2006](#)) suggests species will disperse to

a suitable climate niche as a response to changing temperature. Nevertheless, it is also certain that any change in local conditions determines the efficacy of dispersal at the population level. (Milne and Guichard, 2021) study the dynamics of phase locking and frequency modulation in predator-prey metacommunity with heterogeneity in the carrying capacity. They find that increasing coupling strength led to phase-locked synchrony and constant coupling strength with increasing heterogeneity drives the dynamics from phase-locked synchrony to phase asynchrony and to phase drift, hence illustrating the effect of habitat heterogeneity on dispersal-driven synchrony. Thus, it is critical to understand the role of local species dynamics which indirectly influence dispersal via population abundance.

Species dispersal can have conflicting consequences on population persistence. Asynchrony between the abundance of sub-populations leads towards regional stability (Briggs and Hoopes, 2004). Dispersal promotes stability by allowing recolonization, but at times it can elevate the chance of extinction by globally synchronizing populations. Dispersal, being sensitive to changing climatic conditions (Travis et al, 2013), patch size (Andreassen and Ims, 2001), food availability, population size (Matthysen, 2005), considerably varies within organisms. Moreover, emigration and immigration rates strongly influence the population dynamics in a patch and thus alter the chances of regional persistence. Therefore, various processes in a metacommunity whereby dispersal can inhibit or promote synchrony should be examined. Ims and Andreassen (2005) and Li et al (2005) have shown that dispersal patterns depending upon local abundance result in diminishing synchrony in comparison with density-independent dispersal. Likewise, there is mounting theoretical and empirical evidence accentuating the effect of temperature on metacommunity dynamics. de Boer et al (2014) demonstrated that dispersal reinforced recovery in the biomass of communities subjected to heat stress. Narang et al (2019) found that long-range dispersal at extreme temperatures maintains species' persistence by reducing spatial synchrony. An experimental study by Thompson et al (2015) shows that dispersal promotes asynchronous fluctuations under ambient conditions, but synchrony among species increases with warming. Therefore, the dependency of dispersal on population size and temperature drives us to examine their combined effects in stabilizing or destabilizing the dynamics.

Following the previous investigations, species interactions and density dependence are imperative in determining population abundance under climate warming (Ives and Gilchrist, 1993; Ives, 1995). Hauzy et al (2010) have studied the role of constant and density-dependent dispersal on the stability of a metacommunity. They find that density-dependent dispersal, particularly interspecific density-dependent dispersal, always results in asynchronous fluctuations in population abundance. However, whether dispersal can induce stability under changing environmental conditions is

still unclear. Can rising temperature promote synchrony and erode the stabilizing dynamics by dispersal?

In an attempt to answer these questions, here we consider a metacommunity model with temperature-dependent traits and study how the rising temperature governing species' local dynamics alters dispersal response at the regional scale. We consider different dispersal rates of resource and consumer and analyze the effect of constant and density-dependent dispersal on the stability of metacommunity under changing temperatures. For this, we study spatial synchrony and analyze how coherence or incoherence in species abundance is affected by different dispersal mechanisms and thermal traits. The two aspects: rising temperature and dispersal abilities, together are observed to affect the stability, measured by the coefficient of biomass variation. Our results show that density-dependent dispersal could modify metacommunity stability by affecting spatial synchrony at high temperatures. We then extend our study to a larger spatial scale and determine the coexistence of coherent and incoherent dynamics.

## 5.2 Models and Methods

### 5.2.1 A two patch metacommunity model

We consider a theoretical metacommunity model that includes resource-consumer populations inhabited in patches. Local dynamics of resource and consumer are governed by the Rosenzweig-MacArthur model ([Rosenzweig and MacArthur, 1963](#)), where resource follows the logistic growth rate, and the dynamical evolution of consumer is based upon Holling type-II functional response. For simplicity, we start with a 2-patch metacommunity, where each patch behaves homogeneously in terms of resource-consumer interactions and phenotypes. The model assumes temperature-dependent life-history traits of species, which affect the metacommunity dynamics at the regional scale. The population in each patch is connected by dispersal, and the dispersal propensity depends upon the species abundance of the natal patch. In the  $i$ -th patch, the dynamics of resource ( $N_i$ ) and consumer ( $P_i$ ) abundances are governed by the following equations:

$$\frac{dN_i}{dt} = r(T)N_i\left(1 - \frac{N_i}{K}\right) - \frac{a(T)N_iP_i}{N_0 + N_i} - N_iD_n(N_i, P_i) + N_jD_n(N_j, P_j), \quad (5.1a)$$

$$\frac{dP_i}{dt} = \frac{a(T)N_iP_i}{N_0 + N_i} - m(T)P_i - P_iD_p(N_i, P_i) + P_jD_p(N_j, P_j), \quad (5.1b)$$

where  $i, j = 1, 2$  determine the patch index and  $i \neq j$ ,  $K$  is the carrying capacity of resource and  $N_0$  is the half-saturation constant,  $D_n(N_i, P_i)$  and



$D_p(N_i, P_i)$  are respectively per capita dispersal rates of resource and consumer depending upon either resource ( $N_i$ ) or consumer ( $P_i$ ) abundance. To examine the effects of temperature on resource-consumer interactions, we consider the growth rate of resource  $r$ , attack rate  $a$ , and mortality  $m$  of the consumer as the temperature-dependent parameters. These functional traits of species represent their performance with changing temperatures. Previous research has shown that the thermal response of metabolic traits of ectotherms follows characteristic shapes. The intrinsic growth rate of resource  $r$  and attack rate of consumer  $a$  show a hump-shaped relationship with temperature (Englund et al, 2011; Thomas et al, 2012; Amarasekare, 2015), and mortality of consumer  $m$  increases exponentially with increasing temperature (Savage et al, 2004). Moreover, various studies consider thermal performance curves of ectotherms to be asymmetric (Izem and Kingsolver, 2005; Gilchrist, 1995). Here, temperature-dependent intrinsic resource growth rate  $r$  and consumer attack rate  $a$  are formulated following Gompertz-Gaussian function (Martin and Huey, 2008; Fey and Vasseur, 2016) as:

$$r(T) = r_{opt} \times \exp \left[ -\exp(0.75 \times (T - T_n) - 8) - \frac{(T - T_n)^2}{300} \right], \quad (5.2)$$

and

$$a(T) = a_{opt} \times \exp \left[ -\exp(0.75 \times (T - T_p) - 8) - \frac{(T - T_p)^2}{400} \right], \quad (5.3)$$

where  $r_{opt}$ ,  $a_{opt}$  are the scaling parameters, and  $T_n$ , and  $T_p$  are the optimum temperature of resource and consumer, respectively.

We consider the temperature dependent consumer mortality  $m$  as (Vasseur and McCann, 2005; Kaur and Dutta, 2020):

$$m(T) = m_{opt} \times \exp \left[ A_p \times \left( \frac{1}{T_p} - \frac{1}{T} \right) \right], \quad (5.4)$$

$m_{opt}$  is the scaling parameter, and  $A_p$  is the Arrhenius constant. These temperature-dependent traits take the form as exhibited in Fig. 5.1.

To explore spatial population dynamics, we broadly categorize dispersal in two ways, i.e., constant dispersal (CD) and density-dependent dispersal (DD) (intraspecific and interspecific) (see Fig. 5.2). The model assumes CD in both species, whereas intraspecific DD and interspecific DD in either resource or consumer. Thus per capita dispersal rate for resource and consumer in the  $i$ -th patch correspondingly takes the form (Hauzy et al, 2010):

$$D_n(N_i) = d_n \frac{N_i^{x_{nn}}}{S_{nn}^{x_{nn}} + N_i^{x_{nn}}} \quad \text{or} \quad D_n(P_i) = d_n \frac{P_i^{x_{np}}}{S_{np}^{x_{np}} + P_i^{x_{np}}}, \quad \text{and} \quad (5.5)$$



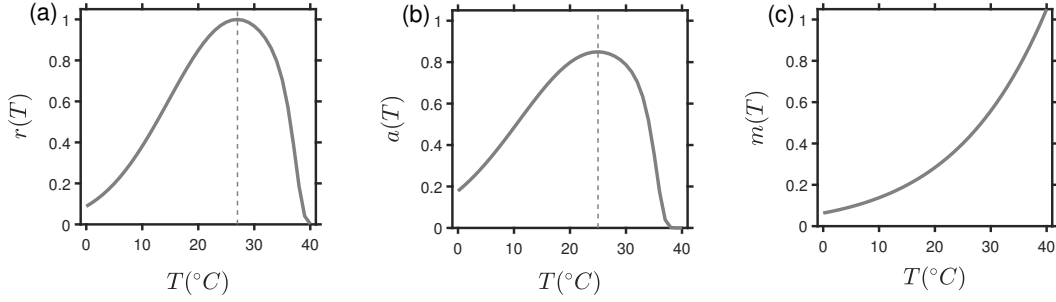


**Figure 5.1.** Temperature-dependent species biological traits: (a) Intrinsic growth of resource with varying temperature ( $T$ ). (b) Thermal response of consumer's attack rate. (c) Temperature-dependent mortality of consumers.

$$D_p(N_i) = d_p \frac{N_i^{x_{pn}}}{S_{pn}^{x_{pn}} + N_i^{x_{pn}}} \quad \text{or} \quad D_p(P_i) = d_p \frac{P_i^{x_{pp}}}{S_{pp}^{x_{pp}} + P_i^{x_{pp}}}, \quad (5.6)$$

where  $d_n$  and  $d_p$  determine the maximal per capita dispersal rates of resource and consumer, respectively.  $S_{\alpha\beta}$  ( $\alpha = n, p$ ;  $\beta = n, p$ ) is close to the mean species abundance of the isolated population (varies with temperature).  $x_{\alpha\beta}$  specifies shape of dispersal:  $x_{\alpha\beta} = 0$  signifies CD with rate  $\frac{d_\alpha}{2}$ ,  $x_{\alpha\beta} > 0$  implies positive relation of species abundance and dispersal, whereas  $x_{\alpha\beta} < 0$  justifies negative effect of species abundance on dispersal. Thus, we consider  $x_{nn} > 0$ ,  $x_{np} > 0$ ,  $x_{pp} > 0$ , and  $x_{pn} < 0$ . [Jenkins et al \(2007\)](#) emphasize the role of body size on dispersal abilities of species, thus suggesting, different dispersal rates of resource and consumer can lead to important dynamics of a system. In this chapter, we focus on two instances, i.e, the maximal dispersal rate  $d_n$  of resource is greater than the maximal dispersal rate  $d_p$  of consumer (i.e.,  $d_n > d_p$ ) and otherwise (i.e.,  $d_n < d_p$ ).

To measure the effect of changing temperature and dispersal strengths on spatial synchrony, we calculate Pearson correlation coefficient  $r_{ij}$  between species abundance in two patches which is defined as:

$$r_{ij} = \frac{\langle x_i x_j \rangle - \langle x_i \rangle \langle x_j \rangle}{\sqrt{\langle x_i^2 \rangle - \langle x_i \rangle^2} \sqrt{\langle x_j^2 \rangle - \langle x_j \rangle^2}}, \quad (5.7)$$

where  $x$  is either resource or consumer abundance,  $\langle \dots \rangle$  denotes the average over a given time  $t$ , denoted as:

$$\langle \dots \rangle = \frac{1}{t' - t_0 + 1} \sum_{t=t_0}^{t=t'} a(t), \quad (5.8)$$

where  $a(t)$  is species abundance at time  $t$  and  $i, j \in \{1, 2\}$ . The more the coefficient to 1, the more the system exhibits synchronous solutions.  $r_{ij} = 1$  represents complete

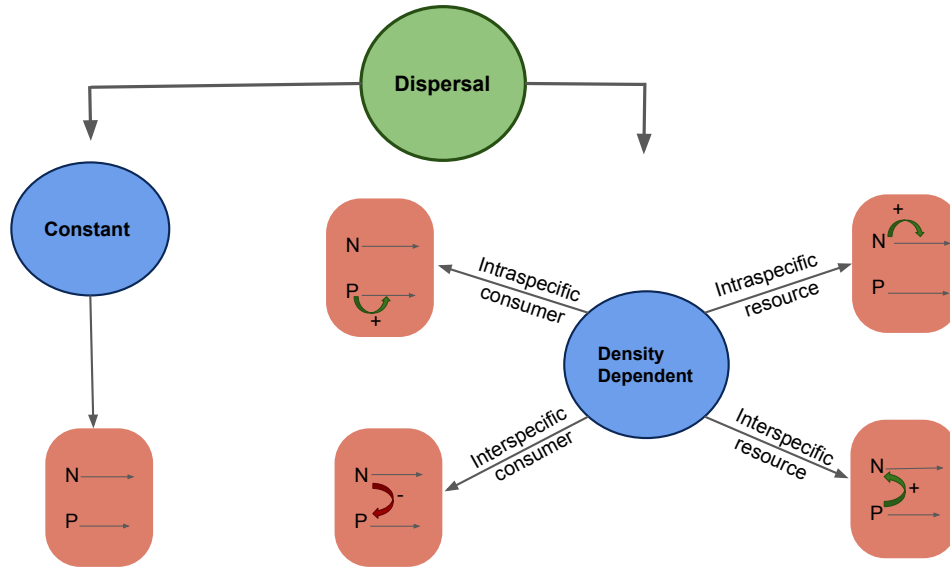


**Figure 5.2.** Schematic representation of different types of dispersal mechanisms, where  $N$  and  $P$  are the resource and consumer abundance, respectively. '+' sign describes the positive effect of resource abundance ( $N$ ) or consumer abundance ( $P$ ) on dispersal, and '-' sign symbolizes the negative effect of resource abundance ( $N$ ) on dispersal of consumer from the patch.

synchrony.

We also determine the persistence of species by analyzing temporal variability and the mean of regional resource and consumer abundance at different temperatures. The temporal variability is calculated by coefficient of variation as:

$$C.V. = \frac{\sqrt{\langle z - \mu_z \rangle^2}}{\mu_z}, \quad (5.9)$$

where  $z$  is the average of species time series at time  $t$  in two patches,  $\mu_z$  denotes the mean regional abundance, and  $\langle \dots \rangle$  is the average over a given time  $t$ . Moreover, for the robustness of our results, we carry out sensitivity analysis for the parameters  $N_0$  (half saturation constant) and  $K$  (carrying capacity), along with changing temperature (see Figs. 5.10(a)-(b)).

### 5.2.2 Metacommunity with a large number of patches

We also study the collective dynamics of a metacommunity model with many patches, i.e.,  $n = 100$  patches. Here, we consider a regular network with the nearest neighboring coupling; specifically, the neighboring patches are accessible by dispersal, which we have particularly taken as CD. The metacommunity model

is written as:

$$\frac{dN_i}{dt} = r(T)N_i\left(1 - \frac{N_i}{K}\right) - \frac{a(T)N_iP_i}{N_0 + N_i} + \frac{d_n}{2}(N_{i+1} + N_{i-1} - 2N_i), \quad (5.10a)$$

$$\frac{dP_i}{dt} = \frac{a(T)N_iP_i}{N_0 + N_i} - m(T)P_i + \frac{d_p}{2}(P_{i+1} + P_{i-1} - 2P_i), \quad (5.10b)$$

where patch indices  $i+1$  and  $i-1$  correspond to modulo  $n$  (total number of patches). A fascinating collective dynamics of complex systems that has emerged as an active research area is the chimera states. A chimera state results in the coexistence of synchronous and asynchronous oscillators in a network of coupled identical oscillators (Zakharova et al, 2014; Dutta and Banerjee, 2015). Depending upon the coupling strength of oscillators strong synchronous groups evolve, while some individual oscillators refuse to synchronize, thus resulting in chimera. (Vandermeer et al, 2021) using the Kuramoto model to study the emergence of one or more synchrony groups, referred to as chimeric elements depending upon the coupling strength of oscillators. Here we take into account CD in both resource and consumer with  $d_n < d_p$  and study the spatiotemporal dynamics at different temperatures. To analyze the effect of these patterns on phase dynamics, we compute mean phase velocity  $w_i$  for each node (Zakharova et al, 2014):

$$w_i = 2\pi M_i / \Delta t, \quad (5.11)$$

where  $M_i$  are the number of oscillations in time  $\Delta t$ . Throughout this work we consider the following parameter values:  $K = 25$ ,  $N_0 = 5$ ,  $r_{opt} = 1$ ,  $a_{opt} = 0.85$ ,  $m_{opt} = 0.4$ ,  $A_p = 6 \times 10^3$ ,  $T_n = 27^\circ C$ , and  $T_p = 25^\circ C$ ,  $x_{nn} = x_{np} = x_{pp} = 4$ , and  $x_{pn} = -4$ .

### 5.3 Results

Ectotherms can thrive in a specific thermal range, and it is believed that temperature rising above their thermal optimum would result in their overheating and thus reduce their fitness. Here, we vary the temperature from  $0^\circ C$  to  $40^\circ C$  and observe that rising temperature above  $31^\circ C$  leads to consumer extinction, and resource abundance saturates at their maximum capacity. However, for a range of temperature from  $0^\circ C$  to  $29^\circ C$  consumer-resource model exhibits oscillatory coexistence. Hence, we explore collective dynamics in the oscillatory range (Vandermeer, 2006) at three different temperatures, low ( $10^\circ C$ ), intermediate ( $20^\circ C$ ), and high ( $29^\circ C$ ).

### 5.3.1 Spatial synchrony

We observe different collective population dynamics depending upon: first, the kind of dispersal exhibited, second, the relative dispersal rate of resource and consumer, and third, the change in local conditions due to varying temperatures.

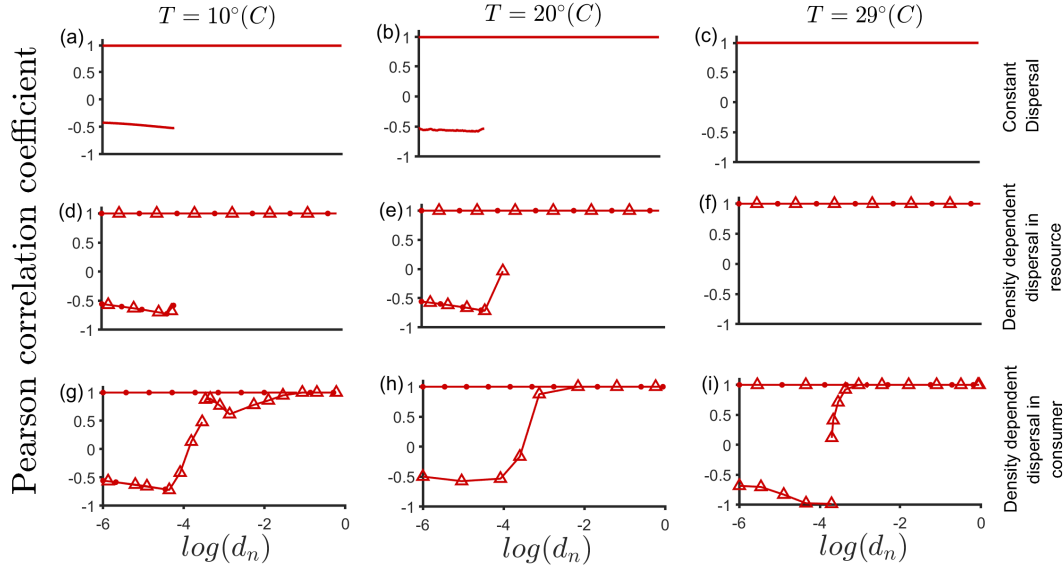


**Figure 5.3.** Species collective dynamics when  $d_n < d_p$ : Spatial synchrony with changing dispersal rates of resource ( $d_n$ ) and consumer ( $d_p = 100d_n$ ) at different temperatures ( $T$ ): For (a), (d), (g)  $T = 10^\circ C$ ; (b), (e), (h)  $T = 20^\circ C$ ; (c), (f), (i)  $T = 29^\circ C$ , in two distinct patches. (a)-(c) correspond to the dynamics for CD where  $x_{\alpha\beta} = 0$ . Intraspecific (dots) and interspecific (triangles) DD in resource and consumer follow the dynamics depicted in (d)-(f) and (g)-(i), respectively.

For constant species dispersal, as in Figs. 5.3(a)-5.3(c) where consumer dispersal is higher than a resource ( $d_n < d_p$ ), and in Figs. 5.4(a)-5.4(c) where resource dispersal is higher than consumer ( $d_n > d_p$ ), we observe that for all the three ranges of temperature, i.e.,  $T = 10^\circ C$ ,  $T = 20^\circ C$ ,  $T = 29^\circ C$  for higher dispersal values, dynamics remain completely synchronous. However, for low and intermediate dispersal strengths, and for  $T = 10^\circ C$  and  $T = 20^\circ C$  (see Figs. 5.3(a)-5.3(b), and Figs. 5.4(a)-5.4(b)), system exhibits two alternative collective dynamics, one with complete synchrony and other with strong asynchrony, as characterized by the Pearson Correlation Coefficient. Despite that, at  $T = 29^\circ C$ , dynamics remain perfectly synchronous for low and intermediate dispersal rates, as is seen in Fig. 5.3(c) and Fig. 5.4(c).

When the resource adopts DD, we notice that interspecific and intraspecific DD follow the same dynamics as CD when  $d_n < d_p$  as in Figs. 5.3(d)-5.3(f). Whilst, dynamics are seen to be affected when resource dispersal is more than that of the consumer ( $d_n > d_p$ ). We discern from Fig. 5.4(d) and Fig. 5.4(e), i.e., at low and intermediate temperatures, though low and high dispersal values maintain similar

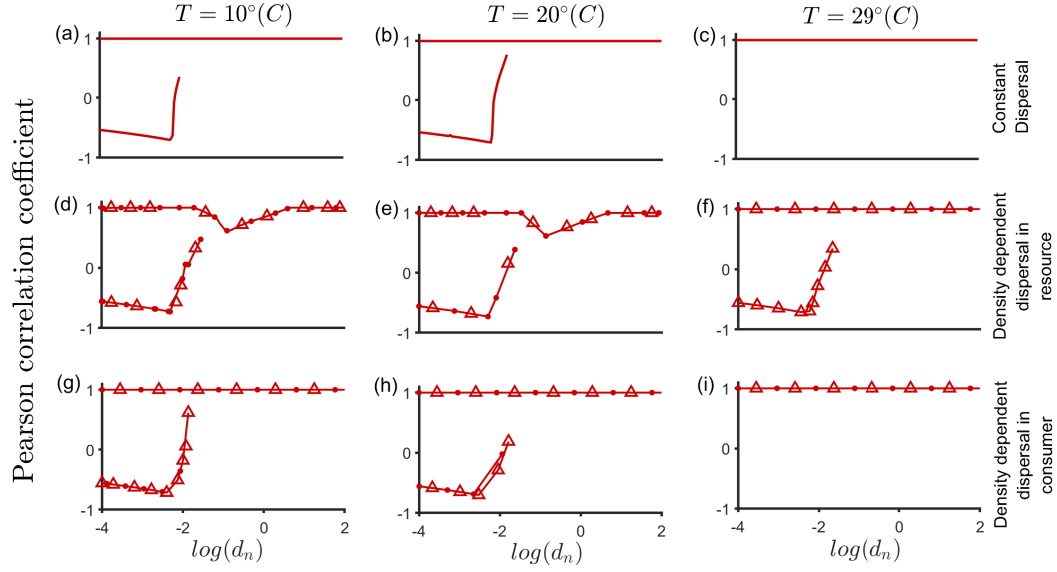


**Figure 5.4.** Species collective dynamics when  $d_n > d_p$ : Spatial synchrony of two patch metacommunity with changing dispersal rates of resource ( $d_n$ ) and consumer ( $d_p = 0.01d_n$ ) at different temperature ( $T$ ). For (a), (d), (g)  $T = 10^\circ\text{C}$ ; (b), (e), (h)  $T = 20^\circ\text{C}$ ; (c), (f), (i)  $T = 29^\circ\text{C}$ , in two distinct patches. (a)-(c) correspond to the dynamics for CD where  $x_{\alpha\beta} = 0$ . Intraspecific (dots) and interspecific (triangles) DD in resource and consumer follow the dynamics depicted in (d)-(f) and (g)-(i), respectively.

dynamics as CD, synchronization decreases at intermediate dispersal values for both inter and intraspecific DD. Moreover, at  $T = 29^\circ\text{C}$ , where intraspecific DD shows perfect synchronization for all dispersal values (see Fig. 5.4(f)), interspecific DD leads the system to manifest both synchronous and asynchronous states for low and intermediate dispersal rates.

Further, the influence of temperature and relative dispersal rates is also clearly evident when consumers trail DD. Inter and intraspecific DD in the consumer does not affect the dynamics when  $d_n > d_p$  (see Figs. 5.4(g)- 5.4(i)). However, when  $d_n < d_p$ , we observe different synchronization behavior for all three temperature ranges. At  $T = 10^\circ\text{C}$ , for intraspecific DD in consumers, we perceive complete synchrony (i.e.,  $r_{ij} = 1$ ) at high dispersal rates and coexistence of synchronous and asynchronous states at low and intermediate dispersal values (Fig. 5.3(g)). However, interspecific DD shows strong asynchrony at low dispersal rates. With an increase in dispersal rates, synchronization increases, and the system eventually reaches perfect synchrony. Next, at  $T = 20^\circ\text{C}$ , we get to see from Fig. 5.3(h) that for all dispersal rates, dynamics show complete synchrony in the case of intraspecific DD. However, synchronization changes from strong asynchrony to complete synchrony with increased dispersal values when the consumer follows interspecific DD. Continuing,  $T = 29^\circ\text{C}$  seems to alter the effect of inter and intraspecific DD on the dynamics of the system (see Fig. 5.3(g)). We observe that intraspecific DD preserves perfect synchrony for all dispersal values. Whereas for

interspecific DD, depending upon the initial conditions the system can exhibit both synchrony and asynchrony for low and intermediate dispersal rates, and complete synchrony for higher dispersal rates. A summary of the observed collective dynamics of species is given in Table 5.1.

**Table 5.1.** Species collective dynamics in two patch system for low to intermediate values of  $d_n$ . For large  $d_n$  values system dynamics synchronize completely ( $r_{ij} = 1$ ).

	Dispersal Mechanisms	$T = 10^\circ C$	$T = 20^\circ C$	$T = 29^\circ C$
$d_n < d_p$	Constant	Coexistence of synchronous and asynchronous states.	Coexistence of synchronous and asynchronous states.	Complete synchrony.
	Intraspecific Resource	Coexistence of synchronous and asynchronous states.	Coexistence of synchronous and asynchronous states.	Complete synchrony.
	Intraspecific Consumer	Coexistence of synchronous and asynchronous states.	Complete synchrony.	Complete synchrony.
	Interspecific Resource	Coexistence of synchronous and asynchronous states.	Coexistence of synchronous and asynchronous states.	Complete synchrony.
	Interspecific Consumer	Strong asynchrony tending to perfect synchrony with dispersal.	Strong asynchrony tending to perfect synchrony with dispersal.	Coexistence of synchronous and asynchronous states.
$d_n > d_p$	Constant	Coexistence of synchronous and asynchronous states.	Coexistence of synchronous and asynchronous states.	Complete synchrony.
	Intraspecific Resource	Coexistence of synchronous and asynchronous states.	Coexistence of synchronous and asynchronous states.	Complete synchrony.
	Intraspecific Consumer	Coexistence of synchronous and asynchronous states.	Coexistence of synchronous and asynchronous states.	Complete synchrony.
	Interspecific Resource	Coexistence of synchronous and asynchronous states.	Coexistence of synchronous and asynchronous states.	Coexistence of synchronous and asynchronous states.
	Interspecific Consumer	Coexistence of synchronous and asynchronous states.	Coexistence of synchronous and asynchronous states.	Complete synchrony.

### 5.3.2 Variance and mean of regional abundance

We observe that different dispersal rates and dispersal strategies alter the species collective dynamics depending upon varying temperatures. As observed from Figs. 5.5 and 5.6 (see Appendix Figs. 5.8 and 5.9), for the synchronous state we get to see high regional variability in resource and consumer abundance, as calculated from the coefficient of variation (Eq. 5.9). However, for the asynchronous state, when  $d_n < d_p$  and dispersal is constant or DD in resource, we notice that at  $T = 10^\circ C$  (Figs. 5.5(a), 5.5(d) and Figs. 5.6(a), 5.6(d)) and  $T = 20^\circ C$  (Figs. 5.5(b), 5.5(e) and Figs. 5.6(b), 5.6(e)), consumer abundance rises, and variability decreases with increasing dispersal values up to the intermediate range, whereas resource abundance shows a simultaneous drop.

The model exhibits different dynamics when consumer dispersal is density-dependent. At  $T = 10^\circ C$  we observe that for lower and intermediate dispersal rates, consumer variability decreases and abundance increases with a parallel decrease in resource abundance for both inter and intraspecific DD (see Figs. 5.5(g) and 5.6(g)). Whereas, at  $T = 20^\circ C$  (Figs. 5.5(h), 5.6(h)) and  $T = 29^\circ C$  (Figs. 5.5(i), 5.6(i)) we get to see that simultaneous increase or decrease in consumer and resource abundance occurs only for interspecific DD. Moreover, at

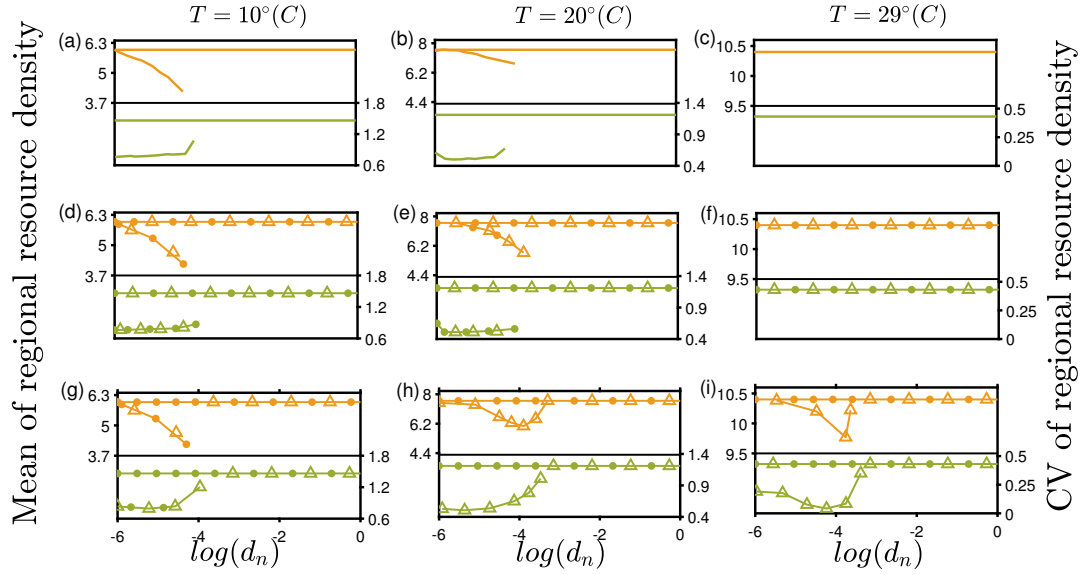


**Figure 5.5.** Mean and CV of resource abundance when  $d_n < d_p$ : Temporal mean (upper sub-graph) and coefficient of variation (lower sub-graph) of regional resource abundance as a function of maximal resource dispersal rates ( $d_n$ ) at different temperatures ( $T$ ). Consumer dispersal rates  $d_p = 100d_n$ . For (a), (d), (g)  $T = 10^\circ C$ ; (b), (e), (h)  $T = 20^\circ C$ ; (c), (f), (i)  $T = 29^\circ C$ , in two distinct patches. (a)-(c) correspond to the dynamics for CD where  $x_{\alpha\beta} = 0$ . Intraspecific (dots) and interspecific (triangles) DD in resource and consumer follow the dynamics depicted in (d)-(f) and (g)-(i), respectively.

the intermediate dispersal range, we notice a drop in consumer abundance and a rise in resource abundance.

As dispersal increases, dynamics become completely synchronized, leading towards high regional variability. Figs. 5.5 and 5.6 (see Appendix Figs. 5.8 and 5.9) show that for a range of dispersal rates, the resource abundance decreases while the consumer's abundance increases, thus insinuating towards top-down control. However, we find that the effectiveness of top-down control varies with increasing temperature and dispersal strengths. At  $T = 10^\circ C$  and  $T = 20^\circ C$ , when the dispersal of resource is less than consumer dispersal (i.e.  $d_n < d_p$ ) (see Figs. 5.5 and 5.6), more attack rate and less mortality rate of consumer (Fig. 5.1), increases the impact of control of consumer on a resource at intermediate dispersal rates for constant and DD. This is governed by increasing consumer abundance and decreasing variability.

### 5.3.3 Spatiotemporal dynamics for a metacommunity with many patches

Amongst the emergent collective dynamics, synchronization is pervasive in a network of coupled oscillators (Strogatz, 2004). A fascinating effect gaining much attention is the partial synchronization patterns, such as the chimera state. Chimera states correspond to a distinctive spatiotemporal pattern, in which identical oscillators

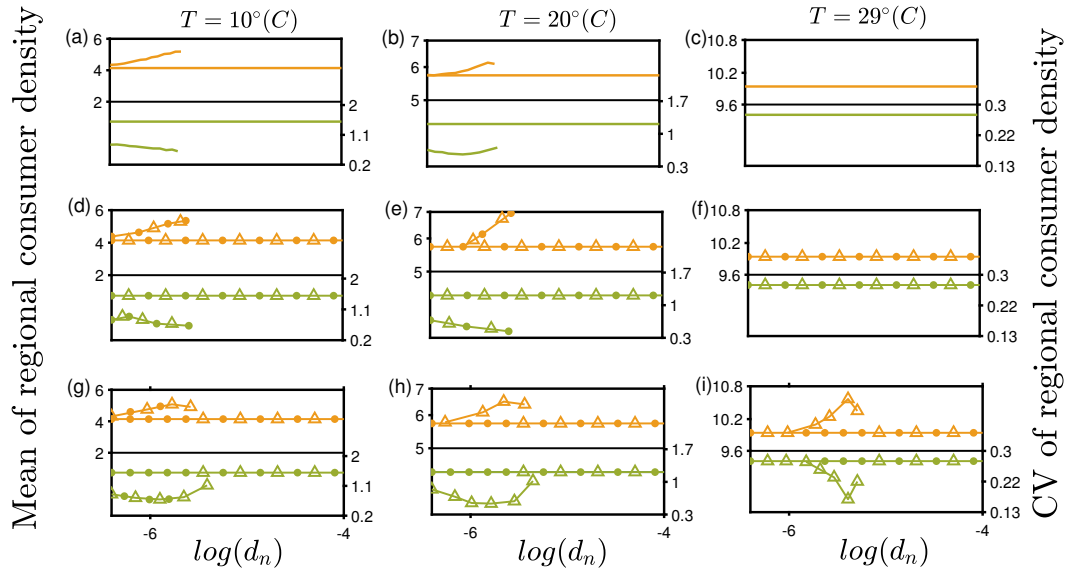


**Figure 5.6.** Mean and CV of consumer abundance when  $d_n < d_p$ : Temporal mean (upper sub-graph) and coefficient of variation (lower sub-graph) of regional consumer abundance as a function of maximal resource dispersal rates ( $d_n$ ) at different temperatures ( $T$ ). Consumer dispersal rates  $d_p = 100d_n$ . For (a), (d), (g)  $T = 10^\circ C$ ; (b), (e), (h)  $T = 20^\circ C$ ; (c), (f), (i)  $T = 29^\circ C$ , in two distinct patches. (a)-(c) correspond to the dynamics for CD where  $x_{\alpha\beta} = 0$ . Intraspecific (dots) and interspecific (triangles) DD in resource and consumer follow the dynamics depicted in (d)-(f) and (g)-(i), respectively.

self-organize into coherent and incoherent co-existing domains. Several theoretical and experimental studies substantiate the existence of chimera in diverse fields of science and engineering (Hagerstrom et al, 2012; Zakharova et al, 2014).

We find the chimera state by considering both constant and DD in species; however, we show the results for CD. In Fig. 5.7(a), we show phase chimera in the presence of CD between nearest neighbors. We observe that the system splits into two coexisting domains: in the coherent domain, where species in several patches oscillate in complete synchrony, whereas, in the incoherent domain, species in the rest of the patches exhibit asynchronous oscillations. Moreover, from Fig. 5.7(b) we find that the mean phase velocity is constant in some nodes, thus, corresponding to coherent regions. In the incoherent regions, the neighboring nodes are not phase-locked, resulting in different mean phase velocities ( $w_i$ ) for each oscillator  $i$ . Different temperature values ( $T = 10^\circ C$  and  $T = 29^\circ C$ ) result in different spatiotemporal dynamics (see Appendix Fig. 5.11 and Fig. 5.12).

## 5.4 Discussion

Climate warming is one of the decisive factors for the apparent range shifts and local extinctions of species (Wilson et al, 2005; Franco et al, 2006). Species dispersal also critically influences the balance between species extinction and recolonization in



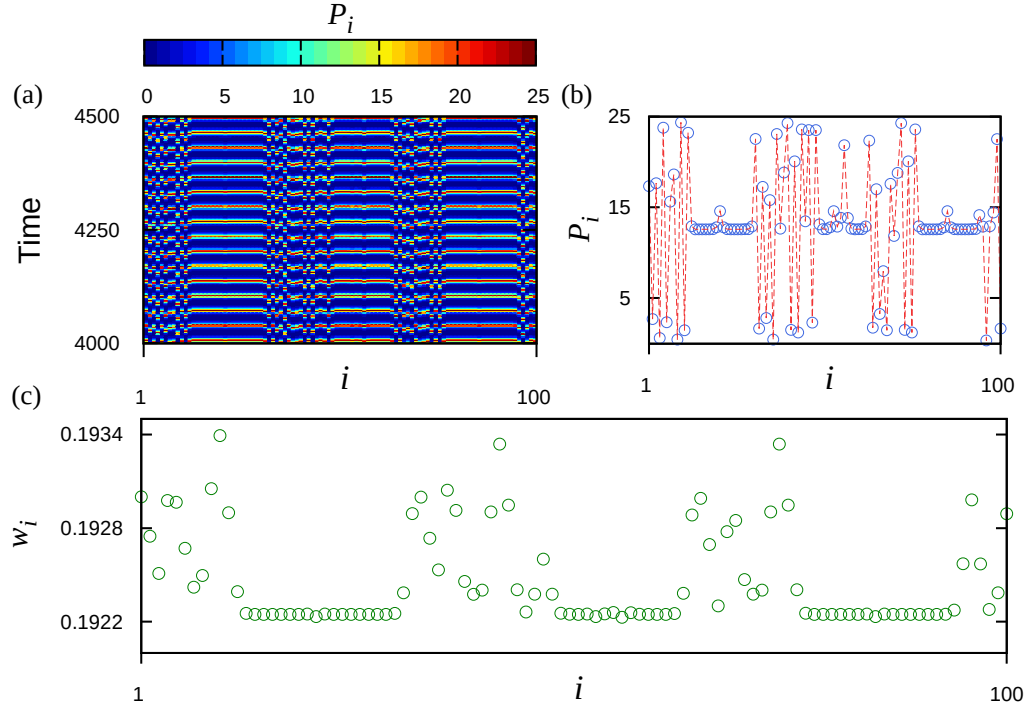


**Figure 5.7.** Interplay of coherence and incoherence in population abundance at an intermediate temperature: (a) Spatiotemporal plot of consumer  $P_i$ , (b) snapshot of  $P_i$  at  $t = 4200$  (red(dotted) lines are for visual guidance), and (c) mean phase velocity ( $w_i$ ), for  $n = 100$  patches. Coupling strength  $d_n = 10^{-6}$  and  $d_p = 10^{-4}$ ,  $T = 20^\circ C$ .

a metacommunity. Hence, species may need effective dispersal strategies to cope with the changing environmental conditions to ensure metacommunity persistence. Here, we emphasize the importance of considering temperature-dependent functional traits of interacting species to anticipate their temporal and spatial associations. We quantify the effects of changing temperature on the dispersal behavior of species. We show that the thermal sensitivity of life-history traits and DD that affect a community at a local and regional scale demands more explorations for ecosystem conservation and management.

Understanding factors influencing ecosystem stability at temporal and spatial scales is critical. Recent years have witnessed increased attention been paid to investigate the relationship between biodiversity and ecosystem stability (Ives and Carpenter, 2007; Hector et al, 2010). While stability has various definitions (Loreau et al, 2002), one of which defines metacommunity stability as long-term species persistence, avoiding extinction (Holling, 1973; Connell and Sousa, 1983). The metacommunity concept suggests that dispersal rates of species (Loreau et al, 2003; Holt, 2004) and resource-consumer interactions (McCann et al, 2005; France and Duffy, 2006) have important consequences on ecosystem stability. Our study highlights how temperature-influenced resource-consumer interactions affect metacommunity persistence depending upon the type of species dispersal.

Synchronization in spatial ecology has always been of great interest (Abbott, 2011). Previous studies suggest that dispersal can influence population synchrony depending on the factors affecting local dynamics. High dispersal rates triggers synchronized dynamics (Bjørnstad et al, 1999), however, for oscillating populations with intrinsic nonlinearities, weak dispersal can also promote population synchrony (Jansen, 1999; Bjørnstad, 2000). Our results show that increasing temperature reduces the stabilizing effect of dispersal that was facilitated by spatially asynchronous dynamics for low and intermediate temperature ranges. As appears for  $10^{\circ}\text{C}$  and  $20^{\circ}\text{C}$ , low and intermediate dispersal rates lead to the coexistence of synchronous and asynchronous states. However, this pattern was not observed at high temperature,  $T = 29^{\circ}\text{C}$  (except for a particular DD, see Table 5.1), because increased mortality of consumers at this temperature decreases the amplitude of fluctuations which lead to the reduced collective differences between the patches.

High temperature in combination with interspecific DD in consumers, with maximal per capita dispersal of consumers being relatively higher than resources (i.e.  $d_n < d_p$ ) contributes towards the stability of metacommunity. Due to  $d_n < d_p$  and interspecific DD in consumers more consumers will disperse from the patch with lower resource abundance to the one with higher abundance, in comparison to resource. The high mortality rate of consumers, and the growth rate of resource being lower than consumer's attack rate at high temperature, increases the rate of increase of resource abundance, relative to that of consumers. Therefore, at this temperature per capita growth rate of resources increases and the emigration of consumers from the low resource abundance patch to the other patch increases consumers' abundance in the dispersed patch, hence, accelerating their growth. This slows down resource growth in that patch, and consequently, here the difference between the abundance of the two patches increases due to high mortality and interspecific DD. Whereas, this is not true for intraspecific DD, where consumers would emigrate from the patch with more consumers due to increasing competition. The effect of this dispersal is neutralized due to the high mortality of consumers at  $29^{\circ}\text{C}$ . The dynamics are altered by interspecific DD in the resource when  $d_n > d_p$ . Hence, in an unfavorable condition, we perceive that interspecific DD can effectively preserve metacommunity stability. We measure the metacommunity stability using temporal variance and the mean of regional species abundance. Variability in population abundance affects the persistence of species. Ecosystems with more variability are known to be less stable (Wang and Loreau, 2014). Our results show that species temporal variability and mean regional abundance are interceded by dispersal strength, dispersal type, and thermal traits.

Our results are in accordance with (Hauzy et al, 2010) on the effect of synchrony on stability. High dispersal rates tend to synchronize dynamics, leading towards

high regional variability, thus decreasing stability. We also found that interspecific DD has a stabilizing effect on metacommunity in agreement with (Hauzy et al, 2010). However, a critical difference is that in (Hauzy et al, 2010), intermediate dispersal rates lead to the emergence of chaotic dynamics, which is in contrast with our results. Moreover, the synchronizing dynamics observed in our study differ based on the changing temperature. Considering,  $d_n < d_p$  and CD, our result of coexisting two periodic attractors is in line with (Hauzy et al, 2010) for  $T = 10^\circ C$  and  $T = 20^\circ C$ , whereas, at  $T = 29^\circ C$  the asynchronous attractor vanishes, trailing the system towards completely synchronized dynamics. Furthermore, for  $d_n > d_p$  and CD,  $T = 10^\circ C$  and  $T = 20^\circ C$  exhibit coexisting attractors and  $T = 29^\circ C$  shows perfect synchrony, which is in contrast to (Hauzy et al, 2010), where, spatial synchrony increases monotonically with dispersal rates, maintaining high value of synchrony. Our study shows the influence of climate warming on the dispersal strategies adapted by species. Dispersal promotes species persistence by maintaining balance in population abundance, whereas synchrony aggravates the chances of extinction. However, dispersal is known to impel population stability by breaking synchrony in ecological networks and thus result in producing chimera states. Emergence of chimera reduces the synchronization domain, thereby enhancing survival probabilities of populations (Dutta and Banerjee, 2015). In this study, we also analyze the role of temperature in the emergence of spatiotemporal patterns as shown in Fig. 5.7. We observed that at intermediate temperature ( $T = 20^\circ C$ ) and for low dispersal strength, the population splits into coherent and incoherent domains. We find that high temperature drives all the oscillators towards complete synchrony, thus weakening population persistence (see Fig. 5.13). Our results suggest that intermediate temperatures potentially enhance the chance of survivability of a metacommunity. Thus, in this chapter, we elucidate the importance of considering the biotic interactions of species by taking into account the thermal response of life-history traits of interacting species. These temperature-dependent key traits indicate the effect of rising temperature on community interactions and dispersal patterns. We have shown that DD and relative dispersal are crucial in understanding metacommunity stability under the effect of global warming.

## 5.5 Appendix

### 5.5.1 Variance and mean of regional abundance for $d_n > d_p$

Here we discuss the case of resource dispersal strength being more than consumer dispersal rate ( $d_n > d_p$ ).

We perceive a change in dynamics when resources carry out DD, for the other kind

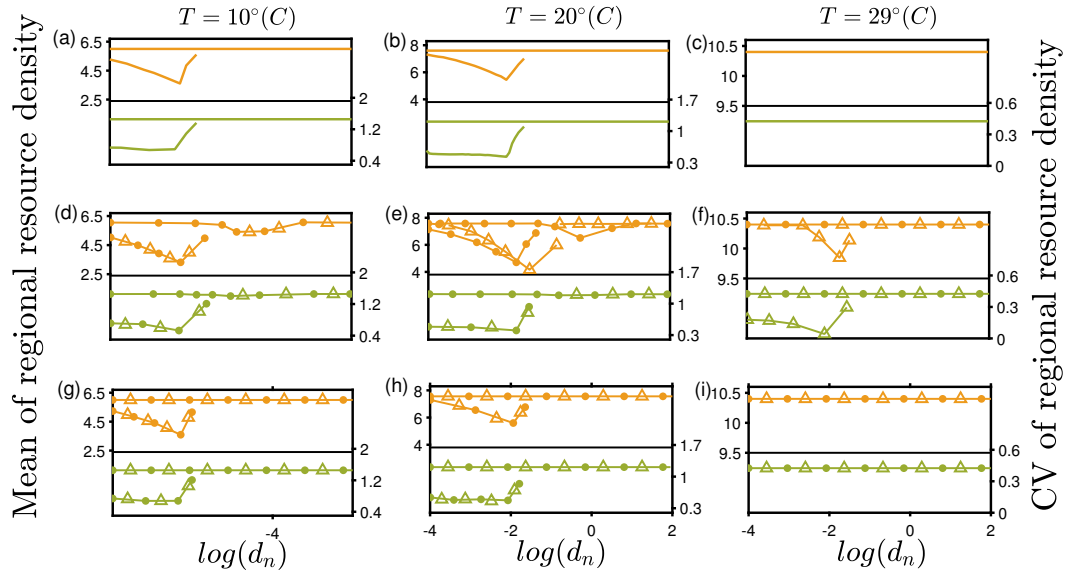


**Figure 5.8.** Mean and CV of resource abundance when  $d_n > d_p$ : Temporal mean (upper sub-graph) and coefficient of variation (lower sub-graph) of regional resource abundance as a function of maximal resource dispersal rates ( $d_n$ ) at different temperature ( $T$ ). Consumer dispersal rates  $d_p = 0.01d_n$ . For (a), (d), (g)  $T = 10^\circ C$ ; (b), (e), (h)  $T = 20^\circ C$ ; (c), (f), (i)  $T = 29^\circ C$ , in two distinct patches. (a)-(c) Correspond to the dynamics for CD where  $x_{\alpha\beta} = 0$ . Intraspecific (dots) and interspecific (triangles) DD in resource and consumer follow the dynamics depicted in (d)-(f) and (g)-(i), respectively.

of dispersal behavior regional abundance is by variations in temperature. When dispersal is constant or when consumers follow DD, we notice that at  $T = 10^\circ C$  (Figs. 5.8((a), (g)) and Figs. 5.9((a), (g))) and at  $T = 20^\circ C$  (Figs. 5.8((b), (h)) and Figs. 5.9((b), (h))), for lower dispersal values, consumer variability decreases as regional abundance of consumer increases, however, resource temporal variability decreases following the same trend as resource regional abundance up to certain dispersal range. Nevertheless, a substantive change in abundance is observed here, when resource abundance rises with a fall in consumer abundance, correspondingly affecting the regional variability. At  $T = 29^\circ C$  we see from Figs. 5.8((c), (i)) and Figs. 5.9((c), (i)) that no change in mean and variability of regional resource and consumer abundances, respectively.

Now, looking at the variations in abundance when resource adopts DD, we find that at  $T = 10^\circ C$  (see Figs. 5.8(d), 5.9(d)) and  $T = 20^\circ C$  (see Figs. 5.8(e), 5.9(e)), for lower dispersal values inter and intra-specific DD leads to decrease in resource abundance and a simultaneous increase in consumer abundance. Here again, we notice that at intermediate dispersal values resource abundance and variability rise, and consumer abundance witnesses a drop with rising variability. However, then with a further increase in dispersal rates, while inter-specific DD moves towards constant regional abundance, intraspecific DD repeats the behavior and then maintains sustained abundance. Next, at  $T = 29^\circ C$ , we observe that inter

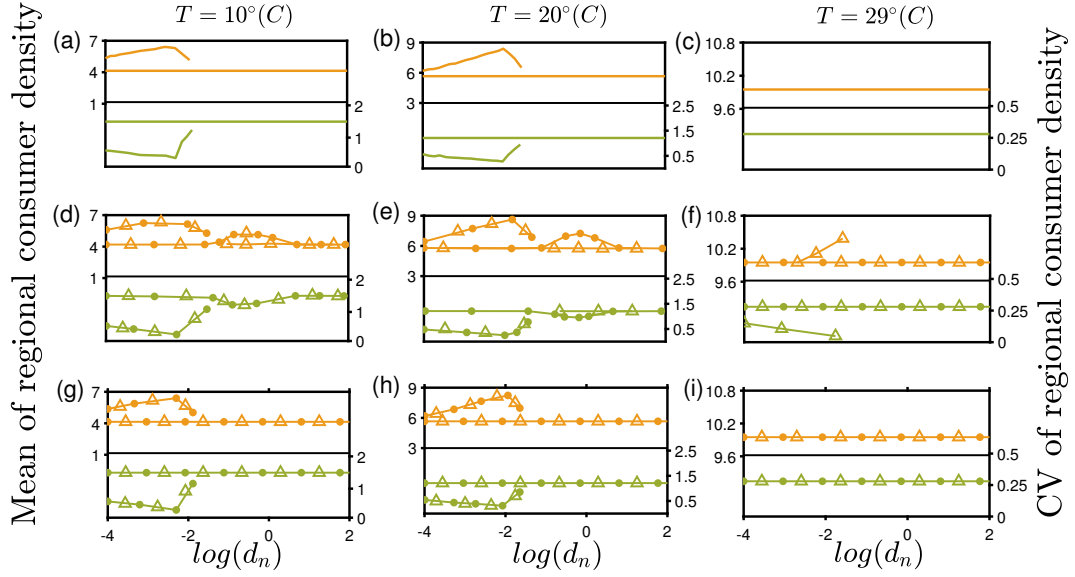


**Figure 5.9.** Mean and CV of consumer abundance when  $d_n > d_p$ : Temporal mean (upper sub-graph) and coefficient of variation (lower sub-graph) of regional consumer abundance as a function of maximal resource dispersal rates ( $d_n$ ) at different temperature ( $T$ ). Consumer dispersal rates  $d_p = 0.01d_n$ . For (a), (d), (g)  $T = 10^\circ C$ ; (b), (e), (h)  $T = 20^\circ C$ ; (c), (f), (i)  $T = 29^\circ C$ , in two distinct patches. (a)-(c) correspond to the dynamics for CD where  $x_{\alpha\beta} = 0$ . Intraspecific (dots) and interspecific (triangles) DD in resource and consumer follow the dynamics depicted in (d)-(f) and (g)-(i), respectively.

and intra-specific DD maintain the same regional abundance as CD, whereas, for inter-specific DD, consumer abundance increases with increasing dispersal values and then drops at intermediate dispersal rate, and contrariwise for resource abundance (see Fig. 5.8(f) and Fig. 5.9(f)).

As noticed, the strength of consumer control weakens at the same dispersal range when dispersal of resource is greater than consumer dispersal ( $d_n > d_p$ ). Moreover, as the dispersal rate increases from low to intermediate values, we see a direct relationship between resource mean abundance and variability. Declining resource abundance comes along with decreasing variability due to the effect of temperature. However, further increase in dispersal rates leads to higher variability in regional resource abundances, but weakening consumer control as observed from increasing resource abundance. Thus, relatively high dispersal rates of the resource may increase the chances of their survival from consumers. High temperatures ( $T = 29^\circ C$ ), where the growth rate of resource and attack and mortality rate of the consumer is significantly higher (see Fig. 5.1), affect the top-down control. We perceive that for both instances, i.e. for a lower dispersal rate of resource than the dispersal rate of consumer ( $d_n < d_p$ ) and another way ( $d_n > d_p$ ), only interspecific DD in consumer and resource, respectively, amplifies consumer control on the resource while moving from low to intermediate dispersal values. Consumers are the most vulnerable species at high temperatures that could stabilize at lower

dispersal rates due to interspecific DD.

### 5.5.2 Temperature sensitivity of the half-saturation constant ( $N_0$ ) and the carrying capacity ( $K$ )

We perform sensitivity analysis (Kaur and Dutta, 2020) for the half-saturation constant ( $N_0$ ) and the carrying capacity ( $K$ ) together with the temperature variation ( $T$ ). Figure 5.10 shows steady state, oscillatory, and extinction regions of species at different temperatures.  $HB$  corresponds to the Hopf bifurcation boundary beyond which the system does not exhibit oscillatory dynamics and  $TB$  is the transcritical bifurcation curve beyond which species fail to co-exist. We observe that at higher temperatures (above  $31^\circ C$ ), irrespective of the parameter values, species do not coexist. As can be seen from Fig. 5.10(a), for a small range of  $N_0$  the system shows oscillatory behavior up to a certain temperature extent. Moderate to high  $N_0$  values, lead towards steady state dynamics across a range of temperature gradients, beyond which the system fails to exhibit the co-existence of species equilibrium abundance.

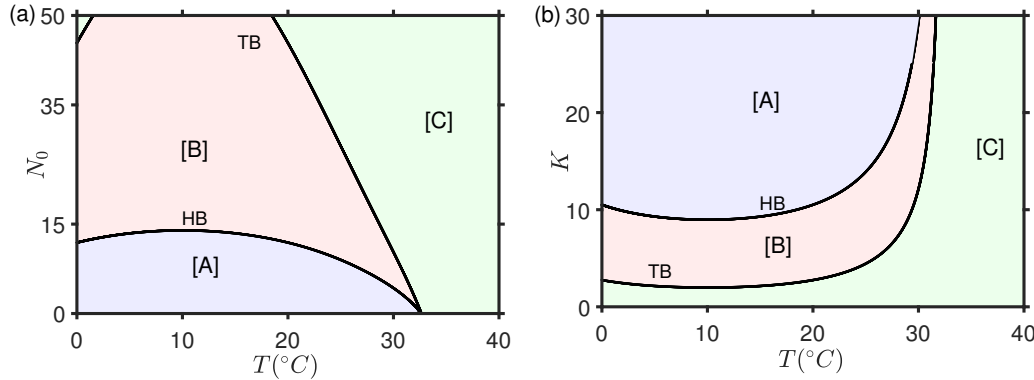


**Figure 5.10.** Thermal sensitivity of species half-saturation constant ( $N_0$ ) and carrying capacity ( $K$ ): Two-parameter bifurcation diagram in the (a)  $T - N_0$  plane, and (b)  $T - K$  plane. Shaded regions: [A] corresponds to the region where species abundance shows oscillatory behavior. [B] determines the region where the system exhibits steady state dynamics, and [C] is the region where stability fails and consumers become extinct.  $HB$ , and  $TB$  represent the Hopf bifurcation and the transcritical bifurcation, respectively.

Moderate to high  $K$  values manifest oscillatory dynamics (see Fig. 5.10(b)), whereas, with lowering  $K$  values oscillations disappear, yet stabilizing dynamics from low to temperature up to  $31^\circ C$ . However, increasing temperature beyond this threshold does not favor the coexistence of species and results in the extinction of consumers. Therefore, the metacommunity dynamics that we have reported for the specific choice of parameters are quite robust and can be found in a larger region of the parameter space.

### 5.5.3 Spatiotemporal dynamics for different choices of temperature

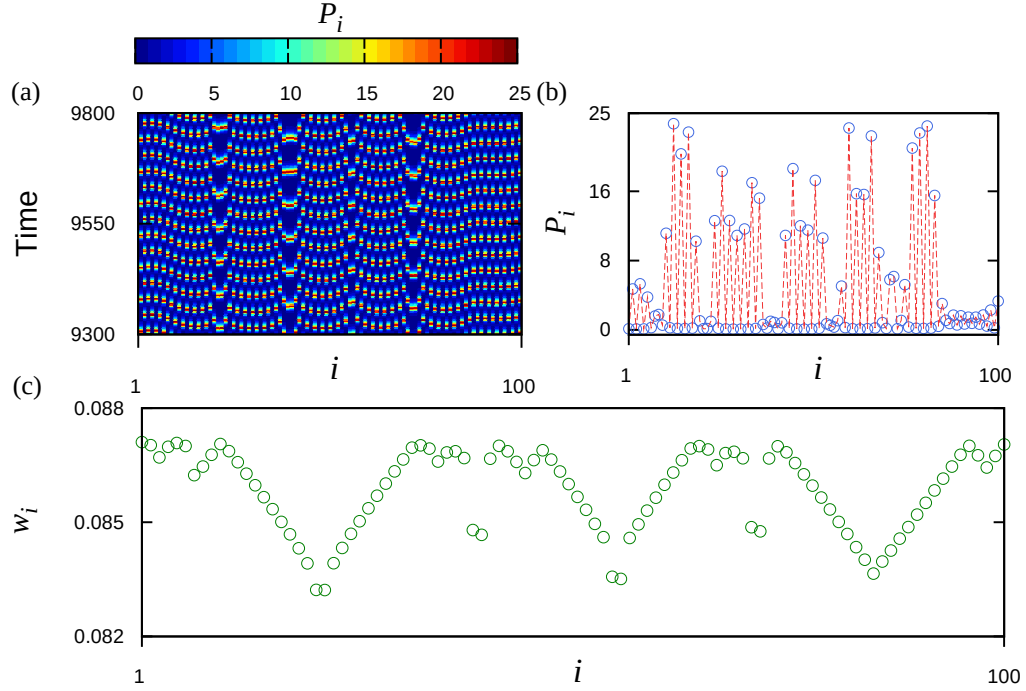


**Figure 5.11.** Interplay of coherence and incoherence in population abundance at  $T = 10^\circ\text{C}$ : (a) Spatiotemporal plot of consumer  $P_i$ , (b) snapshot of  $P_i$  at  $t = 9500$  (red (dotted) lines are for visual guidance), and (c) mean phase velocity ( $w_i$ ), for  $n = 100$  patches. Coupling strength  $d_n = 10^{-6}$  and  $d_p = 10^{-4}$ .

Here, considering a large metacommunity of  $n = 100$  interacting patches with CD (constant dispersal) we illustrate the effect of temperature on species spatiotemporal dynamics. We find the occurrence of chimera patterns (Abrams and Strogatz, 2004) illustrated by the coexistence of coherent and incoherent domains for  $T = 10^\circ\text{C}$  and  $T = 20^\circ\text{C}$ , as can be seen from Fig. 5.11(a) and Fig. 5.12(a), respectively. However, on changing the temperature to  $T = 29^\circ\text{C}$  all the oscillators converge to the coherent state (see Fig. 5.13(a)). These results have a resemblance with the dynamics of two patch metacommunity which is also evident from Table 1 (main draft).



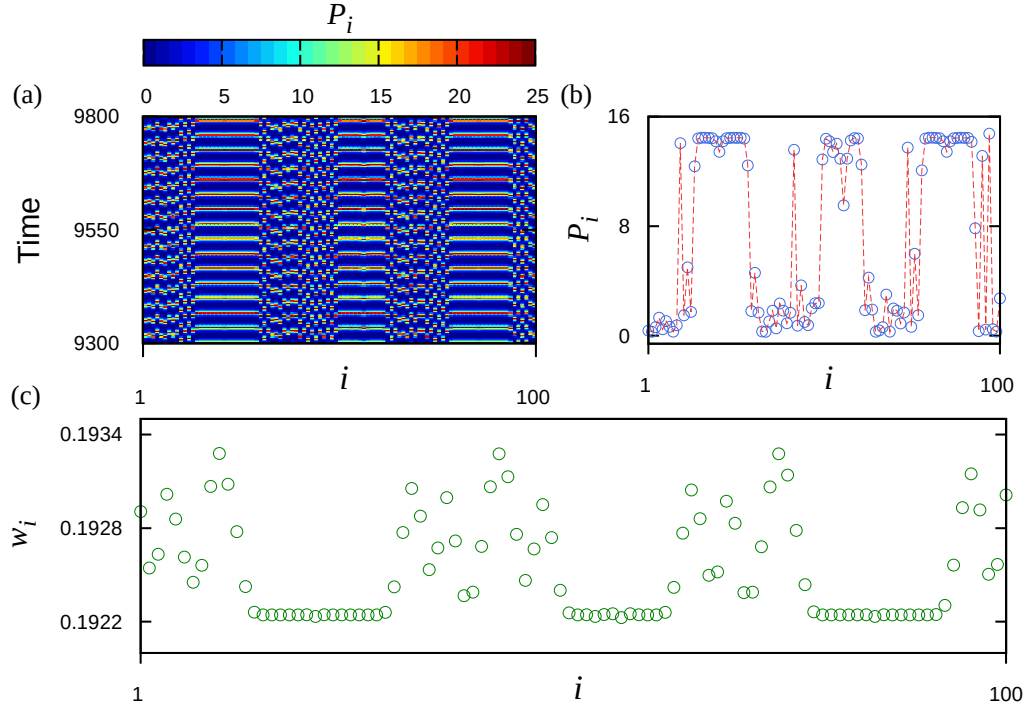


**Figure 5.12.** Interplay of coherence and incoherence in population abundance at  $T = 20^\circ\text{C}$ : (a) Spatiotemporal plot of consumer  $P_i$ , (b) snapshot of  $P_i$  at  $t = 9500$  (red(dotted) lines are for visual guidance), and (c) mean phase velocity ( $w_i$ ), for  $n = 100$  patches. Coupling strength  $d_n = 10^{-6}$  and  $d_p = 10^{-4}$ .

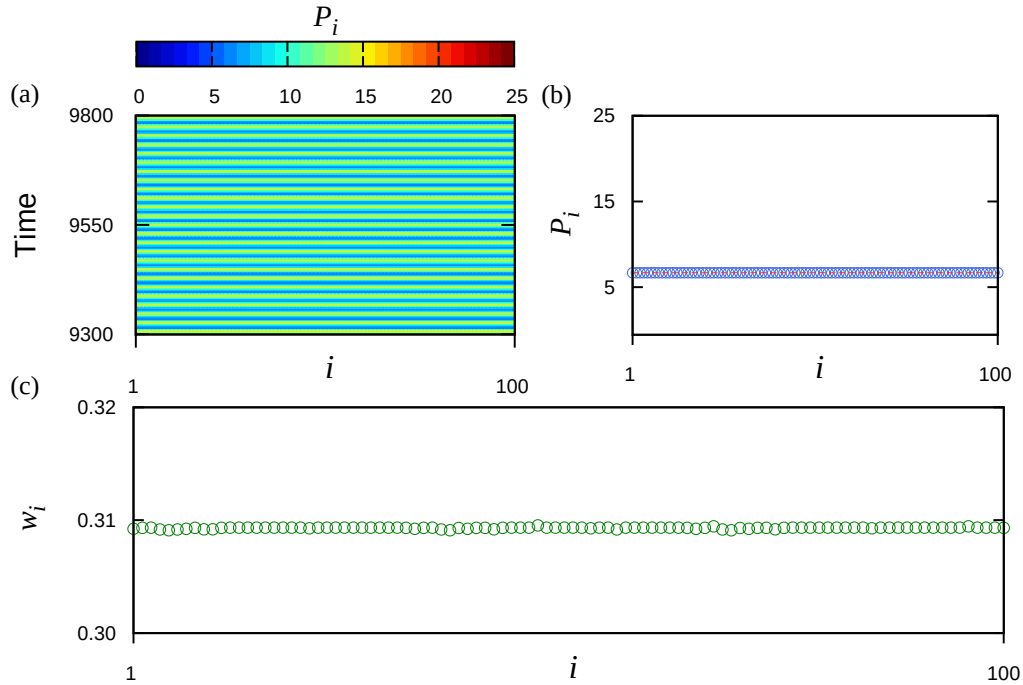


**Figure 5.13.** Global synchronized oscillations at  $T = 29^\circ\text{C}$ : (a) Spatiotemporal plot of consumer  $P_i$ , (b) snapshot of  $P_i$  at  $t = 9500$  (red(dotted) lines are for visual guidance), and (c) mean phase velocity ( $w_i$ ), for  $n = 100$  patches. Coupling strength  $d_n = 10^{-6}$  and  $d_p = 10^{-4}$ .



# Chapter 6

## Long-range dispersal promotes species persistence in climate extremes

---

### 6.1 Introduction

The study of spatial ecological systems has a strong significance in our understanding of large-scale population dynamics concerning the evolutionary outcomes ([Tilman and Kareiva, 2018](#); [Williams, 2018](#)). Spatial ecologists often find metapopulation theory of utmost importance to understand the processes of regional extinction and recolonization of species. The metapopulation approach adopts the view that local populations interact via dispersal and gene flow ([Hanski et al, 2004](#)). Dispersal is expressed through the interaction of an organism with its environment, therefore it is likely to be influenced by environmental effects ([Clobert et al, 2012](#)). One of the major environmental factors responsible for altering the costs and benefits of dispersal is climate warming. Climate change has a considerable impact on species composition ([Walther et al, 2002](#); [Foden et al, 2009](#)) and current global warming is expected to cause an irreparable change to ecosystems ([Tylianakis et al, 2008](#)). Eventually, dispersal will become a central subject to predict species responses to environmental change ([Travis et al, 2013](#)). Therefore, it is of natural interest to explore the effect of temperature on species dispersal. According to earlier studies, dispersal, which is considered to be an impelling cause for the persistence and stability of metapopulations could also drive the population towards extinction by increasing the degree of spatial synchrony ([Tanaka et al, 1997](#); [Jansen, 1999](#); [Hopson and Fox, 2019](#)). Population stability means that the minimum density of populations in all patches is not too low, and the probability of extinction is less in a given time ([Briggs and Hoopes, 2004](#)). Other than dispersal, environmental factors are also one of the reasons for dynamical connection ([GRØTAN et al, 2005](#); [Post and Forchhammer, 2004](#)), which results in the synchronization of spatial populations. If dispersal, induces synchrony, then the synchronized populations will continue to remain in synchrony until and unless any large external perturbation drives them

away (Goldwyn and Hastings, 2011). Spatial *asynchrony* in density fluctuations is known to strengthen the metapopulation persistence. This indicates the importance of examining species dynamics due to dispersal and the extrinsic factor, which we consider to be temperature, on synchrony.

Range interaction in species dispersal is an important factor that drives interesting spatial dynamics (Banerjee et al, 2016). Dispersal, under the influence of climate change, has an impact on species range shifts (Thomas and Lennon, 1999; Battisti et al, 2006; Brooker et al, 2007), either resulting in long-distance dispersal (LDD) or short-distance dispersal (SDD). We incorporate dispersal kernels which refer to the probability to disperse to certain distances. Several different functions are used for dispersal kernels in theoretical models of dispersal including the inverse power law (Banerjee et al, 2016), for the present study we consider that the network of spatially separated patches is connected by a long-range interaction that obeys a distance-dependent power law. Our choice of this particular type of dispersal kernel is also motivated by the fact that long-range interaction plays a crucial role in many physical and biological systems. For example, in the one-dimensional Ising spin model (Aizenman et al, 1988) and spin-glass model (Kotliar et al, 1983b) interaction among the spins is governed by long-range interaction that obeys a distance-dependent power law. In neuronal systems, long-range interaction with a specific scaling has been found that controls the connectivity among the neurons (Szaro and Tompkins, 1987).

An appreciable amount of work has been done to study the effects of climate change and dispersal on ecosystems (Eklöf et al, 2012; Lande et al, 1999; Kendall et al, 2000; Peltonen et al, 2002; Travis et al, 2013; Bestion et al, 2015; Urban et al, 2012; Levy et al, 2016; Nevai and Van Gorder, 2012; Shen and Van Gorder, 2017; Bani et al, 2019; Hutchison et al, 2020). A mathematical model (predator-prey subsidy model) involving temperature to study seasonal fluctuations (Levy et al, 2016), and also to measure the impact of global warming and seasonality (Nevali and Van Gorder, 2012) has been investigated. Further, the influence of network structures was examined on the predator-prey subsidy system (Shen and Van Gorder, 2017). It was observed that in spatial structures with food scarcity, an increase in migration rates would result in the possibility of extinction of predators. Investigating delayed migration to study spatial dynamics has also been an important perspective (Levy et al, 2016; Eide et al, 2018). Consequently, considerable research has been done to examine the effect of dispersal on predator-prey dynamics (Levin, 1976; Kareiva, 1990; Yaari et al, 2012). However, a direct approach that incorporates temperature in spatial population models to study dispersal-induced dynamics is yet to be explored. Models that investigate migratory effects are generally classified into one of three categories: Island models, Stepping-Stone models, and Continuum

models (Shen and Van Gorder, 2017). The key feature of the “Island” model (Levin, 1976; Kareiva, 1990) is the inclusion of a set of patches. It involves instantaneous migration between patches without explicitly including spatial dimensions. The “Stepping-Stone” models again consider populations being divided into patches but the patches are now assigned fixed spatial coordinates. In such models, spatial structures significantly contribute towards determining predator-prey dynamics (Shen and Van Gorder, 2017). The “Continuum” models involve partial differential equations to elucidate migration of populations in the continuous domain (Levin, 1976). In this chapter, we link changing global mean temperature with the dispersal behavior of species by considering an ecological system, namely a spatial Rosenzweig-MacArthur model (Rosenzweig and MacArthur, 1963; Holland and Hastings, 2008) or a “Stepping-Stone” model. We demonstrate that the natal dispersal tendency depends upon the changing temperature, which further will have an impact on the species’ survival. We consider that at very low and high-temperature ranges, species dispersal within patches is low; this arises mainly as a consequence of species ‘Thermal Performance Curves’ (TPCs) (Amarasekare and Savage, 2011). These curves show an exponentially inclining trend at low temperatures, attain a maximum at the thermal optimum and then decline with further increase in the temperature. Hence, as the species’ thermal performance is low at extreme temperatures, this suppresses the species’ ability to move and thus disperse within patches. In this chapter, we try to address the following questions: How does the temperature-dependent dispersal influence the dynamics of a metapopulation? Can dispersal promote the persistence of species by reducing the degree of spatial synchrony, even in the least favorable environmental conditions? Can transient state work as an indicator of species behavior in their final dynamics? To address the above questions, we begin by analyzing the fluctuations in species density, over time. We carry out different measures to learn the coherence/incoherence in species dynamics characterized by their amplitude of fluctuations, density correlations, and transient dynamics. Furthermore, we use cross-wavelet analyses to understand the long-term dynamics of the system through transients. Temperature variations that influence species dispersal lead to interesting spatiotemporal dynamics. We observe that the amplitude of fluctuations in species density averaged over a large number of the system replicates, and suppresses along the thermal axis up to optimum temperatures. These findings are conserved while investigating the cluster count, depicting relatively similar responses of a large number of species along the changing temperatures. Further, the robustness of observations is rooted in the increasing synchrony measure and decreasing transients of the system. Importantly, we also find that the transient phase of the system can trace the long-term synchronous or asynchronous distance-dependent dynamics.

In all, our study reveals that the synchrony is minimal at the extreme conditions and comparatively more synchronized behavior is observed around the optimum temperatures, which may also be hinted by the transient state, using cross wavelet analyses.

The chapter is organized as follows: In Subsec. 6.2A, we introduce the temperature-dependent metapopulation model. The measures used to analyze the model are defined in Subsec. 6.2B. In Sec. 6.3, we first discuss cluster analysis and transients which are related to the collective dynamics of the model. Then, we present the cross-wavelet analysis which depicts the effects of different temperature together with the distance between patches in Subsec. 6.3E. Finally, in Sec. 6.4 we discuss the importance of our results and future directions.

## 6.2 Materials and Methods

To study the influence of temperature-dependent dispersal on spatial population dynamics, we consider prey-predator interactions within a patch and between  $n$ -spatially distributed patches. Each patch exhibits homogeneous behavior in the sense of species interactions and phenotypes. Spatial heterogeneity is introduced into the system due to temperature-dependent dispersal phenomenon as well as by accounting short-range and long-range interactions of species between the patches.

### 6.2.1 A metapopulation model

We start with the dimensionless form of a spatial Rosenzweig-MacArthur model (Goldwyn and Hastings, 2008; Rosenzweig and MacArthur, 1963). The dynamics of a prey density ( $h_i$ ) and a predator density ( $p_i$ ) in the  $i$ -th patch (node) are given as:

$$\frac{dh_i}{dt} = h_i(1 - \theta h_i) - \frac{p_i h_i}{1 + h_i} + \epsilon_h \left( \frac{1}{\zeta(f(T))} \sum_{d=1}^m \frac{h_{i-d} + h_{i+d}}{df(T)} - h_i \right), \quad (6.1a)$$

$$\frac{dp_i}{dt} = \frac{\phi p_i h_i}{1 + h_i} - \eta p_i + \epsilon_p \left( \frac{1}{\zeta(f(T))} \sum_{d=1}^m \frac{p_{i-d} + p_{i+d}}{df(T)} - p_i \right), \quad (6.1b)$$

where  $i$  ( $= 1, 2, \dots, n$ ) determines the index of a patch. All the indices with modulo the number of patches in the network (i.e.  $n$ ).  $\theta$  is the self-regulation of prey,  $\phi$  is the conversion efficiency of the predator to convert and assimilate acquired food into energy and  $\eta$  determines the predator's natural mortality. These factors govern the local dynamics of the interaction network. Spatiotemporal dynamics of the metapopulation are characterized by dispersal strengths of prey and predator as  $\epsilon_h$

and  $\epsilon_p$ , respectively.  $d$  is the distance between  $i$ -th and  $j$ -th patches, defined by the minimum number of edges required to disperse from the  $i$ -th to the  $j$ -th patch. We consider a regular network where all the patches are connected and hence accessible by the dispersing species from any patch (i.e.  $m=(n-1)/2$ , when the total number of patches is odd), but the dispersal density may vary depending upon the distance between the patches as well as the temperature of the habitat.

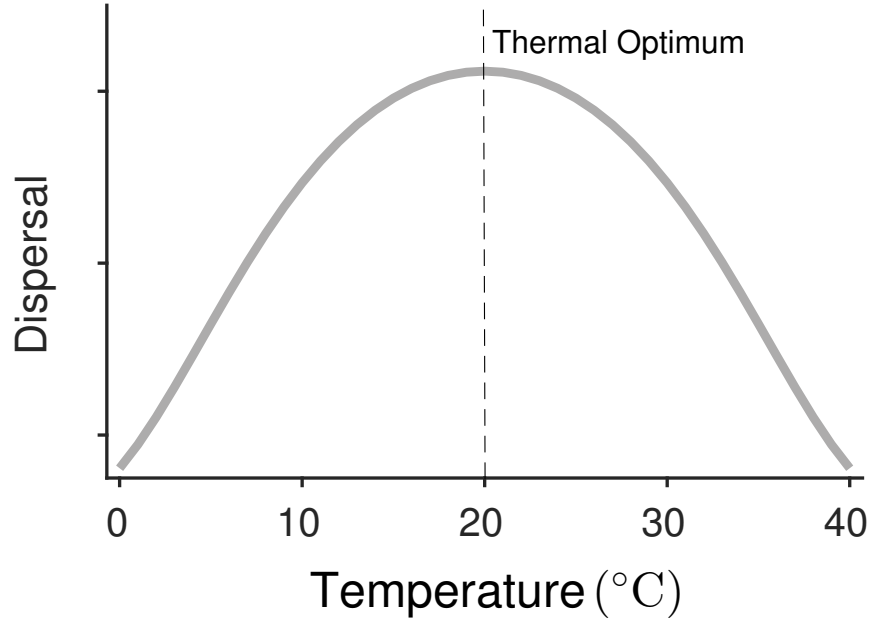


**Figure 6.1.** Thermal dependence of dispersal of spatially separated species. At extreme temperatures (either very low or high) species are less likely to disperse.

In the network, every patch is connected to all the other patches via the dispersal strength  $\epsilon_h$  or  $\epsilon_p$ , which is modulated by the distance between patches and temperature-dependent power law function  $d^{-f(T)}$ , where  $T$  is the temperature.  $\zeta(f(T)) = 2 \sum_{d=1}^m d^{-f(T)}$  is the normalization constant. We consider the hypothesis that dispersal is strongest at the optimal temperature (see Fig. 6.1). This is because the intermediate temperature being a favorable temperature for the growth and survival (Pellerin et al, 2019) of species results in the active biological traits of species (Amarasekare and Savage, 2011; Amarasekare and Johnson, 2017). For example, species attack rate follows an increasing trend, attains a maximum at the optimum temperature, and then declines, moreover, handling time also attains an optimum value at the intermediate temperature (Amarasekare, 2015). The temperature-dependent power law exponent  $f(T)$  governing the distance-dependent interaction strength is represented by a Gaussian function (Amarasekare, 2015):

$$f(T) = f_{opt} \times e^{\frac{(T-T_{opt})^2}{2s^2}}, \quad (6.2)$$

where  $f_{opt}$  is the value of  $f$  at the optimal temperature  $T_{opt}$ . Temperature sensitivity of the function  $f(T)$  is determined by the parameter  $s$ , which also determines the performance breadth of the dispersal between the coupled patches. Throughout this chapter, we have considered  $f_{opt} = 0.27$ ,  $T_{opt} = 20^\circ\text{C}$  and  $s = 11.5$ . The function  $f(T)$  holds relatively large values at extreme temperatures as compared to intermediate temperatures. Furthermore, large values of  $f(T)$  imply fewer chances of species to disperse to the further habitat as compared to lower values of  $f(T)$  (except the nearest neighboring patches, i.e. for  $d = 1$ ) as prey-predator dispersal strengths are modulated via  $d^{-f(T)}$  (see Fig. 6.1). Therefore, species dispersal is more likely to further patches at intermediate temperatures in comparison with the extreme temperatures.

### 6.2.2 Characteristic measures

We study the spatiotemporal dynamics of the system (see Eqn. (6.1)) for a fragmented land of 11 patches. When there is no dispersal of species from one patch to another (i.e. with  $\epsilon_h = \epsilon_p = 0$ ), species dynamics are determined by their local interaction and they exhibit oscillatory behavior. Setting it up as a benchmark for spatiotemporal interaction, first, we examine the time series of the species in the 11 patches and observe the impact of changing temperature on the species dynamics. Our major concern is to understand, what role dispersal plays in the survival of species under different thermal conditions. For this we compute the total predator amplitude (Holland and Hastings, 2008), defined as:

$$\text{Total predator amplitude} = \log_{10} \left( \frac{\max(\sum_{i=1}^n p_i)}{\min(\sum_{i=1}^n p_i)} \right), \quad (6.3)$$

over a window of  $4\overline{M_p}$ , with  $\overline{M_p}$  as the mean period of the population cycle which is averaged over a sufficiently long time period. A synchronous system signifies more possibility of obtaining high values of predator amplitude compared to asynchrony. To analyze the same, we also calculate the cumulative probability of various predator amplitudes for different values of  $T$ .

Likewise, to explore the outcomes of interactions between patches, we calculate the correlation coefficient  $\rho_{ij}$  of a species time series at time  $t$ , between the  $i$ -th and the  $j$ -th patch for different values of the temperature  $T$ . Thereafter, a set of patches having identical behavior are considered to form a cluster. Here, for identical behavior, we refer to patches having  $\rho_{ij} > 0.999$ . Out of the  $n$  patches, we can have a  $k$ -cluster solution, where  $1(\text{global synchrony}) \leq k \leq n(\text{complete asynchrony})$ . The

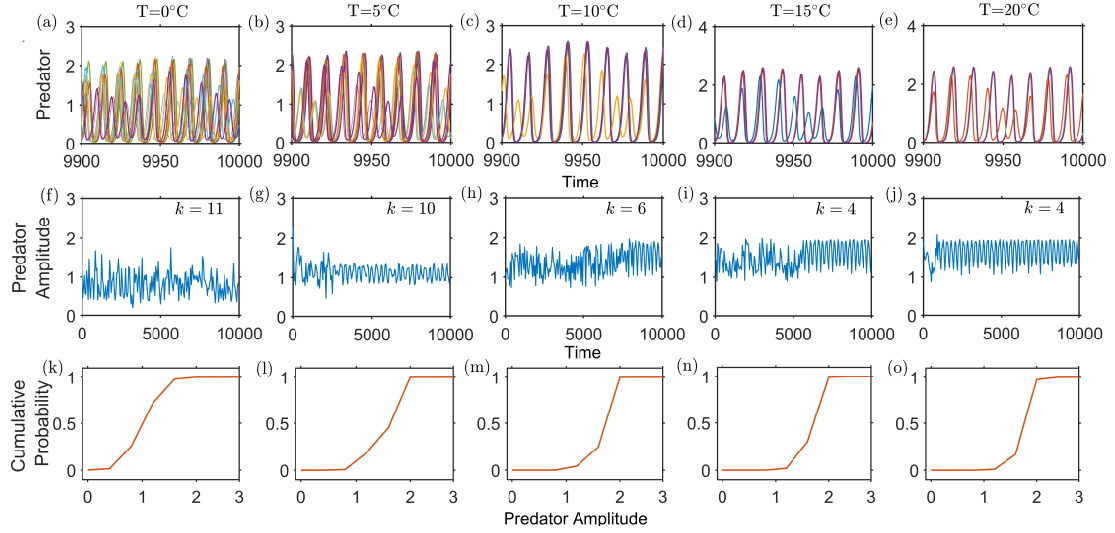


**Figure 6.2.** Time series of predator species, predator amplitude, and cumulative distributions of predator amplitude along the thermal gradient  $T$ : for (a), (f), (k)  $T = 0^\circ\text{C}$ ; (b), (g), (l)  $T = 5^\circ\text{C}$ ; (c), (h), (m)  $T = 10^\circ\text{C}$ ; (d), (i), (n)  $T = 15^\circ\text{C}$ ; and (e), (j), (o)  $T = 20^\circ\text{C}$ . Local dynamics are governed by  $\theta = 0.3$ ,  $\eta = 1$  and  $\phi = 3$ . Dispersal strengths are:  $\epsilon_h = 2^{-5}$  and  $\epsilon_p = 2^{-6}$ .  $k$  denotes clusters count at different values of  $T$ .

correlation coefficient is calculated at each time and is given by (Gupta et al, 2017):

$$\rho_{ij} = \frac{\langle x_i x_j \rangle - \langle x_i \rangle \langle x_j \rangle}{\sqrt{\langle x_i^2 \rangle - \langle x_i \rangle^2} \sqrt{\langle x_j^2 \rangle - \langle x_j \rangle^2}}, \quad (6.4)$$

where  $x$  is the species density and  $\langle \dots \rangle$  is the average over the window  $[t, t + 4\overline{M}_p]$ . Using the correlation coefficient  $\rho_{ij}$ , the frequency of the occurrence of a  $k$ -cluster solution with time evolutions is calculated as:

$$\text{Frequency of } k\text{-cluster} = \frac{\text{No. of } \leq k\text{-clusters}}{\text{No. of simulations}}. \quad (6.5)$$

Due to the possibility of the occurrence of multiple stable attractors in higher dimensional dynamical systems, here we perform large ensembles of simulations for a set of randomly chosen initial conditions.

For the permanence of our results, we carry forward our investigation by calculating the synchrony measure  $\sigma$  (Komin et al, 2010) concerning the changing temperature  $T$ . The synchrony order parameter  $\sigma$  measures the amount of change in synchrony between patches along the temperature gradient and is defined as:

$$\sigma = \sqrt{1 - \left\langle \frac{\sum_{i=1}^n [x_i(t) - \overline{x}(t)]^2}{\sum_{i=1}^n x_i(t)^2} \right\rangle}, \quad (6.6)$$



where  $\overline{x(t)} = \frac{1}{n} \sum_{i=1}^n x_i(t)$  and  $\langle \dots \rangle$  represents the average over a given time. The quantity  $\sigma$  varies at intervals 0 and 1, i.e. from no synchrony to perfect synchrony of the populations. Any intermediate value of  $\sigma$  accounts for partial synchronization of populations in the system.

The study of asymptotic or long-term dynamics is influential in understanding a natural system. The asymptotic dynamics may display a constant or a periodic phase evolution or even chaos. However, while considering the large-scale dynamics it is of great importance to realize how the population evolves with time. Another important aspect of ecological time scales is the transients, i.e. the dynamics far from the final state of a system. A lot of attention has been given to the study of transient dynamics (Saravia et al, 2000; Hastings, 2001) and it is believed that the final behavior of a system may be quite different from the transient dynamics (Hastings et al, 2018). Therefore, it is essential to study the variations in both the transient and asymptotic dynamics.

We also split the total predator amplitude into transient and asymptotic time series, and take the median of these time series called the *median predator amplitude* (MPA) for transient and asymptotic states. To estimate the transient time, we first used the low pass filter on the time series obtained by numerically integrating the Eqn. (6.1) following an algorithm as described in (Holland and Hastings, 2008). MPA is taken to be an ensemble average of 100 simulations for different sets of randomly chosen initial conditions to avoid uncertainty. We also calculate the mean fraction of time spent in the transient state along with changing global mean temperature to estimate the time taken by the populations to reach a steady state under different warming conditions.

Also, there is a possibility of long transients, i.e. the system reaches asymptotic behavior after a very long time (Schreiber, 2003), and it is even possible that the system never attains an asymptotic state within a given time frame. Therefore, to understand how a system evolves with time, it is important to study the behavior of the system away from its final asymptotic dynamics. Here, we use wavelet analysis to study synchronization and phase relations between interacting species when the system is in a transient state. Wavelet analysis is a commonly used statistical tool for investigating nonstationary time series (Torrence and Compo, 1998). Usually, periodic signals are analyzed by spectral analysis, which uses stationary time series. This sometimes works as a limitation since the majority of ecological time series are nonstationary in nature and hence it may not be able to characterize signals whose frequency content changes with time. It is possible to overcome this hindrance by wavelet analysis, which is now regularly being used for the investigation of ecological time series (Grenfell et al, 2001; Keitt and Fischer, 2006). In the interest of studying



the relative behavior of two-time series, here we use cross-wavelet analysis. It examines the fluctuations of two-time series and also estimates the phase difference between these fluctuations (Grinsted et al, 2004). The cross-wavelet analysis is a powerful tool for testing the possibility of linkages between two-time series (Becks and Arndt, 2013). To study the effect of temperature and distance on species dynamics, we perform the cross-wavelet analysis by considering  $n = 33$  patches. We use the 4th order Runge-Kutta method with  $10^{-2}$  step size to numerically integrate the Eqn. (6.1). Initial conditions of prey are independently and identically distributed, with  $\log_{10}(h_i(0))$  following a uniform distribution on the interval  $(-5, 1 + \log_{10} \hat{h})$ . Parallely, predator initial conditions are independently and identically distributed, with  $\log_{10}(p_i(0))$  uniformly distributed on the interval  $(-5, 1 + \log_{10} \hat{p})$ .  $\hat{h} = \frac{\eta}{\phi - \eta}$  and  $\hat{p} = (1 + \hat{h})(1 - \theta \hat{h})$  are the respective equilibrium densities of prey and predator.

## 6.3 Results

As per the choice of  $f(T)$  and the associated thermal optimum (Eqn. (6.2)), the system has a reflection symmetry on either side of the thermal optimum  $T_{opt} = 20^\circ\text{C}$  (see Fig. 6.1). For example, the results that hold for  $T = 0^\circ\text{C}$  will also hold for  $T = 40^\circ\text{C}$ . Hence, in general, we carry out the numerical experiments for the temperature ranging from  $T = 0^\circ\text{C}$  to  $T = 20^\circ\text{C}$ .

### 6.3.1 Time series analyses and predator amplitude

We observe diverse species dynamics for different values of the temperature  $T$ . Examining the time series of predator density as well as total predator amplitude (Eqn. (6.3)), we find that increasing temperature  $T$  up to the line of symmetry (i.e. the line at  $T = 20^\circ\text{C}$  in Fig. 6.1), moves the system from low to high amplitude values and, hence, less number of clusters  $k$ . Figure 6.2 shows the amplitude fluctuations with time for different values of temperature and it is visible by analyzing cumulative probability (see Figs. 6.2(k)-6.2(o)) that the expectation of getting high amplitude values increases with the increasing temperature.

### 6.3.2 Cluster analysis

The total predator amplitude reveals the oscillatory behavior of populations indicating that the solutions of Eqn. (6.1) can result in different synchronous states of spatially connected species depending upon the number of clusters. Hence, we perform the cluster analysis using the Eqns. (6.4) and (6.5). We observe different

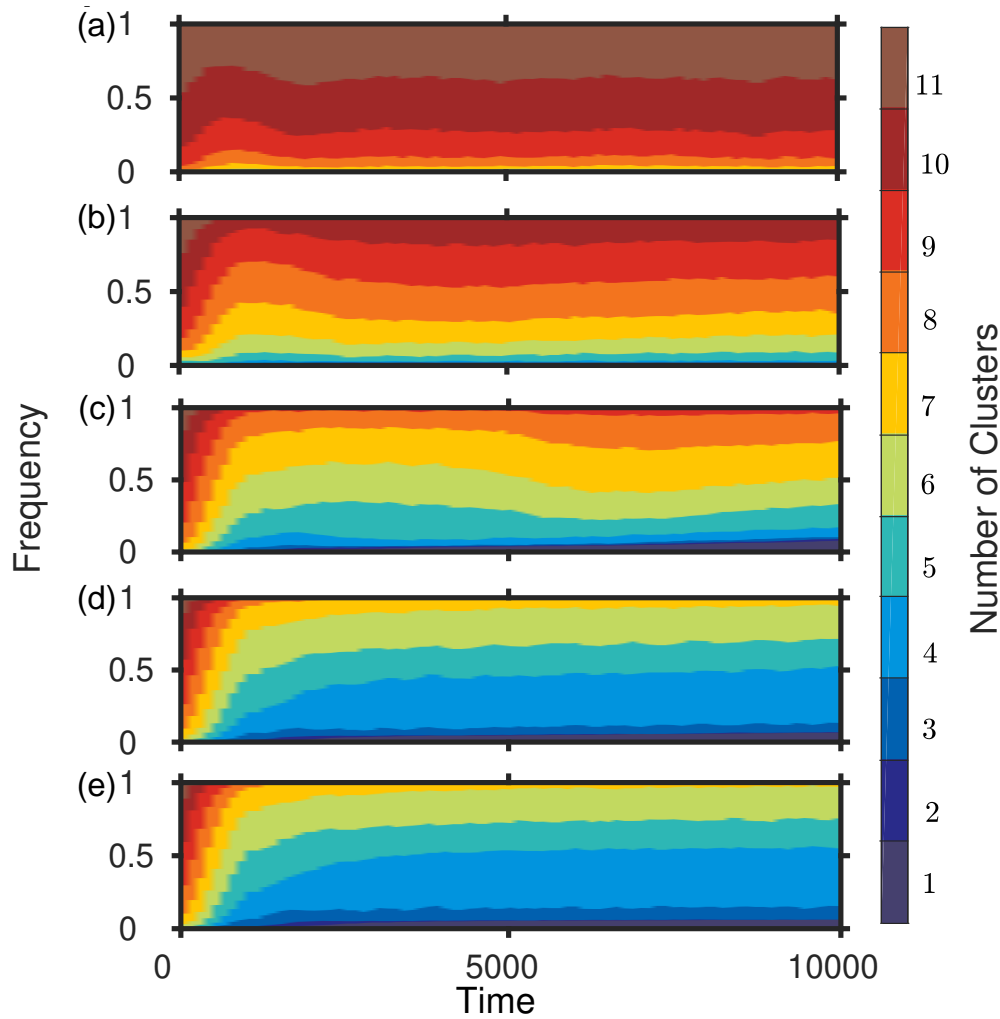


**Figure 6.3.** Frequency of cluster states for different values of  $T$ : (a)  $T = 0^\circ\text{C}$ , (b)  $T = 5^\circ\text{C}$ , (c)  $T = 10^\circ\text{C}$ , (d)  $T = 15^\circ\text{C}$ , and (e)  $T = 20^\circ\text{C}$ . The system converges to high or low number of clusters depending upon the temperature. The number of clusters decreases with the increasing temperature. Local dynamics are governed by  $\theta = 0.3$ ,  $\eta = 1$  and  $\phi = 3$ . Dispersal strengths are:  $\epsilon_h = 2^{-5}$  and  $\epsilon_p = 2^{-6}$ . Each panel is the result of 100 independent simulations.

$k$ -cluster solutions for different warming conditions of the habitat patch,  $k$  ranging from 1 to  $n$  cluster(s).

Analyzing the distribution of clusters (see Fig. 6.3) with changing temperature reveals important information about the collective dynamics of the system. We observe that an increase in the temperature up to the thermal optimum converges the system from a high to a low number of clusters.

### 6.3.3 Interpatch synchrony

Synchrony is highly influenced by species interaction strength. High interaction strength between patches drives more synchronous behavior, when compared to low

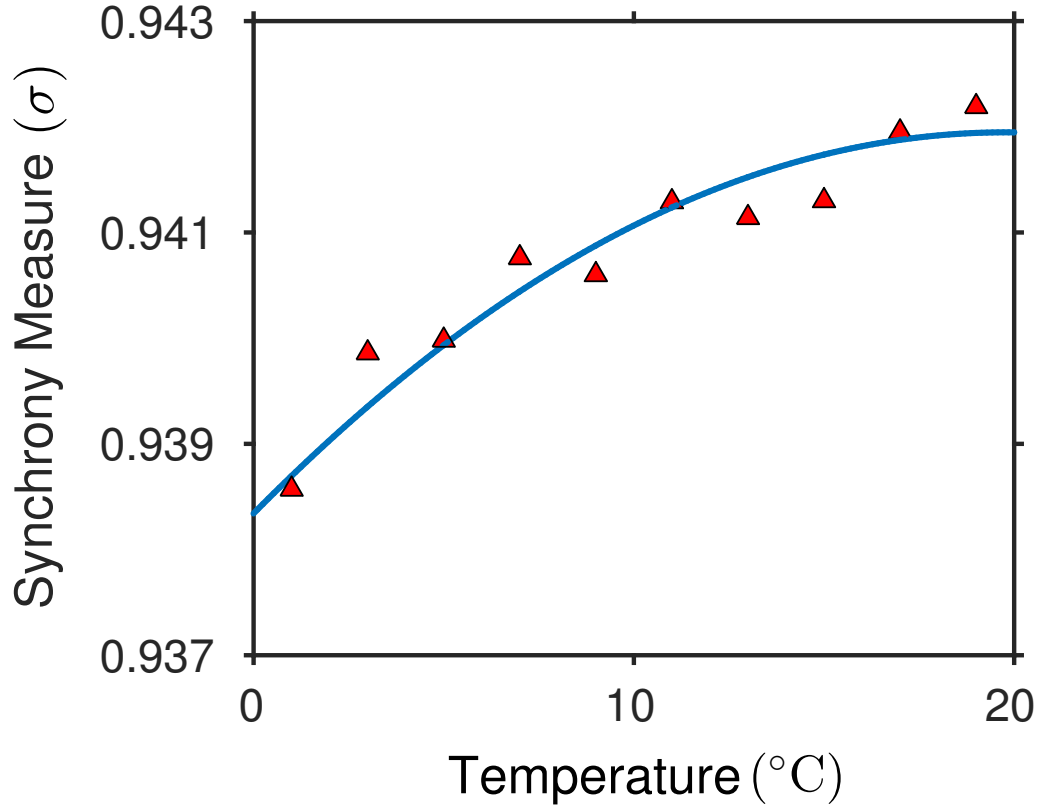


**Figure 6.4.** Synchrony measure  $\sigma$  with changing  $T$ . The triangles represent the estimated value of  $\sigma$  at different values of  $T$ . The solid line is the best curve fit to the estimations. The other parameters are  $\epsilon_h = 2^{-10}$ ,  $\epsilon_p = 2^{-10}$ ,  $\phi = 2$ ,  $\eta = 1$ , and  $\theta = 0.3$ .

interaction strength. We calculate the synchrony order parameter  $\sigma$  (Eqn. (6.6)) to measure the change in synchrony between patches with variations in  $T$ , which explains the qualitative synchronous dynamics of the interaction network. Figure 6.4 depicts that the value of  $\sigma$  increases with the increasing temperature up to the thermal optimum. In fact, synchrony is strongest at the thermal optimum and weakest at both the temperature extremes (extreme low and extreme high temperatures).

#### 6.3.4 Median predator amplitude and mean transient fraction

The MPA depicts the fluctuations in total population density, a low value of MPA implies lower fluctuations and hence high chances of species persistence. It is observed from Fig. 6.5(a) that both transient and asymptotic MPA hold lower values at low temperatures and comparatively higher values at intermediate temperatures. On a related note, we also calculate the mean transient fraction (see Fig. 6.5(b)), the high value of transient time corresponds to asynchronous solutions. We notice that

the transient time is high around low temperatures and decreases with the increasing temperature. Hence, increasing temperature up to the thermal optimum drives the system from long transients and low amplitude solutions to lower transients and higher amplitude solutions.

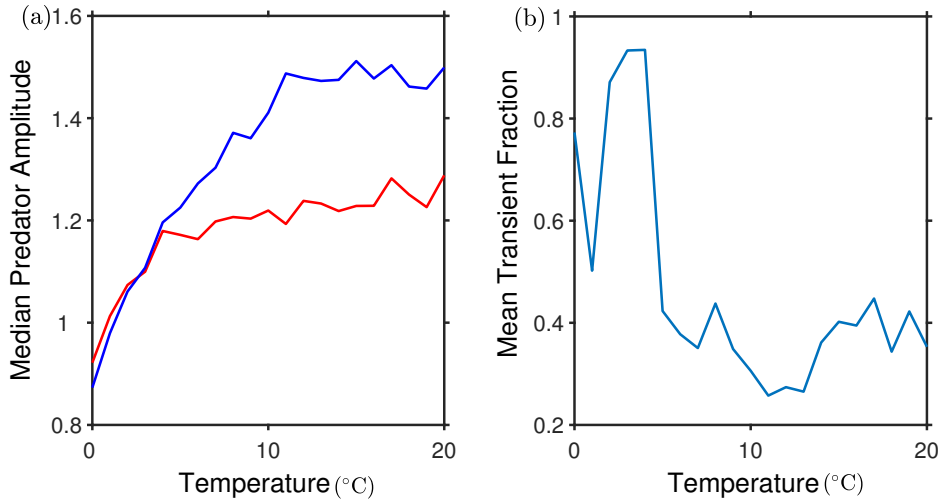


**Figure 6.5.** Median predator amplitude and transient duration. (a) Median predator amplitude for the transient (red) and asymptotic (blue) solution values of  $T$ . (b) The mean fraction of the total time duration the system remains in the transient solutions concerning temperature  $T$ . Parameter values are:  $\theta = 0.3$ ,  $\eta = 1$ ,  $\phi = 3$ ,  $\epsilon_h = 2^{-5}$ , and  $\epsilon_p = 2^{-6}$ .

### 6.3.5 Cross wavelet analysis

Wavelet analysis can be helpful to quantify and interpret powerful information stored in the transient state (Torrence and Compo, 1998). To study the interactions between different time series and to understand how the behavioral state changes in a given period we perform cross wavelet analysis (see Fig. 6.6). Black contour lines enclose a region of 95% confidence level. Wavelet transform at any point at a given time also contains information on the nearby data points and since we have considered time series of finite length, there are chances of error at the beginning and end of the time series, known as the edge effects. Cone of influence is the region of the power spectrum where edge effects might distort the signal, and which is represented by the shaded region on both sides of the contour. Therefore, we confine our study to the non-shaded regions.

By the cross-wavelet analysis, the density fluctuations between predator species of two distinct patches with high common power (yellow band) are observed at a considerable periodicity of 8 – 16 units of time. To study the coordination between predator species of two distinct patches we analyze the phase shift between them. At the extreme temperature  $T = 0^\circ\text{C}$ , the arrows in the eloquent common power

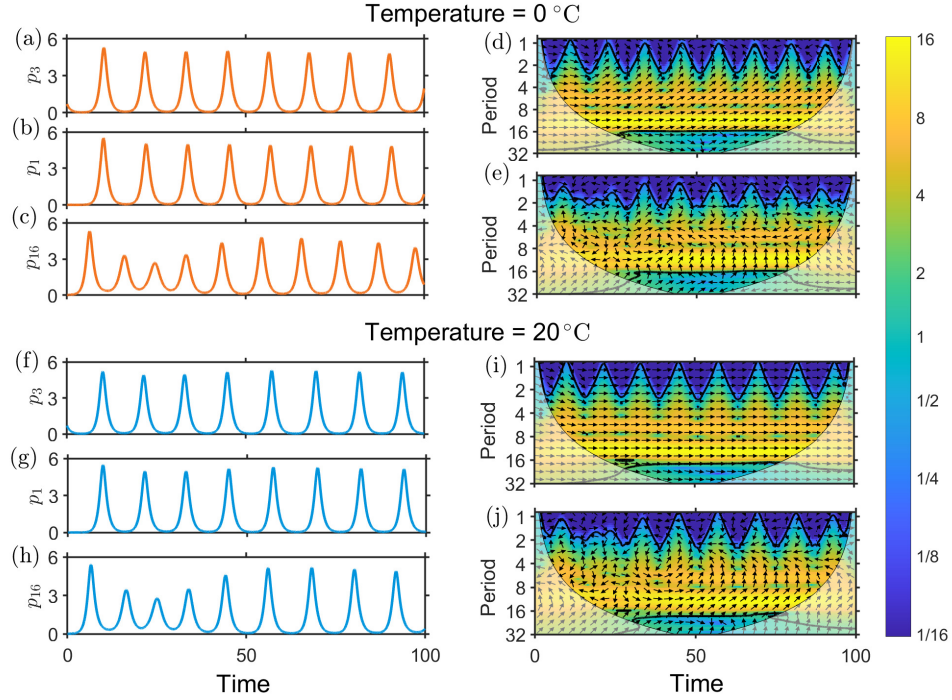


**Figure 6.6.** Time series (left panels) and cross wavelet spectra (right panels) of the predator  $p_i$ . For two distinct temperatures: (a)-(c)  $T = 0^\circ\text{C}$  and (f)-(h)  $T = 20^\circ\text{C}$ , are the time series of predator density  $p_i$ , where  $i = 1, 3, 16$  is the patch index, in three distinct patches. (d), (i) Cross-wavelet spectra of the predator in two nearest patches  $p_1$  and  $p_3$ . (e), (j) Cross-wavelet spectra of the predator in two farthest patches  $p_1$  and  $p_{16}$ . At  $T = 0^\circ\text{C}$ , in case of nearest patches ((a), (b); (d)) the predator species oscillates in phase angle of  $\approx 30^\circ$ ; for the farthest patches ((b), (c); (e)) interactions lead to different phase angles ( $\approx 90^\circ$ ). At  $T = 20^\circ\text{C}$ , species, in the nearest patches oscillate in phase i.e  $0^\circ$  ((f), (g); (i)); in case of farthest patches ((g), (h); (j)) predator species show a phase drift of  $\approx 45^\circ$ . The black contour in cross-wavelet spectra encloses a significant region (95% confidence level) of consideration. The color code follows a pattern from blue to yellow; the blue color indicates the region with low power whereas the yellow region is with high power. Other parameter values are:  $n = 33$ ,  $\theta = 0.3$ ,  $\eta = 1$ ,  $\phi = 3$ ,  $\epsilon_h = 2^{-5}$ , and  $\epsilon_p = 2^{-6}$ .

(yellow band) reflect a phase difference of  $\approx 30^\circ$  between the fluctuations in predator density of the two nearest patches, i.e.  $p_1$  and  $p_3$  (we consider those nearest patches where  $d$  is not equal to 1) (see Fig. 6.6(d)). On the other side, a phase shift of  $\approx 90^\circ$  is observed between the fluctuations of predator species of two farthest patches, i.e.  $p_1$  and  $p_{16}$  (see Fig. 6.6(e)). When analyzed the dynamics at the thermal optimum  $T = 20^\circ\text{C}$ , the phase angle is centred around  $0^\circ$  for the predator species of nearest patches (see Fig. 6.6(i)), whereas, the fluctuations between two predator species of farthest patches show a phase drift of  $\approx 45^\circ$  (Fig. 6.6(j)).

## 6.4 Discussion

Understanding the effects of dispersal on population dynamics is one of the major issues in spatial ecology. Dispersal is considered to be a “double-edged sword” (Hudson and Cattadori, 1999), since dispersal not only contributes towards species

persistence by preventing local extinctions due to recolonization, but at some time it can also be responsible for synchronizing the populations which can trigger the possibility of global extinction. The realization that the changing climate has a strong impact on spatial populations, communities, and whole ecosystems, triggered a lot of interest in investigating the effects of temperature-influenced dispersal on metapopulations (Bestion et al, 2015; Watkinson and Gill, 2002). Here, we have presented a mathematical framework elucidating the effects of temperature on species dispersal. This framework illustrates how the dispersal strength that promotes synchrony at temperature results in some form of ecological stability at different extreme temperatures via asynchrony.

Range or habitat shifts are one of the natural ecological responses to climate change. When the temperature is not favourable, i.e. at extreme temperatures, we have claimed interaction strength to be low which corresponds to low species dispersal, hence the intensity of LDD is low. This persuades the asynchronous behavior of the population at the extreme temperatures. Whereas, at the intermediate temperatures due to active biological traits of species, dispersal is more prompt, which makes a species efficient in going to any habitat patch. Thus, resulting in high intensity of SDD as well as moderate LDD. For instance, at the extreme temperatures, we get comparatively more clusters and a lower value of predator amplitude than at the intermediate temperatures, which depicts variations in the spatial dynamics. For different values of the temperature sensitivity  $s$ , the results are qualitatively similar. We have also observed the change in the measure of synchrony with the changing temperature. Our study indicates that the synchrony order parameter holds a low value at extreme temperatures when compared with the value at intermediate temperatures, including the thermal optimum.

These results hold important implications for understanding how temperature variations affect dispersal, which further has an impact on population persistence. We find that long-range dispersal at extreme temperatures turns out to be beneficial for the species' persistence. The asynchronous behavior of populations at extreme temperatures signifies that the minimum densities of species occur at different time instances for most of the patches, thus making the dispersing species more persistent by reducing their vulnerability towards environmental perturbation.

We also emphasize the importance of understanding dynamics during the transient time. Corresponding to this we study the behavior of MPA differently for transient as well as asymptotic phase. The lower amplitude asymptotic solutions with higher transient duration at low temperatures (see Fig 6.5(a) and Fig 6.5(b)) reveals the asynchronous behavior of the system. Our study demonstrates how dispersal in a regular network under the influence of increasing global temperature drives the system from asynchrony to synchrony and asynchrony.

Further, our study interprets the effects of climate warming on species dispersal, influencing their persistence. In view of a better understanding of the evolution of such dynamics, we figure out the interactions between species of distinct patches at different temperatures through cross-wavelet analysis of a few transient time series. At the extreme temperature  $T = 0^{\circ}\text{C}$ , the cross wavelet analysis explores the asynchrony between the species oscillations of two nearer patches, however, the degree of asynchrony becomes stronger when we consider two further patches. This is because the dispersal strength becomes weaker between furthest patches which results in stronger asynchrony, in comparison with the asynchrony between nearer patches. Similarly, at the optimum temperature  $T = 20^{\circ}\text{C}$ , we see almost synchrony in species oscillations between two nearer patches and the degree of synchrony reduces when we consider the two furthest patches. In conformity with the phase shifts observed at  $T = 0^{\circ}\text{C}$  between the fluctuations of predator species of nearer and farthest patches, we state that the intensity of SDD is much more than that of LDD. On another note, based on the analysis of phase shifts at  $T = 20^{\circ}\text{C}$  by examining our results (Fig. 6.3 and Fig. 6.6), we claim that at intermediate temperatures, the species are resilient towards long-distance dispersal as well.

In conclusion, our study demonstrates the dispersal-temperature relationship from the perspectives of dynamical systems. We have considered a uniform model with a difference in dispersal strengths of prey and predators in each patch. Developing more mechanistic models elucidating temperature effects on dispersal by taking into account heterogeneity in the structure, and also considering intra-specific competition, which are equally substantial for the survivorship of species, is an important future direction. Further, the assumption that different species have different temperature sensitivity may reveal interesting results. It is also important to study the dynamics of the spatial system where temperature is a function of time. This can be done by considering the increase in temperature at a very slow rate (global warming ([Wieczorek et al, 2011](#))) or by assuming a periodic function (to model seasonality ([Levy et al, 2016](#))). Moreover, there is a need to understand the influence of climate change on both the local and spatial ecological processes simultaneously and the long-term dynamics driven by their mutual interactions.





# Chapter 7

## Conclusions

---

### 7.1 Key findings

This thesis focuses on different factors that determine the stability and functioning of spatial ecological systems. In particular, from the mathematical modeling perspective, we demonstrate how the movement patterns of metapopulations, changes in network structure, landscape layout, and ecosystem stochasticity can greatly influence complex communities' dynamics.

After extensive research on stochastic ecological systems, the genesis and robustness of noise-induced symmetry breaking (NISB) remains challenging. To fill this gap, we study the simultaneous effect of network structure and noise on an ecological network of excitable systems. We find that while in the absence of noise, the system resides in a single steady state, the presence of noise drives the system out of the resting state, leading to various collective dynamics. Varying noise intensity and network topology results in a transition from a homogeneous steady state to inhomogeneous steady states via NISB, before turning into noise-induced asynchronous oscillations. The system exhibits oscillatory dynamics for adequate noise intensity and non-local coupling, or it breaks into two sub-populations with two distinct (inhomogeneous) noise-induced steady states. Further, for fixed noise intensity and changing the coupling range from local to global, we identify a transition from an oscillatory domain to a region of homogeneous steady state through inhomogeneous steady states. Overall, our results can have significant implications for understanding the positive effects of noise on species diversity. We thus emphasize the need to study the interplay between noise and deterministic mechanisms, which have significance for biological conservation.

The study on networks has focused on the interactions between the node states mediated by links. However, including higher-order interactions can alter the behavior of complex networks. We consider an ecological network of spatially separated patches subjected to pairwise interactions and three-body higher-order interactions using simplicial complexes to investigate this. We study the collective behavior and elucidate the effect of network structure and higher-order interactions on ecological dynamics. We find that where, in the presence of only dyadic

couplings, a random network could increase the stability of a metacommunity by inducing asynchronous oscillations, higher-order interactions suppress asynchrony and pave the way to synchronous solutions (two clusters). On the contrary, in all-to-all coupling (high node degree), the system with increasing higher-order coupling strength results in a transition from a region of asynchronous oscillations to a complete synchrony (one cluster solution). In all, our results illustrate how higher-order interactions impact the characteristics and dynamics of a system depending upon the interacting units of the network, which thus hold important implications in the stability and persistence of a community.

Further, habitat loss and fragmentation have raised major concerns about its consequences on the functioning and services of ecosystems. Movement strategies are key in maintaining connectivity and increasing survival in a fragmented landscape. We consider a spatially explicit stochastic vegetation-grazer model in a fragmented landscape and study the interplay between foraging behavior, resource pulse, and the survival rates of species. Our work unveils the important interdependence of movement behavior and species' survival rate. It highlights the significant aspect of resource pulse on the persistence and stability of populations in a fragmented landscape. Our analysis shows that the optimal foraging strategy highly depends upon the survival conditions and the amount of resources. We observe that Lévy walk is always an effective movement strategy; however, the optimal foraging behavior changes from the Brownian to ballistic with the increase in the rate of mortality of grazers. Overall, our study shows that a movement may counterbalance the effect of adverse conditions and promote species coexistence.

Climate warming is one of the decisive factors for the apparent range shifts and local extinctions of species. Species may need effective dispersal strategies to cope with the changing environmental conditions to ensure metacommunity persistence. We investigate how the rising temperature governing species' local dynamics alters dispersal response at the regional scale. We study spatial synchrony and analyze how coherence or incoherence in species abundance is affected by different dispersal mechanisms and thermal traits. High dispersal rates tend to synchronize dynamics, leading towards high regional variability, thus decreasing stability. Whereas, for low dispersal rates, at low and intermediate temperatures, the existence of two alternative collective dynamics, one with complete synchrony and the other with strong asynchrony, enhances the chances of persistence of species. However, high temperatures completely synchronize the population trailing constant dispersal, thus weakening the stabilizing dynamics. It is also observed that density-dependent dispersal (DD) could modify metacommunity stability by inducing asynchronous fluctuations in population abundance at high temperatures. We also demonstrate the role of temperature in the emergence of chimera (coexistence of coherent

and incoherent solutions) in constant dispersal. We observe that at intermediate temperature and for low dispersal strength, the population splits into coherent and incoherent domains, thus resulting in chimera. In contrast, high temperature drives all the oscillators towards complete synchrony, thus weakening population persistence. Our results elucidate that DD and relative dispersal are crucial in understanding metacommunity stability under the effect of global warming.

Finally, we study a spatial consumer-resource model where the distance between patches and the temperature-dependent power law function modulates the dispersal strengths of species. Our study yields how the temperature influences species' decision of dispersal, resulting in either short-range or long-range dispersal. We examine species' synchronous or asynchronous behavior under their thermal dependence of dispersal. The dispersal strength that promotes synchrony at a specific temperature is observed to result in some form of ecological stability at different extreme temperatures via asynchrony. We also emphasize the importance of understanding species dynamics during the transient time. We determine the interactions between species of nearest and farthest patches at different temperatures through cross-wavelet analysis using transient time series. In conformity with the phase shifts observed at extreme temperatures between the fluctuations of species, we state that the intensity of short-distance dispersal is much more than that of long-distance dispersal. On another note, we claim that at intermediate temperatures, the species are resilient towards long-distance dispersal as well.

Overall, our work develops a better understanding of various dynamic processes persuaded by different factors in spatial ecological networks.

## 7.2 Future directions

Our research findings center on investigating the impacts of noise, network topology, dispersal patterns, and landscape structure within complex ecological systems. Nonetheless, various factors that dictate the persistence of populations and communities necessitate a thorough comprehension of their repercussions on ecosystems. There are still many unknowns about this topic. Here are some questions that could be considered for future research:

We analyzed the influence of noise on an ecological network and explored how changes in the network structure impact the system's dynamics. Further, it could be intriguing to understand the extent to which these criteria remain valid if the network inhabits temporal structural change. Additionally, an essential future exploration could involve examining a two-dimensional lattice of excitable systems and analyzing how spatiotemporal dynamics are influenced when demographic noise is introduced.

Exploring the Fokker-Planck equation for stochastic ecological networks is essential for future research. This analytical approach has the potential to enhance our understanding of the observed collective dynamics.

We've noticed that higher-order interactions incorporated result in distinct collective behavior compared to the standard pairwise approach. Numerous unresolved challenges must be addressed when exploring higher-order interactions in spatial ecological systems. We have focused on studying simplicial complexes. It's unclear how our results would change if we consider different higher-order structures, like hypergraphs. Furthermore, exploring multilayer and temporal networks has the potential to unveil new phenomena and insights.

Our research uncovers how movement behavior impacts ecological systems and emphasizes the significant role of resource pulses in maintaining the persistence and stability of populations within a fragmented landscape. We introduced resource pulses into the system following a regular pattern. Examining how dynamics change when the resource pulse becomes aperiodic could reveal intriguing and diverse patterns. Considering the higher trophic interactions in a heterogeneous landscape, which incorporates the dispersal costs, is an important future direction to investigate the effect of movement on landscape connectivity and ecological stability.

We emphasize that considering temperature and distance when studying dispersal patterns is crucial for comprehending metacommunity stability. Further, considering different species' climate niches in understanding their response, i.e., either adapt or disperse ([Berg et al, 2010](#)), is much needed. Moreover, [Kuussaari et al \(2016\)](#) found an increase in dispersal rates with increasing temperature and population abundance of the *Clouded Apollo* butterfly. In contrast, a study by [Jourdan et al \(2019\)](#) on the crane fly *Tipula maxima* reveals the negative effect of rising temperatures on their dispersal in dealing with changing climatic conditions. Moreover, the analysis done by [Pärn et al \(2012\)](#) on the house sparrow *Passer domesticus* demonstrates the effect of temperature on dispersal rates depending upon the habitat quality. They found that dispersal rates increased with temperature on islands that lacked food resources; however, they are independent of temperature on islands with farms. Therefore, analyzing how species' dispersal abilities can vary following their thermal tolerance is crucial for conserving a metacommunity.

# References

---

- Abbott KC (2011) A dispersal-induced paradox: synchrony and stability in stochastic metapopulations. *Ecology Letters* 14(11):1158–1169
- Abrams DM, Strogatz SH (2004) Chimera states for coupled oscillators. *Physical Review Letters* 93(17):174,102
- Aizenman M, Chayes JT, Chayes L, Neuman CM (1988) Synchronization and plateau splitting of coupled oscillators with long-range power-law interactions. *J Stat Phys* 50:1
- Albert R, Barabási AL (2002) Statistical mechanics of complex networks. *Reviews of Modern Physics* 74(1):47
- Alvarez-Rodriguez U, Battiston F, de Arruda GF, Moreno Y, Perc M, Latora V (2021) Evolutionary dynamics of higher-order interactions in social networks. *Nature Human Behaviour* 5(5):586–595
- Amaral LAN, Scala A, Barthélemy M, Stanley HE (2000) Classes of small-world networks. *Proceedings of the National Academy of Sciences* 97(21):11,149–11,152
- Amarasekare P (2015) Effects of temperature on consumer–resource interactions. *Journal of Animal Ecology* 84(3):665–679
- Amarasekare P, Johnson C (2017) Evolution of thermal reaction norms in seasonally varying environments. *The American Naturalist* 189(3):E31–E45
- Amarasekare P, Savage V (2011) A framework for elucidating the temperature dependence of fitness. *The American Naturalist* 179(2):178–191
- Amritkar R, Rangarajan G (2006) Spatially synchronous extinction of species under external forcing. *Physical Review Letters* 96(25):258,102
- Andreassen HP, Ims RA (2001) Dispersal in patchy vole populations: role of patch configuration, density dependence, and demography. *Ecology* 82(10):2911–2926
- Arenas A, Díaz-Guilera A, Kurths J, Moreno Y, Zhou C (2008) Synchronization in complex networks. *Physics Reports* 469(3):93–153
- Armstrong RA, McGehee R (1980) Competitive exclusion. *The American Naturalist* 115(2):151–170

- Armsworth PR, Roughgarden JE (2005) The impact of directed versus random movement on population dynamics and biodiversity patterns. *The American Naturalist* 165(4):449–465
- Arnaudon A, Peach RL, Petri G, Expert P (2022) Connecting hodge and sakaguchi-kuramoto through a mathematical framework for coupled oscillators on simplicial complexes. *Communications Physics* 5(1):211
- Austin D, Bowen W, McMillan J (2004) Intraspecific variation in movement patterns: modeling individual behaviour in a large marine predator. *Oikos* 105(1):15–30
- Bairey E, Kelsic ED, Kishony R (2016) High-order species interactions shape ecosystem diversity. *Nature communications* 7(1):12,285
- Baker MB, Rao S (2004) Incremental costs and benefits shape natal dispersal: theory and example with *hemilepistus reaumuri*. *Ecology* 85(4):1039–1051
- Balvanera P, Pfisterer AB, Buchmann N, He JS, Nakashizuka T, Raffaelli D, Schmid B (2006) Quantifying the evidence for biodiversity effects on ecosystem functioning and services. *Ecology Letters* 9(10):1146–1156
- Banerjee T, Dutta PS, Zakharova A, Schöll E (2016) Chimera patterns induced by distance-dependent power-law coupling in ecological networks. *Physical Review E* 94(3):032,206
- Bani R, Fortin MJ, Daigle RM, Guichard F (2019) Dispersal traits interact with dynamic connectivity to affect metapopulation growth and stability. *Theoretical Ecology* 12:111–127
- Barabási AL, Albert R (1999) Emergence of scaling in random networks. *Science* 286(5439):509–512
- Barahona M, Pecora LM (2002) Synchronization in small-world systems. *Physical Review Letters* 89(5):054,101
- Barkham J, Hance C (1982) Population dynamics of the wild daffodil (*narcissus pseudonarcissus*): Iii. implications of a computer model of 1000 years of population change. *The Journal of Ecology* pp 323–344
- Bartumeus F, Catalan J (2009) Optimal search behavior and classic foraging theory. *Journal of Physics A: Mathematical and Theoretical* 42(43):434,002

- Bartumeus F, Peters F, Pueyo S, Marrasé C, Catalan J (2003) Helical lévy walks: adjusting searching statistics to resource availability in microzooplankton. *Proceedings of the National Academy of Sciences* 100(22):12,771–12,775
- Bartumeus F, da Luz MGE, Viswanathan GM, Catalan J (2005) Animal search strategies: a quantitative random-walk analysis. *Ecology* 86(11):3078–3087
- Bascompte J, Solé RV (1996) Habitat fragmentation and extinction thresholds in spatially explicit models. *Journal of Animal Ecology* pp 465–473
- Battisti A, Stastny M, Buffo E, Larsson S (2006) A rapid altitudinal range expansion in the pine processionary moth produced by the 2003 climatic anomaly. *Global Change Biology* 12(4):662–671
- Battiston F, Cencetti G, Iacopini I, Latora V, Lucas M, Patania A, Young JG, Petri G (2020) Networks beyond pairwise interactions: Structure and dynamics. *Physics Reports* 874:1–92
- Becks L, Arndt H (2013) Different types of synchrony in chaotic and cyclic communities. *Nature Communications* 4:1359
- Bell WJ (2012) Searching behaviour: the behavioural ecology of finding resources. Springer Science & Business Media
- Benhamou S, Bovet P (1989) How animals use their environment: a new look at kinesis. *Animal Behaviour* 38(3):375–383
- Beninca E, Dakos V, Van Nes EH, Huisman J, Scheffer M (2011) Resonance of plankton communities with temperature fluctuations. *The American Naturalist* 178(4):E85–E95
- Benincà E, Ballantine B, Ellner SP, Huisman J (2015) Species fluctuations sustained by a cyclic succession at the edge of chaos. *Proceedings of the National Academy of Sciences USA* 112(20):6389–6394
- Benzi R, Sutera A, Vulpiani A (1981) The mechanism of stochastic resonance. *Journal of Physics A: Mathematical and General* 14(11):L453
- Berg MP, Kiers ET, Driessen G, Van Der HEIJDEN M, Kooi BW, Kuenen F, Liefing M, Verhoef HA, Ellers J (2010) Adapt or disperse: understanding species persistence in a changing world. *Global Change Biology* 16(2):587–598
- Berge C (1973) *Graphs and hypergraphs*. north-holl math. libr

- Bestion E, Clobert J, Cote J (2015) Dispersal response to climate change: scaling down to intraspecific variation. *Ecology Letters* 18(11):1226–1233
- Bhandary S, Biswas D, Banerjee T, Dutta PS (2022) Effects of time-varying habitat connectivity on metacommunity persistence. *Physical Review E* 106(1):014,309
- Biancalani T, Dyson L, McKane AJ (2014) Noise-induced bistable states and their mean switching time in foraging colonies. *Physical Review Letters* 112(3):038,101
- Billings L, Schwartz IB (2002) Exciting chaos with noise: unexpected dynamics in epidemic outbreaks. *Journal of Mathematical Biology* 44(1):31–48
- Bjørnstad ON (2000) Cycles and synchrony: two historical ‘experiments’ and one experience. *Journal of Animal Ecology* 69(5):869–873
- Bjørnstad ON, Ims RA, Lambin X (1999) Spatial population dynamics: analyzing patterns and processes of population synchrony. *Trends in Ecology & Evolution* 14(11):427–432
- Blasius B, Huppert A, Stone L (1999) Complex dynamics and phase synchronization in spatially extended ecological systems. *Nature* 399(6734):354–359
- Boccaletti S, Latora V, Moreno Y, Chavez M, Hwang DU (2006) Complex networks: Structure and dynamics. *Physics Reports* 424(4-5):175–308
- Boccaletti S, Pisarchik AN, Del Genio CI, Amann A (2018) Synchronization: from coupled systems to complex networks. Cambridge University Press
- de Boer MK, Moor H, Matthiessen B, Hillebrand H, Eriksson BK (2014) Dispersal restricts local biomass but promotes the recovery of metacommunities after temperature stress. *Oikos* 123(6):762–768
- Boschi CDE, Louis E, Ortega G (2001) Triggering synchronized oscillations through arbitrarily weak diversity in close-to-threshold excitable media. *Physical Review E* 65(1):012,901
- Briggs CJ, Hoopes MF (2004) Stabilizing effects in spatial parasitoid–host and predator–prey models: a review. *Theoretical Population Biology* 65(3):299–315
- Brooker RW, Travis JM, Clark EJ, Dytham C (2007) Modelling species’ range shifts in a changing climate: the impacts of biotic interactions, dispersal distance and the rate of climate change. *Journal of Theoretical Biology* 245(1):59–65
- Brown JH, Kodric-Brown A (1977) Turnover rates in insular biogeography: effect of immigration on extinction. *Ecology* 58(2):445–449



- Buldú JM, García-Ojalvo J, Mirasso CR, Torrent M, Sancho J (2001) Effect of external noise correlation in optical coherence resonance. *Physical Review E* 64(5):051,109
- Cardinale BJ, Srivastava DS, Emmett Duffy J, Wright JP, Downing AL, Sankaran M, Jouseau C (2006) Effects of biodiversity on the functioning of trophic groups and ecosystems. *Nature* 443(7114):989–992
- Carletti T, Battiston F, Cencetti G, Fanelli D (2020) Random walks on hypergraphs. *Physical review E* 101(2):022,308
- Cayan DR, Kammerdiener SA, Dettinger MD, Caprio JM, Peterson DH (2001) Changes in the onset of spring in the western united states. *Bulletin of the American Meteorological Society* 82(3):399–416
- Cencetti G, Battiston F, Lepri B, Karsai M (2021) Temporal properties of higher-order interactions in social networks. *Scientific Reports* 11(1):7028
- Chapin Iii FS, Zavaleta ES, Eviner VT, Naylor RL, Vitousek PM, Reynolds HL, Hooper DU, Lavorel S, Sala OE, Hobbie SE, et al (2000) Consequences of changing biodiversity. *Nature* 405(6783):234–242
- Chavez M, Hwang DU, Amann A, Hentschel H, Boccaletti S (2005) Synchronization is enhanced in weighted complex networks. *Physical Review Letters* 94(21):218,701
- Chesson P (2000) Mechanisms of maintenance of species diversity. *Annual Review of Ecology and Systematics* pp 343–366
- Chesson PL, Ellner S (1989) Invasibility and stochastic boundedness in monotonic competition models. *Journal of Mathematical Biology* 27(2):117–138
- Chesson PL, Warner RR (1981) Environmental variability promotes coexistence in lottery competitive systems. *The American Naturalist* 117(6):923–943
- Clark JS, Silman M, Kern R, Macklin E, HilleRisLambers J (1999) Seed dispersal near and far: patterns across temperate and tropical forests. *Ecology* 80(5):1475–1494
- Clobert J, Baguette M, Benton TG, Bullock JM (2012) Dispersal ecology and evolution. Oxford University Press
- Connell JH (1961) Effects of competition, predation by *thais lapillus*, and other factors on natural populations of the barnacle *balanus balanoides*. *Ecological Monographs* 31(1):61–104

- Connell JH, Sousa WP (1983) On the evidence needed to judge ecological stability or persistence. *The American Naturalist* 121(6):789–824
- Crist TO, Guertin DS, Wiens JA, Milne BT (1992) Animal movement in heterogeneous landscapes: an experiment with eleodes beetles in shortgrass prairie. *Functional Ecology* pp 536–544
- Dakos V, Bascompte J (2014) Critical slowing down as early warning for the onset of collapse in mutualistic communities. *Proceedings of the National Academy of Sciences USA* 111(49):17,546–17,551
- Dannemann T, Boyer D, Miramontes O (2018) Lévy flight movements prevent extinctions and maximize population abundances in fragile lotka–volterra systems. *Proceedings of the National Academy of Sciences* 115(15):3794–3799
- Del Genio CI, Gómez-Gardeñes J, Bonamassa I, Boccaletti S (2016) Synchronization in networks with multiple interaction layers. *Science Advances* 2(11):e1601,679
- Denno RF, Cheng J, Roderick GK, Perfect TJ (1994) Density-related effects on the components of fitness and population dynamics of planthoppers. In: *Planthoppers: their ecology and management*, Springer, pp 257–281
- Diffendorfer JE, Gaines MS, Holt RD (1995) Habitat fragmentation and movements of three small mammals (*sigmodon*, *microtus*, and *peromyscus*) ecological archives e076-002. *Ecology* 76(3):827–839
- Dillon ME, Wang G, Huey RB (2010) Global metabolic impacts of recent climate warming. *Nature* 467(7316):704–706
- Dixon A (1969) Population dynamics of the sycamore aphid *drepanosiphum platanoides* (schr.)(hemiptera: Aphididae): migratory and trivial flight activity. *The Journal of Animal Ecology* pp 585–606
- D’Odorico P, Laio F, Ridolfi L (2005) Noise-induced stability in dryland plant ecosystems. *Proceedings of the National Academy of Sciences* 102(31):10,819–10,822
- Dunn PO, Winkler DW (1999) Climate change has affected the breeding date of tree swallows throughout north america. *Proceedings of the Royal Society of London Series B: Biological Sciences* 266(1437):2487–2490
- Dutta PS, Banerjee T (2015) Spatial coexistence of synchronized oscillation and death: A chimera-like state. *Physical Review E* 92(4):042,919

- Dutta PS, Kooi BW, Feudel U (2014) Multiple resource limitation: nonequilibrium coexistence of species in a competition model using a synthesizing unit. *Theoretical Ecology* 7(4):407–421
- Dutta PS, Kooi BW, Feudel U (2017) The impact of a predator on the outcome of competition in the three-trophic food web. *Journal of Theoretical Biology* 417:28–42
- Eide RM, Krause AL, Fadaei NT, Van Gorder RA (2018) Predator-prey-subsidy population dynamics on stepping-stone domains with dispersal delays. *Journal of Theoretical Biology* 451:19–34
- Eklöf A, Kaneryd L, Mürger P (2012) Climate change in metacommunities: dispersal gives double-sided effects on persistence. *Philosophical Transactions of the Royal Society B: Biological Sciences* 367(1605):2945–2954
- Elton CS (1924) Periodic fluctuations in the numbers of animals: their causes and effects. *Journal of Experimental Biology* 2(1):119–163
- Englund G, Öhlund G, Hein CL, Diehl S (2011) Temperature dependence of the functional response. *Ecology Letters* 14(9):914–921
- Erdős P, Rényi A (1959) On random graphs i. *Publ Math Debrecen* 6(290-297):18
- Ergon T, Lambin X, Stenseth NC (2001) Life-history traits of voles in a fluctuating population respond to the immediate environment. *Nature* 411(6841):1043–1045
- Eveleigh ES, McCann KS, McCarthy PC, Pollock SJ, Lucarotti CJ, Morin B, McDougall GA, Strongman DB, Huber JT, Umbanhowar J, et al (2007) Fluctuations in density of an outbreak species drive diversity cascades in food webs. *Proceedings of the National Academy of Sciences* 104(43):16,976–16,981
- Fahrig L (2003) Effects of habitat fragmentation on biodiversity. *Annual Review of Ecology, Evolution, and Systematics* 34(1):487–515
- Fahrig L, Merriam G (1985) Habitat patch connectivity and population survival: Ecological archives e066-008. *Ecology* 66(6):1762–1768
- Fey SB, Vasseur DA (2016) Thermal variability alters the impact of climate warming on consumer–resource systems. *Ecology* 97(7):1690–1699
- Focardi S, Marcellini P, Montanaro P (1996) Do ungulates exhibit a food density threshold? a field study of optimal foraging and movement patterns. *Journal of Animal Ecology* pp 606–620

- Foden WB, Mace GM, Vié JC, Angulo A, Butchart SH, DeVantier L, Dublin HT, Gutsche A, Stuart S, Turak E (2009) Species susceptibility to climate change impacts. *Wildlife In A Changing World—An Analysis Of The 2008 IUCN Red List of Threatened Species* 77
- Fortuna MA, Gómez-Rodríguez C, Bascompte J (2006) Spatial network structure and amphibian persistence in stochastic environments. *Proceedings of the Royal Society B: Biological Sciences* 273(1592):1429–1434
- France KE, Duffy JE (2006) Diversity and dispersal interactively affect predictability of ecosystem function. *Nature* 441(7097):1139–1143
- Franco AM, Hill JK, Kitschke C, Collingham YC, Roy DB, Fox R, Huntley B, Thomas CD (2006) Impacts of climate warming and habitat loss on extinctions at species' low-latitude range boundaries. *Global Change Biology* 12(8):1545–1553
- Gambuzza LV, Di Patti F, Gallo L, Lepri S, Romance M, Criado R, Frasca M, Latora V, Boccaletti S (2021) Stability of synchronization in simplicial complexes. *Nature Communications* 12(1):1255
- Gammaitoni L, Hänggi P, Jung P, Marchesoni F (1998) Stochastic resonance. *Reviews of Modern Physics* 70(1):223
- Gang H, Ditzinger T, Ning CZ, Haken H (1993) Stochastic resonance without external periodic force. *Physical Review Letters* 71(6):807
- Ganopolski A, Rahmstorf S (2002) Abrupt glacial climate changes due to stochastic resonance. *Physical Review Letters* 88(3):038,501
- García-Ojalvo J, Schimansky-Geier L (1999) Noise-induced spiral dynamics in excitable media. *Europhysics Letters* 47(3):298
- Gause G (1935) Experimental demonstration of volterra's periodic oscillations in the numbers of animals. *Journal of Experimental Biology* 12(1):44–48
- Gilarranz LJ, Bascompte J (2012) Spatial network structure and metapopulation persistence. *Journal of Theoretical Biology* 297:11–16
- Gilchrist GW (1995) Specialists and generalists in changing environments. i. fitness landscapes of thermal sensitivity. *The American Naturalist* 146(2):252–270
- Goldwasser L, Cook J, Silverman E (1994) The effects of variability on metapopulation dynamics and rates of invasion. *Ecology* 75(1):40–47

- Goldwyn EE, Hastings A (2008) When can dispersal synchronize populations? *Theoretical Population Biology* 73(3):395–402
- Goldwyn EE, Hastings A (2011) The roles of the moran effect and dispersal in synchronizing oscillating populations. *Journal of Theoretical Biology* 289:237–246
- Gong CC, Pikovsky A (2019) Low-dimensional dynamics for higher-order harmonic, globally coupled phase-oscillator ensembles. *Physical Review E* 100(6):062,210
- Grenfell BT, Bjørnstad ON, Kappey J (2001) Travelling waves and spatial hierarchies in measles epidemics. *Nature* 414(6865):716
- Grilli J, Barabás G, Michalska-Smith MJ, Allesina S (2017) Higher-order interactions stabilize dynamics in competitive network models. *Nature* 548(7666):210–213
- Grinsted A, Moore JC, Jevrejeva S (2004) Application of the cross wavelet transform and wavelet coherence to geophysical time series. *Nonlinear Processes in Geophysics* 11(5/6):561–566
- GRØTAN V, SÆTHER BE, Engen S, Solberg EJ, Linnell JD, Andersen R, BRØSETH H, Lund E (2005) Climate causes large-scale spatial synchrony in population fluctuations of a temperate herbivore. *Ecology* 86(6):1472–1482
- Gu HG, Jia B, Li YY, Chen GR (2013) White noise-induced spiral waves and multiple spatial coherence resonances in a neuronal network with type i excitability. *Physica A: Statistical Mechanics and its Applications* 392(6):1361–1374
- Gupta A, Banerjee T, Dutta PS (2017) Increased persistence via asynchrony in oscillating ecological populations with long-range interaction. *Physical Review E* 96(4):042,202
- Guttal V, Jayaprakash C (2009) Spatial variance and spatial skewness: leading indicators of regime shifts in spatial ecological systems. *Theoretical Ecology* 2:3–12
- Haddad NM (1999) Corridor and distance effects on interpatch movements: a landscape experiment with butterflies. *Ecological Applications* 9(2):612–622
- Hagerstrom AM, Murphy TE, Roy R, Hövel P, Omelchenko I, Schöll E (2012) Experimental observation of chimeras in coupled-map lattices. *Nature Physics* 8(9):658–661
- Haken H (1975) Cooperative phenomena in systems far from thermal equilibrium and in nonphysical systems. *Reviews of Modern Physics* 47(1):67

- Hanski I (1998) Metapopulation dynamics. *Nature* 396(6706):41–49
- Hanski I, Gilpin M (1991) Metapopulation dynamics: brief history and conceptual domain. *Biological journal of the Linnean Society* 42(1-2):3–16
- Hanski I, Kuussaari M, Nieminen M (1994) Metapopulation structure and migration in the butterfly *melitaea cinxia*. *Ecology* 75(3):747–762
- Hanski IA, Gaggiotti OE, Gaggiotti OF (2004) Ecology, genetics and evolution of metapopulations. Academic Press
- Harrington R, Woiwod I, Sparks T (1999) Climate change and trophic interactions. *Trends in Ecology & Evolution* 14(4):146–150
- Harris TE (1974) Contact interactions on a lattice. *The Annals of Probability* 2(6):969–988
- Hastings A (1992) Age dependent dispersal is not a simple process: Density dependence, stability, and chaos. *Theoretical Population Biology* 41(3):388–400
- Hastings A (1993) Complex interactions between dispersal and dynamics: lessons from coupled logistic equations. *Ecology* 74(5):1362–1372
- Hastings A (2001) Transient dynamics and persistence of ecological systems. *Ecology Letters* 4(3):215–220
- Hastings A, Powell T (1991) Chaos in a three-species food chain. *Ecology* 72(3):896–903
- Hastings A, Abbott KC, Cuddington K, Francis T, Gellner G, Lai YC, Morozov A, Petrovskii S, Scranton K, Zeeman ML (2018) Transient phenomena in ecology. *Science* 361(6406):eaat6412
- Hastings A, Abbott KC, Cuddington K, Francis TB, Lai YC, Morozov A, Petrovskii S, Zeeman ML (2021) Effects of stochasticity on the length and behaviour of ecological transients. *Journal of the Royal Society Interface* 18(180):20210,257
- Hauzy C, Gauduchon M, Hulot FD, Loreau M (2010) Density-dependent dispersal and relative dispersal affect the stability of predator–prey metacommunities. *Journal of Theoretical Biology* 266(3):458–469
- Hector A, Hautier Y, Saner P, Wacker L, Bagchi R, Joshi J, Scherer-Lorenzen M, Spehn EM, Bazeley-White E, Weilenmann M, et al (2010) General stabilizing effects of plant diversity on grassland productivity through population asynchrony and overyielding. *Ecology* 91(8):2213–2220

- Hidalgo J, Seoane LF, Cortès JM, Munoz MA (2012) Stochastic amplification of fluctuations in cortical up-states. *PloS One* 7(8):1–8
- Higgins K, Hastings A, Sarvela JN, Botsford LW (1997) Stochastic dynamics and deterministic skeletons: population behavior of dungeness crab. *Science* 276(5317):1431–1435
- Hillenbrand U (2002) Subthreshold dynamics of the neural membrane potential driven by stochastic synaptic input. *Physical Review E* 66(2):021,909
- Holland MD, Hastings A (2008) Strong effect of dispersal network structure on ecological dynamics. *Nature* 456(7223):792–794
- Holling CS (1973) Resilience and stability of ecological systems. *Annual Review of Ecology and Systematics* 4(1):1–23
- Holt RD (2004) Implications of system openness for local community structure and ecosystem function. *Food Webs at the Landscape Level* University of Chicago Press, Chicago pp 96–114
- Hooper DU, Chapin III FS, Ewel JJ, Hector A, Inchausti P, Lavorel S, Lawton JH, Lodge DM, Loreau M, Naeem S, et al (2005) Effects of biodiversity on ecosystem functioning: a consensus of current knowledge. *Ecological Monographs* 75(1):3–35
- Hopson J, Fox JW (2019) Occasional long distance dispersal increases spatial synchrony of population cycles. *Journal of Animal Ecology* 88(1):154–163
- Hu B, Zhou C (2000) Phase synchronization in coupled nonidentical excitable systems and array-enhanced coherence resonance. *Physical Review E* 61(2):R1001
- Hudson PJ, Cattadori IM (1999) The moran effect: a cause of population synchrony. *Trends in Ecology & Evolution* 14(1):1–2
- Huffaker C (1958) Experimental studies on predation: dispersion factors and predator-prey oscillations. *Hilgardia* 27:343–383
- Hutchison C, Guichard F, Legagneux P, Gauthier G, Bêty J, Berteaux D, Fauteux D, Gravel D (2020) Seasonal food webs with migrations: multi-season models reveal indirect species interactions in the canadian arctic tundra. *Philosophical Transactions of the Royal Society A* 378(2181):20190,354
- Hutt A, Mierau A, Lefebvre J (2016) Dynamic control of synchronous activity in networks of spiking neurons. *PloS One* 11(9):e0161,488

- Ims RA, Andreassen HP (2005) Density-dependent dispersal and spatial population dynamics. *Proceedings of the Royal Society B: Biological Sciences* 272(1566):913–918
- Ives A, Gilchrist G (1993) Climate change and ecological interactions. *Biotic Interactions and Global Change* pp 120–146
- Ives AR (1995) Predicting the response of populations to environmental change. *Ecology* 76(3):926–941
- Ives AR, Carpenter SR (2007) Stability and diversity of ecosystems. *Science* 317(5834):58–62
- Izem R, Kingsolver JG (2005) Variation in continuous reaction norms: quantifying directions of biological interest. *The American Naturalist* 166(2):277–289
- Izhikevich EM (2007) *Dynamical systems in neuroscience*. MIT press
- Jacoby DM, Freeman R (2016) Emerging network-based tools in movement ecology. *Trends in Ecology & Evolution* 31(4):301–314
- Jafarpour F, Biancalani T, Goldenfeld N (2017) Noise-induced symmetry breaking far from equilibrium and the emergence of biological homochirality. *Physical Review E* 95(3):032,407
- Jánosi IM, Scheuring I (1997) On the evolution of density dependent dispersal in a spatially structured population model. *Journal of Theoretical Biology* 187(3):397–408
- Jansen VA (1999) Phase locking: another cause of synchronicity in predator–prey systems. *Trends in Ecology & Evolution* 7(14):278–279
- Jenkins DG, Brescacin CR, Duxbury CV, Elliott JA, Evans JA, Grablow KR, Hillegass M, Lyon BN, Metzger GA, Olandese ML, et al (2007) Does size matter for dispersal distance? *Global Ecology and Biogeography* 16(4):415–425
- Jourdan J, Baranov V, Wagner R, Plath M, Haase P (2019) Elevated temperatures translate into reduced dispersal abilities in a natural population of an aquatic insect. *Journal of Animal Ecology* 88(10):1498–1509
- Jung P, Mayer-Kress G (1995) Spatiotemporal stochastic resonance in excitable media. *Physical Review Letters* 74(11):2130
- Kareiva P (1990) Population dynamics in spatially complex environments: theory and data. *Philosophical Transactions of the Royal Society of London Series B: Biological Sciences* 330(1257):175–190



- Kareiva P, Odell G (1987) Swarms of predators exhibit "preytaxis" if individual predators use area-restricted search. *The American Naturalist* 130(2):233–270
- Kareiva P, Shigesada N (1983) Analyzing insect movement as a correlated random walk. *Oecologia* 56:234–238
- Kareiva P, Wennergren U (1995) Connecting landscape patterns to ecosystem and population processes. *Nature* 373(6512):299–302
- Kaur T, Dutta PS (2020) Persistence and stability of interacting species in response to climate warming: The role of trophic structure. *Theoretical Ecology* 13(3):333–348
- Keitt TH, Fischer J (2006) Detection of scale-specific community dynamics using wavelets. *Ecology* 87(11):2895–2904
- Keitt TH, Lewis MA, Holt RD (2001) Allee effects, invasion pinning, and species' borders. *The American Naturalist* 157(2):203–216
- Kendall BE, Bjørnstad ON, Bascompte J, Keitt TH, Fagan WF (2000) Dispersal, environmental correlation, and spatial synchrony in population dynamics. *The American Naturalist* 155(5):628–636
- Khatun T, Bandyopadhyay B, Banerjee T (2022) Diverse coherence-resonance chimeras in coupled type-i excitable systems. *Physical Review E* 106(5):054,208
- Kingsland SE, Kingsland SE (1995) *Modeling nature*. University of Chicago Press
- Knappe J, de Valpine P (2012) Are patterns of density dependence in the global population dynamics database driven by uncertainty about population abundance? *Ecology Letters* 15(1):17–23
- Kobayashi TJ (2011) Connection between noise-induced symmetry breaking and an information-decoding function for intracellular networks. *Physical Review Letters* 106(22):228,101
- Komin N, Murza AC, Hernández-García E, Toral R (2010) Synchronization and entrainment of coupled circadian oscillators. *Interface Focus* 1(1):167–176
- Kot M, Lewis MA, van den Driessche P (1996) Dispersal data and the spread of invading organisms. *Ecology* 77(7):2027–2042
- Kotliar G, Anderson P, Stein DL (1983a) One-dimensional spin-glass model with long-range random interactions. *Physical Review B* 27(1):602

- Kotliar G, Anderson PW, Stein DL (1983b) Discontinuity of the magnetization in one-dimensional ising and potts models. *Phys Rev B* 27:602
- Kovalenko K, Dai X, Alfaro-Bittner K, Raigorodskii A, Perc M, Boccaletti S (2021) Contrarians synchronize beyond the limit of pairwise interactions. *Physical Review Letters* 127(25):258,301
- Kuehn C, Bick C (2021) A universal route to explosive phenomena. *Science Advances* 7(16):eabe3824
- Kuo HY, Wu KA (2015) Synchronization and plateau splitting of coupled oscillators with long-range power-law interactions. *Physical Review E* 92(6):062,918
- Kurrer C, Schulten K (1995) Noise-induced synchronous neuronal oscillations. *Physical Review E* 51(6):6213
- Kuussaari M, Rytteri S, Heikkinen RK, Heliölä J, von Bagh P (2016) Weather explains high annual variation in butterfly dispersal. *Proceedings of the Royal Society B: Biological Sciences* 283(1835):20160,413
- Lande R, Engen S, Sæther BE (1999) Spatial scale of population synchrony: environmental correlation versus dispersal and density regulation. *The American Naturalist* 154(3):271–281
- Langmead O, Sheppard C (2004) Coral reef community dynamics and disturbance: a simulation model. *Ecological Modelling* 175(3):271–290
- Levin SA (1976) Population dynamic models in heterogeneous environments. *Annual Review of Ecology and Systematics* 7(1):287–310
- Levin SA, Durrett R (1996) From individuals to epidemics. *Philosophical Transactions of the Royal Society of London Series B: Biological Sciences* 351(1347):1615–1621
- Levine JM, Bascompte J, Adler PB, Allesina S (2017) Beyond pairwise mechanisms of species coexistence in complex communities. *Nature* 546(7656):56–64
- Levins R (1969) Some demographic and genetic consequences of environmental heterogeneity for biological control. *American Entomologist* 15(3):237–240
- Levy D, Harrington HA, Van Gorder RA (2016) Role of seasonality on predator–prey–subsidy population dynamics. *Journal of Theoretical Biology* 396:163–181

- Lewontin RC (1969) The meaning of stability. In: Brookhaven Symposia in Biology, vol 22, pp 13–24
- Li Zz, Gao M, Hui C, Han Xz, Shi H (2005) Impact of predator pursuit and prey evasion on synchrony and spatial patterns in metapopulation. *Ecological Modelling* 185(2-4):245–254
- Liebholt A, Koenig WD, Bjørnstad ON (2004) Spatial synchrony in population dynamics. *Annu Rev Ecol Evol Syst* 35:467–490
- Lima SL, Zollner PA (1996) Towards a behavioral ecology of ecological landscapes. *Trends in Ecology & Evolution* 11(3):131–135
- Lindenmayer DB, Fischer J (2013) Habitat fragmentation and landscape change: an ecological and conservation synthesis. Island Press
- Lindner JF, Chandramouli S, Bulsara AR, Löcher M, Ditto WL (1998) Noise enhanced propagation. *Physical Review Letters* 81(23):5048
- Logofet DO (2018) Matrices and graphs: stability problems in mathematical ecology. CRC press
- Loreau M, Downing A, Emmerson M, Gonzalez A, Hughes J, Inchausti P, Joshi J, Norberg J, Sala O (2002) A new look at the relationship between diversity and stability. *Biodiversity and Ecosystem Functioning: Synthesis and Perspectives* pp 79–91
- Loreau M, Mouquet N, Gonzalez A (2003) Biodiversity as spatial insurance in heterogeneous landscapes. *Proceedings of the National Academy of Sciences* 100(22):12,765–12,770
- Lundberg P, Ranta E, Ripa J, Kaitala V (2000) Population variability in space and time. *Trends in Ecology & Evolution* 15(11):460–464
- Majumder S, Das A, Kushal A, Sankaran S, Guttal V (2021) Finite-size effects, demographic noise, and ecosystem dynamics. *The European Physical Journal Special Topics* 230(16):3389–3401
- Martin TL, Huey RB (2008) Why “suboptimal” is optimal: Jensen’s inequality and ectotherm thermal preferences. *The American Naturalist* 171(3):E102–E118
- Matthysen E (2005) Density-dependent dispersal in birds and mammals. *Ecography* 28(3):403–416

- May RM (1974) Biological populations with nonoverlapping generations: stable points, stable cycles, and chaos. *Science* 186(4164):645–647
- McCann KS, Rasmussen J, Ulanowicz J (2005) The dynamics of spatially coupled food webs. *Ecology Letters* 8(5):513–523
- McMahon SM, Harrison SP, Armbruster WS, Bartlein PJ, Beale CM, Edwards ME, Kattge J, Midgley G, Morin X, Prentice IC (2011) Improving assessment and modelling of climate change impacts on global terrestrial biodiversity. *Trends in Ecology & Evolution* 26(5):249–259
- Melbourne BA, Hastings A (2008) Extinction risk depends strongly on factors contributing to stochasticity. *Nature* 454(7200):100–103
- Meron E (1992) Pattern formation in excitable media. *Physics Reports* 218(1):1–66
- Millán AP, Torres JJ, Bianconi G (2019) Synchronization in network geometries with finite spectral dimension. *Physical Review E* 99(2):022,307
- Milne R, Guichard F (2021) Coupled phase-amplitude dynamics in heterogeneous metacommunities. *Journal of Theoretical Biology* 523:110,676
- Moilanen A, Hanski I (2001) On the use of connectivity measures in spatial ecology. *Oikos* 95(1):147–151
- Moilanen A, Nieminen M (2002) Simple connectivity measures in spatial ecology. *Ecology* 83(4):1131–1145
- Moilanen A, Franco AM, Early RI, Fox R, Wintle B, Thomas CD (2005) Prioritizing multiple-use landscapes for conservation: methods for large multi-species planning problems. *Proceedings of the Royal Society B: Biological Sciences* 272(1575):1885–1891
- Molofsky J (1994) Population dynamics and pattern formation in theoretical populations. *Ecology* 75(1):30–39
- Montoya JM, Pimm SL, Solé RV (2006) Ecological networks and their fragility. *Nature* 442(7100):259–264
- Moorcroft PR, Lewis MA (2013) Mechanistic home range analysis.(MPB-43). Princeton University Press
- Moran P (1953) The statistical analysis of the canadian lynx cycle. 1. structure and prediction. *Australian Journal of Zoology* 1(2):163–173

- Murray JD (1993) *Mathematical biology*. second corrected edition. Springer-Verlag Berlin Heidelberg 21:225–272
- Mysterud A, Stenseth NC, Yoccoz NG, Langvatn R, Steinheim G (2001) Nonlinear effects of large-scale climatic variability on wild and domestic herbivores. *Nature* 410(6832):1096–1099
- Naeem S, Thompson LJ, Lawler SP, Lawton JH, Woodfin RM (1994) Declining biodiversity can alter the performance of ecosystems. *Nature* 368:734–737
- Narang A, Bhandary S, Kaur T, Gupta A, Banerjee T, Dutta PS (2019) Long-range dispersal promotes species persistence in climate extremes. *Chaos: An Interdisciplinary Journal of Nonlinear Science* 29(10):103,136
- Nauta J, Simoens P, Khaluf Y, Martinez-Garcia R (2022) Foraging behaviour and patch size distribution jointly determine population dynamics in fragmented landscapes. *Journal of the Royal Society Interface* 19(191):20220,103
- Neiman A, Schimansky-Geier L, Cornell-Bell A, Moss F (1999) Noise-enhanced phase synchronization in excitable media. *Physical Review Letters* 83(23):4896
- Nesse WH, Del Negro CA, Bressloff PC (2008) Oscillation regularity in noise-driven excitable systems with multi-time-scale adaptation. *Physical Review Letters* 101(8):088,101
- Nevai AL, Van Gorder RA (2012) Effect of resource subsidies on predator–prey population dynamics: a mathematical model. *Journal of Biological Dynamics* 6(2):891–922
- Newlands NK, Lutcavage ME, Pitcher TJ (2004) Analysis of foraging movements of atlantic bluefin tuna (*thunnus thynnus*): individuals switch between two modes of search behaviour. *Population Ecology* 46:39–53
- Newman M (2018) *Networks*. Oxford University Press
- Niebuhr B, Wosniack ME, Santos MC, Raposo EP, Viswanathan GM, Da Luz MG, Pie MR (2015) Survival in patchy landscapes: the interplay between dispersal, habitat loss and fragmentation. *Scientific Reports* 5(1):1–10
- Nolet BA, Mooij WM (2002) Search paths of swans foraging on spatially autocorrelated tubers. *Journal of Animal Ecology* pp 451–462
- Olla P (2013) Effect of demographic noise in a phytoplankton-zooplankton model of bloom dynamics. *Physical Review E* 87(1):012,712

- Ostfeld RS, Keesing F (2000) Pulsed resources and community dynamics of consumers in terrestrial ecosystems. *Trends in Ecology & Evolution* 15(6):232–237
- Ovaskainen O, Luoto M, Ikonen I, Rekola H, Meyke E, Kuussaari M (2008) An empirical test of a diffusion model: predicting clouded apollo movements in a novel environment. *The American Naturalist* 171(5):610–619
- Pal K, Deb S, Dutta PS (2022) Tipping points in spatial ecosystems driven by short-range correlated noise. *Physical Review E* 106(5):054,412
- Parastesh F, Mehrabbeik M, Rajagopal K, Jafari S, Perc M (2022) Synchronization in hindmarsh–rose neurons subject to higher-order interactions. *Chaos: An Interdisciplinary Journal of Nonlinear Science* 32(1)
- Parmesan C (2006) Ecological and evolutionary responses to recent climate change. *Annu Rev Ecol Evol Syst* 37:637–669
- Pärn H, Ringsby TH, Jensen H, Sæther BE (2012) Spatial heterogeneity in the effects of climate and density-dependence on dispersal in a house sparrow metapopulation. *Proceedings of the Royal Society B: Biological Sciences* 279(1726):144–152
- Pascual M, Roy M, Guichard F, Flierl G (2002) Cluster size distributions: signatures of self-organization in spatial ecologies. *Philosophical Transactions of the Royal Society of London Series B: Biological Sciences* 357(1421):657–666
- Pecora LM, Carroll TL (1998) Master stability functions for synchronized coupled systems. *Physical Review Letters* 80(10):2109
- Pellerin F, Cote J, Bestion E, Aguilée R (2019) Matching habitat choice promotes species persistence under climate change. *Oikos* 128(2):221–234
- Peltonen M, Liebhold AM, Bjørnstad ON, Williams DW (2002) Spatial synchrony in forest insect outbreaks: roles of regional stochasticity and dispersal. *Ecology* 83(11):3120–3129
- Pereira HM, Leadley PW, Proença V, Alkemade R, Scharlemann JP, Fernandez-Manjarrés JF, Araújo MB, Balvanera P, Biggs R, Cheung WW, et al (2010) Scenarios for global biodiversity in the 21st century. *Science* 330(6010):1496–1501
- Petri G, Expert P, Turkheimer F, Carhart-Harris R, Nutt D, Hellyer PJ, Vaccarino F (2014) Homological scaffolds of brain functional networks. *Journal of The Royal Society Interface* 11(101):20140,873

- Pikovsky AS, Kurths J (1997) Coherence resonance in a noise-driven excitable system. *Physical Review Letters* 78(5):775
- Pimm SL (2009) Climate disruption and biodiversity. *Current Biology* 19(14):R595–R601
- Poethke HJ, Hovestadt T (2002) Evolution of density- and patch-size-dependent dispersal rates. *Proceedings of the Royal Society of London Series B: Biological Sciences* 269(1491):637–645
- Post E, Forchhammer MC (2004) Spatial synchrony of local populations has increased in association with the recent northern hemisphere climate trend. *Proceedings of the National Academy of Sciences, USA* 101(25):9286–9290
- Rands MR, Adams WM, Bennun L, Butchart SH, Clements A, Coomes D, Entwistle A, Hodge I, Kapos V, Scharlemann JP, et al (2010) Biodiversity conservation: challenges beyond 2010. *Science* 329(5997):1298–1303
- Ranta E, Kaitala V, Lundberg P (1997) The spatial dimension in population fluctuations. *Science* 278(5343):1621–1623
- Rayfield B, Fortin MJ, Fall A (2011) Connectivity for conservation: a framework to classify network measures. *Ecology* 92(4):847–858
- Reynolds A, Reynolds D, Smith A, Svensson G, Löfstedt C (2007a) Appetitive flight patterns of male *agrotis segetum* moths over landscape scales. *Journal of Theoretical Biology* 245(1):141–149
- Reynolds AM, Smith AD, Reynolds DR, Carreck NL, Osborne JL (2007b) Honeybees perform optimal scale-free searching flights when attempting to locate a food source. *Journal of Experimental Biology* 210(21):3763–3770
- Ritz A, Tegge AN, Kim H, Poirel CL, Murali T (2014) Signaling hypergraphs. *Trends in Biotechnology* 32(7):356–362
- Rohani P, Earn DJ, Grenfell BT (1999) Opposite patterns of synchrony in sympatric disease metapopulations. *Science* 286(5441):968–971
- Rosenzweig ML, MacArthur RH (1963) Graphical representation and stability conditions of predator-prey interactions. *The American Naturalist* 97(895):209–223
- Salnikov V, Cassese D, Lambiotte R (2018) Simplicial complexes and complex systems. *European Journal of Physics* 40(1):014,001

- Sankaran S, Majumder S, Viswanathan A, Guttal V (2019) Clustering and correlations: Inferring resilience from spatial patterns in ecosystems. *Methods in Ecology and Evolution* 10(12):2079–2089
- Saravia LA, Ruxton GD, Coviella CE (2000) The importance of transient's dynamics in spatially extended populations. *Proceedings of The Royal Society of London Series B: Biological Sciences* 267(1454):1781–1785
- Savage VM, Gillooly JF, Brown JH, West GB, Charnov EL (2004) Effects of body size and temperature on population growth. *The American Naturalist* 163(3):429–441
- Schmidt KA, Ostfeld RS (2003) Songbird populations in fluctuating environments: predator responses to pulsed resources. *Ecology* 84(2):406–415
- Schneidman E, Still S, Berry MJ, Bialek W, et al (2003) Network information and connected correlations. *Physical Review Letters* 91(23):238,701
- Schreiber SJ (2003) Allee effects, extinctions, and chaotic transients in simple population models. *Theoretical Population Biology* 64(2):201–209
- Schwabedal JT, Pikovsky A (2010) Effective phase dynamics of noise-induced oscillations in excitable systems. *Physical Review E* 81(4):046,218
- Sekara V, Stopczynski A, Lehmann S (2016) Fundamental structures of dynamic social networks. *Proceedings of the National Academy of Sciences* 113(36):9977–9982
- Semenova N, Zakharova A, Anishchenko V, Schöll E (2016) Coherence-resonance chimeras in a network of excitable elements. *Physical Review Letters* 117(1):014,102
- Shahal S, Wurzburg A, Sibony I, Duadi H, Shniderman E, Weymouth D, Davidson N, Fridman M (2020) Synchronization of complex human networks. *Nature Communications* 11(1):3854
- Shen L, Van Gorder RA (2017) Predator–prey–subsidy population dynamics on stepping-stone domains. *Journal of Theoretical Biology* 420:241–258
- Shlesinger MF, Klafter J (1986) Lévy walks versus lévy flights. *On growth and Form: Fractal and Non-Fractal Patterns in Physics* pp 279–283
- Sieber M, Malchow H, Schimansky-Geier L (2007) Constructive effects of environmental noise in an excitable prey–predator plankton system with infected prey. *Ecological Complexity* 4(4):223–233



- Sigeti D, Horsthemke W (1989) Pseudo-regular oscillations induced by external noise. *Journal of Statistical Physics* 54(5):1217–1222
- Sims DW, Southall EJ, Humphries NE, Hays GC, Bradshaw CJ, Pitchford JW, James A, Ahmed MZ, Brierley AS, Hindell MA, et al (2008) Scaling laws of marine predator search behaviour. *Nature* 451(7182):1098–1102
- Sole RV, Valls J, Bascompte J (1992) Spiral waves, chaos and multiple attractors in lattice models of interacting populations. *Physics Letters A* 166(2):123–128
- Sommer U, Worm B, Sommer U (2002) Competition and coexistence in plankton communities. Springer
- Sparks T, Carey P (1995) The responses of species to climate over two centuries: an analysis of the marsham phenological record, 1736–1947. *Journal of Ecology* pp 321–329
- Steffen W, Crutzen PJ, McNeill JR, et al (2007) The anthropocene: are humans now overwhelming the great forces of nature. *Ambio-Journal of Human Environment Research and Management* 36(8):614–621
- Stenseth NC, Bjørnstad ON, Saitoh T (1996) A gradient from stable to cyclic populations of *clethrionomys rufocanus* in hokkaido, japan. *Proceedings of the Royal Society of London Series B: Biological Sciences* 263(1374):1117–1126
- Strogatz S (2004) *Sync: The emerging science of spontaneous order*. Penguin UK
- Szaro BG, Tompkins R (1987) Effect of tetraploidy on dendritic branching in neurons and glial cells of the frog, *xenopus laevis*. *J Comp Neurol* 258:304–316
- Szaro BG, Tompkins R, Szaro BG (1987) Effect of tetraploidy on dendritic branching in neurons and glial cells of the frog, *xenopus laevis*. *Journal of Comparative Neurology* 258(2):304–316
- Tanaka HA, Lichtenberg AJ, Oishi S (1997) Self-synchronization of coupled oscillators with hysteretic responses. *Physica D: Nonlinear Phenomena* 100(3-4):279–300
- Taylor PD, Fahrig L, Henein K, Merriam G (1993) Connectivity is a vital element of landscape structure. *Oikos* pp 571–573
- Thomas CD, Lennon JJ (1999) Birds extend their ranges northwards. *Nature* 399(6733):213

- Thomas CD, Cameron A, Green RE, Bakkenes M, Beaumont LJ, Collingham YC, Erasmus BF, De Siqueira MF, Grainger A, Hannah L, et al (2004) Extinction risk from climate change. *Nature* 427(6970):145–148
- Thomas MK, Kremer CT, Klausmeier CA, Litchman E (2012) A global pattern of thermal adaptation in marine phytoplankton. *Science* 338(6110):1085–1088
- Thompson PL, Beisner BE, Gonzalez A (2015) Warming induces synchrony and destabilizes experimental pond zooplankton metacommunities. *Oikos* 124(9):1171–1180
- Thuiller W, Araújo MB, Pearson RG, Whittaker RJ, Brotons L, Lavorel S (2004) Uncertainty in predictions of extinction risk. *Nature* 430(6995):34–34
- Tilman D (1996) Biodiversity: population versus ecosystem stability. *Ecology* 77(2):350–363
- Tilman D, Kareiva P (2018) Spatial ecology: the role of space in population dynamics and interspecific interactions (MPB-30), vol 30. Princeton University Press
- Tilman D, Lehman CL, Kareiva P (1997) Population dynamics in spatial habitats. Spatial ecology: The role of space in population dynamics and interspecific interactions pp 3–20
- Tischendorf L, Fahrig L (2000) On the usage and measurement of landscape connectivity. *Oikos* 90(1):7–19
- Torrence C, Compo GP (1998) A practical guide to wavelet analysis. *Bulletin of the American Meteorological Society* 79(1):61–78
- Travis JM, Murrell DJ, Dytham C (1999) The evolution of density-dependent dispersal. *Proceedings of the Royal Society of London Series B: Biological Sciences* 266(1431):1837–1842
- Travis JM, Delgado M, Bocedi G, Baguette M, Bartoń K, Bonte D, Boulangéat I, Hodgson JA, Kubisch A, Penteriani V, et al (2013) Dispersal and species' responses to climate change. *Oikos* 122(11):1532–1540
- Truscott J, Brindley J (1994) Ocean plankton populations as excitable media. *Bulletin of Mathematical Biology* 56(5):981–998
- Turchin P (1991) Translating foraging movements in heterogeneous environments into the spatial distribution of foragers. *Ecology* 72(4):1253–1266

- Turchin P (1998) Quantitative analysis of movement: measuring and modeling population redistribution in animals and plants. Sinauer associates
- Turchin P, Ellner SP (2000) Living on the edge of chaos: population dynamics of fennoscandian voles. *Ecology* 81(11):3099–3116
- Turner MG (1989) Landscape ecology: the effect of pattern on process. *Annual Review of Ecology and Systematics* 20(1):171–197
- Tylianakis JM, Didham RK, Bascompte J, Wardle DA (2008) Global change and species interactions in terrestrial ecosystems. *Ecology Letters* 11(12):1351–1363
- Urban D, O’NEILL R, Shugart Jr H (1987) Landscape ecology. the study of landscape is emerging as a new discipline in the field of ecology. *BioScience* 37(2):119–127
- Urban MC, Tewksbury JJ, Sheldon KS (2012) On a collision course: competition and dispersal differences create no-analogue communities and cause extinctions during climate change. *Proceedings of the Royal Society B: Biological Sciences* 279(1735):2072–2080
- Vandermeer J (2006) Oscillating populations and biodiversity maintenance. *Bioscience* 56(12):967–975
- Vandermeer J, Hajian-Forooshani Z, Medina N, Perfecto I (2021) New forms of structure in ecosystems revealed with the kuramoto model. *Royal Society Open Science* 8(3):210,122
- Vasseur DA, McCann KS (2005) A mechanistic approach for modeling temperature-dependent consumer-resource dynamics. *The American Naturalist* 166(2):184–198
- Viswanathan GM, Buldyrev SV, Havlin S, Da Luz M, Raposo E, Stanley HE (1999) Optimizing the success of random searches. *Nature* 401(6756):911–914
- Viswanathan GM, Da Luz MG, Raposo EP, Stanley HE (2011) The physics of foraging: an introduction to random searches and biological encounters. Cambridge University Press
- Vitousek PM, Mooney HA, Lubchenco J, Melillo JM (1997) Human domination of earth’s ecosystems. *Science* 277(5325):494–499
- Walther GR (2007) Ecology. tackling ecological complexity in climate impact research. *Science (New York, NY)* 315(5812):606–607

- Walther GR, Post E, Convey P, Menzel A, Parmesan C, Beebee TJ, Fromentin JM, Hoegh-Guldberg O, Bairlein F (2002) Ecological responses to recent climate change. *Nature* 416(6879):389
- Walther GR, Berger S, Sykes MT (2005) An ecological ‘footprint’ of climate change. *Proceedings of the Royal Society B: Biological Sciences* 272(1571):1427–1432
- Wang S, Loreau M (2014) Ecosystem stability in space:  $\alpha$ ,  $\beta$  and  $\gamma$  variability. *Ecology Letters* 17(8):891–901
- Warner RR, Chesson PL (1985) Coexistence mediated by recruitment fluctuations: a field guide to the storage effect. *The American Naturalist* 125(6):769–787
- Watkinson AR, Gill JA (2002) Climate change and dispersal. *Dispersal Ecology* pp 410–428
- Watts DJ, Strogatz SH (1998) Collective dynamics of ‘small-world’ networks. *Nature* 393(6684):440–442
- WF F (2006) Quantifying connectivity: balancing metric performance with data requirements. *Connectivity Conservation* pp 297–317
- Wieczorek S, Ashwin P, Luke CM, Cox PM (2011) Excitability in ramped systems: the compost-bomb instability. *Proceedings of the Royal Society of London A: Mathematical, Physical and Engineering Sciences* 467(2129):1243–1269
- Wiens JA, Chr N, Van Horne B, Ims RA (1993) Ecological mechanisms and landscape ecology. *Oikos* pp 369–380
- Williams GC (2018) Adaptation and natural selection: A critique of some current evolutionary thought, vol 61. Princeton University Press
- Wilson RJ, Gutiérrez D, Gutiérrez J, Martínez D, Agudo R, Monserrat VJ (2005) Changes to the elevational limits and extent of species ranges associated with climate change. *Ecology Letters* 8(11):1138–1146
- With KA, Gardner RH, Turner MG (1997) Landscape connectivity and population distributions in heterogeneous environments. *Oikos* pp 151–169
- Witman JD, Genovese SJ, Bruno JF, McLaughlin JW, Pavlin BI (2003) Massive prey recruitment and the control of rocky subtidal communities on large spatial scales. *Ecological Monographs* 73(3):441–462
- Yaari G, Ben-Zion Y, Shnerb NM, Vasseur DA (2012) Consistent scaling of persistence time in metapopulations. *Ecology* 93(5):1214–1227

- Yang LH, Bastow JL, Spence KO, Wright AN (2008) What can we learn from resource pulses. *Ecology* 89(3):621–634
- Yoder JM, Marschall EA, Swanson DA (2004) The cost of dispersal: predation as a function of movement and site familiarity in ruffed grouse. *Behavioral Ecology* 15(3):469–476
- Zakharova A, Kapeller M, Schöll E (2014) Chimera death: Symmetry breaking in dynamical networks. *Physical Review Letters* 112(15):154,101
- Zollner PA, Lima SL (1999) Search strategies for landscape-level interpatch movements. *Ecology* 80(3):1019–1030

## List of Publications

- 1 Narang, A., Banerjee, T., and Dutta, P. S., *Noise-induced symmetry breaking in a network of excitable ecological systems*, Physical Review E, APS, Vol. 107 (2), 024410 (2023). <https://doi.org/10.1103/PhysRevE.107.024410>
- 2 Narang, A., Banerjee, T., and Dutta, P. S., *Increased habitat connectivity induces diversity via noise-induced symmetry breaking*, Chaos: An Interdisciplinary Journal of Nonlinear Science, AIP, Vol. 33 (6), 063118 (2023). <https://doi.org/10.1063/5.0150943>
- 3 Narang, A., and Dutta, P. S., *Climate warming and dispersal strategies determine species persistence in a metacommunity*, Theoretical Ecology, Springer, Vol. 15 (1), 81-92 (2022). <https://doi.org/10.1007/s12080-022-00531-3>
- 4 Sarkar, S., Narang, A., Sinha, S., and Dutta, P. S., *Effects of stochasticity and social norms on complex dynamics of fisheries*, Physical Review E, APS, Vol. 103 (2), 022401 (2021). <https://doi.org/10.1103/PhysRevE.103.022401>
- 5 Narang, A., Bhandary, S., Kaur, T., Gupta, A., Banerjee, T., and Dutta, P. S., *Long-range dispersal promotes species persistence in climate extremes*, Chaos: An Interdisciplinary Journal of Nonlinear Science, AIP, Vol. 29 (10), 103136 (2019). <https://doi.org/10.1063/1.5120105>
- 6 Narang, A., Guttal, V., and Dutta, P. S., *Resource pulses and foraging behavior shape spatial population dynamics*, (to be submitted).
- 7 Narang, A. and Dutta, P. S., *Effects of higher-order interactions on the stability of ecological communities*, (to be submitted).